Towards Flexibility in Body Area Sensing Systems: A Signal Processing Approach

By:

Roya Haratian

Submitted in partial fulfilment of the requirements of the Degree of Doctor of Philosophy

Queen Mary University of London

School of Electronic Engineering and Computer Science

2014

Statement of Originality

Required statement of originality for inclusion in research degree theses

I, Roya Haratian, confirm that the research included within this thesis is my own work or that where it has been carried out in collaboration with, or supported by others, that this is duly acknowledged below and my contribution indicated. Previously published material is also acknowledged below.

I attest that I have exercised reasonable care to ensure that the work is original, and does not to the best of my knowledge break any UK law, infringe any third party's copyright or other Intellectual Property Right, or contain any confidential material.

I accept that the College has the right to use plagiarism detection software to check the electronic version of the thesis.

I confirm that this thesis has not been previously submitted for the award of a degree by this or any other university.

Signature: Roya Haratian

Date: 10.09.2014

Details of collaboration and publications:

Roya Haratian, Richard Twycross-Lewis, Tijana Timotijevic, and Chris Phillips, "Towards Flexibility in Sensor Placement for Motion Capture Systems: A Signal Processing Approach", *IEEE Sensors Journal*, vol. 14, issue 3, pp. 701-709, 2014.

Roya Haratian, Tijana Timotijevic, and Chris Phillips "A PCA-based technique for compensating the effect of sensor position changes in motion data" in *6th International IEEE conference on Intelligent System,.* pp. 126-131, Sofia, Bulgaria, 2012.

Roya Haratian, Tijana Timotijevic, and Chris Phillips "A data-driven functional PCA filter for compensating the effect of sensor position changes in motion data," *7th International ACM Conference on Body Area Networks*, pp 5-8, Oslo, Norway, 2012.

Abstract

On-body sensors are used in the application of wearable sensing systems. These systems can capture different information such as physiological activities and motion. Wearable sensor systems designed specifically for motion capture need to consider the wearer's comfort and wearability criteria. The weight and size of the system need to be kept small and the system should not interfere with the user's movements or actions. In general, body motion sensors are bulky or have large batteries. They are also sensitive to positioning. Accurate sensor placement with respect to anatomical landmarks is one of the main factors determining the accuracy of motion capture systems. Changes in the position of the sensors cause increased variability in the motion data, so isolating the characteristic features that represent the most important motion patterns from those affected by such kind of changes is our main concern. We consider an automated computation approach to address this problem. As accurate sensor placement is time-consuming and hard to achieve we investigate a signal processing technique that can enable salient data to be isolated. Our goal is to permit a more flexible motion capture system to be developed whilst compensating for the effect of changes in the position of sensors. Furthermore, for the first time we test whether functional data analysis can allow the sampling rate to be reduced so we can increase energy efficiency. This would permit the use of smaller batteries and thus increase the wearer's comfort. We use functional principal component analysis (fPCA) to compensate for the reduced sampling rate and for the effect of random changes in the position of the sensors. More precisely, we investigate the use of fPCA for filtering and interpreting motion data whilst accounting for variability in the sensor origin. Data are collected through a marker-based motion capture system in experiments using human body and robot arm movements. The proposed post-processing technique can compensate for uncertainties due to sensor positional changes, whilst supporting more energy efficient systems, thus enabling a step towards flexibility in on-body sensing.

Acknowledgment

I would like to thank my supervisors, Dr Chris Phillips and Dr Tijana Timotijevic, for their guide, supports and feedbacks. I learnt a lot from them. I would like to thank my friends for their encouragements. The last but not the least, I would like to thank all my family for their love and support. It wouldn't have been possible without them.

Contents

List of Figures

List of Tables

Abbreviations

2D	Two Dimensions
3D	Three Dimensions
PCA	Principal Component Analysis
ICA	Independent Component Analysis
fPCA	functional Principal Component Analysis
FIR	Finite Impulse Response
IIR	Infinite Impulse Response
BSS	Blind Source Separation
SVD	Singular Value Decomposition
SVF	Singular Value Filter
SVM	Support Vector Machine
RB	Rigid Body
DOF	Degree of Freedom
LED	Light Emitting Diode
DFT	Discrete Fourier transform
SSE	Sum of Squared Errors
EVB	Embedded Vector Basis

1. Introduction

Human body parameters can be captured by a network of on-body sensors, which is used in the application of wearable computing devices. These systems can be worn on human body to capture different kinds of information such as motion and physiological changes [1]- [2]- [3]. Wearable system design needs to consider the wearers' comfort and fitting requirements while considering measurement performance. For example, the weight and the size of the system need to be kept small and the system should not interfere with the user's movements or actions [4]. Recent developments of wearable biosensor systems include advances in miniature bio-sensing devices, smart textiles, microelectronics, wireless communications and advanced algorithms for signal processing [5]- [6]- [7].

Sensors are the key components for wearable electronics systems. They gather data from the wearer and relay the information to a processing unit. Wearable systems comprise various types of miniature sensors, wearable or implantable. The sensors measure physiological parameters like heart rate, blood pressure, body and skin temperature, oxygen saturation, respiration rate, electrocardiogram, motion, etc [1]. The type, position and number of sensors used depend on the application of the wearable systems. One area of development is smart clothing and textiles, for which flexible sensors have been developed. Smart textiles are capable of changing properties with the environmental conditions, e.g., change in pressure, moisture, temperature, etc [8]- [9].

Sensor technologies in motion capture for rehabilitation have received great attention recently. Motion capture is the process of recording movement of body and translating that movement onto a digital model [10]. The goal of motor rehabilitation is to enable a person with motor function impairment to overcome the impediment and recover full motor function [11]. There are several kinds of sensor technologies that have been developed in the field of motion capture and tracking to collect movement information. In general, a tracking system can be visual-based (marker and marker-less based), non-visual, or a combination of both.

In capturing of human motion via on-body sensors, the motion of a body can be thought of as a collection of time series streams describing the joint angles, which is called motion data. Motion data can be used in applications such as animation, sports biomechanics, rehabilitation, and so on. In many applications, the human body is approximated by a collection of articulated limbs that form a kinematic tree. Accurate sensor placement with respect to anatomical landmarks plays a vital role in motion capture. Special care must be taken to achieve levels of reliability sufficient to justify the results of motion capture systems despite measurement variability.

1.1. Motivation

In general, on-body sensors are very sensitive to positioning and are bulky due to large batteries. In our research the focus is on motion capture using on-body sensors as a potential part of smart clothing and thus enable their widespread use for improving people's quality of life for example in home-based rehabilitation, evidence-based rehabilitation and sport sciences applications. The disadvantages of such on-body systems are being cumbersome, uncomfortable to wear and the sensors are easy to displace as shown in figure 1.1.

Figure 1.1, An inertial based motion capture system with attached sensors on body [34]

In rehabilitation, costs of medicine and an aging population are driving the need for the provision of care and treatments at home [12]. In addition, advances in virtual technologies have enabled systems with biofeedback, which enhance motor learning and make motor rehabilitation more effective. Recent literature on rehabilitation platforms with biofeedback demonstrates how biofeedback can increase the effectiveness and improve the outcomes of rehabilitation [11]. However, these systems rely on accurate measurements and representation of motion, which are only possible at the moment with bulky and expensive optical systems, which rely on expert technical support for equipment and platform set-up as well as operation. For these systems to

become more widely adopted as home-based rehabilitation platforms, challenges of overcoming human errors due to non-expert operation, power efficiency, and size or bulkiness need to be overcome.

In evidence-based medicine the need to control spiralling costs of medical treatments has brought about evidence-based decision-making in designing care pathways. This requires that treatments, that is, their outcomes are compared in terms of their clinical performance and cost-effectiveness. Treatment outcomes need to be assessed and compared using objective, quantifiable measures [13]. The effect of this trend on rehabilitation means that the measurement of motor function before and after the treatment using optical motion capture is increasingly being used to gather clinical evidence of rehabilitation treatment effectiveness.

Motion capture in a lab setting has been criticised as inappropriate for measuring the true extent (i.e. limitation) of motor function. Measurements of motor function in everyday patients' settings are becoming more important as the focus of care shifts towards the quality of life [14]. For example, measuring gait in the lab is limited to level-walking or a few steps on a short staircase at best. A more valid measurement results from capturing patient's motion across a broader range of scenarios, in a home setting or outside. This demand drives the need for portable motion capture devices [1].

In sports science, motion capture technologies that can be used outside or in a field setting are needed to support sport science [15]- [16]. Here, high performance in terms of both processing speed and measurement accuracy is particularly critical. Motion capture systems need to be able to measure an increased, or broader-than-normal, range and speed of motion, and do so without hindering movement.

Motion artefacts, sensitivity to sensor placement and insufficient battery life are among the issues that need to be overcome for wider acceptance of body area sensing systems in the aforementioned applications [17]. Recent technological developments have enabled sensor miniaturization, power-efficient design and improved biocompatibility. In our research we look at signal processing approaches to overcome these problems. Our goal is to have a more flexible motion capture system that can compensate for the effect of changes in position of sensors as well as have an increasing energy efficiency that would enable a reduction in battery size.

In motion capture, failure to place markers/sensors accurately is probably the single greatest contributor to measurement variability. Placing markers accurately with respect to specific anatomical landmarks and determining the location of joint centres and other anatomical features in relation to these markers is very important in determining the anthropometry of the individual subject [13]. Particular care should be taken to ensure that sweating, rapid movements and the placement of markers on the subject's body during different motion capture trials and sessions, do not affect sensor/marker positioning according to the marker placement guidelines.

Changes in the position of sensors can be influenced by their fitting on or within smart sensing garments, which in turn affects accuracy of measurements. Tight-fitting clothes are frequently perceived uncomfortable, while most sensors and their applications benefit from a close textile-body coupling [18]. For less-tight garments, selecting appropriate sensor positions is essential and it is often performed empirically by expert opinion, which may not be optimal, or generalized to a population aggravating measurement variability [19]- [20].

Instrumented motion analysis is inherently at risk from both marker placement errors and skin motion artefacts – both of which are difficult to correct after the measurements have been taken. Our research addresses the context of computer-assisted rehabilitation within a home environment, to enhance motor learning or in a setting where an objective assessment of motor function improvement over time is required. By removing the noise due to placement variation between sessions, the data inherent to the movement can be analysed. In a home setting in particular, the potential for placement errors is greater, and may affect the way movement is interpreted and feedback given to the user.

1.2. Contribution

We show how uncertainties in motion data due to mentioned challenges can be compensated for by using signal processing techniques. We assess a number of signal processing techniques with respect to their ability to eliminate undesired signal variability due to random changes in the positioning of sensors. We use functional data analysis techniques including a fitting function for data sampled at reduced rate and principal component analysis to overcome undesired signal variability and increase power efficiency. As discussed increased variability in motion data can be associated with arbitrary changes in position of sensors, so discovering the characteristic features that represent the main motion pattern is our concern.

To reflect the true nature of motion data variability, we investigate the use of fPCA as a filter not previously reported in the literature and to interpret data while accounting for their positional variability. We show how uncertainties due to random changes in position of sensors can be compensated for and how energy consumption is reduced in order to reduce sensing system size and thus have a more convenient on-body system. The technique finds the greatest source of variation in the data and allows

the effect of these variations to be isolated from other changes. It also can be used to remove unwanted sources of variation and thus increasing accuracy.

By showing the way that this technique can be applied to motion capture, we are opening up the possibility of the widespread use of motion capture away from lab setting. In summary the contributions of this thesis are:

- Illustrating and measuring the effect of random changes in position of sensors on motion data of human subjects and a robot arm,
- Separating the effect of random changes in the position of sensors on motion data via signal separation techniques and carrying out a comparative analysis with respect to their performance in signal separating [21]. This comprises:
    - Using functional PCA in source separation of motion data and showing the advantages of functional PCA over other source separation techniques such as *a priory* and adaptive ones,
    - Demonstrating the suitability of a functional PCA based technique to enabling greater power efficiency through sample rate reduction without loss of salient data,
- Possibility of applying the approach to other motion capture systems as we consider joint angles as variables in our analysis, thus the results are agnostic to the technology used to measure the motion,
- Enabling improved flexibility and usability of on-body sensing systems as the proposed post-processing technique can compensate for uncertainties due to sensor positional changes, whilst allowing the sensor units to be more energy efficient and lighter.

1.3. Thesis outline

Following the introduction, we review the relevant state of the art in Chapter 2. After introducing body motion and the human body motion model, techniques for motion capture of humans are discussed. We see that motion capture is very sensitive to the positioning of sensors. We review the studies using data mining techniques to extract variability features in the data in Chapter 3. Research method and proposed filtering technique are described in Chapter 4. The experiments carried out in Human Performance Lab of Queen Mary University of London are described in Chapter 5. In Chapter 6, we describe and compare signal processing techniques. Their ability to compensate for variability of the motion data due to positional changes of sensors on the collected motion data is examined. We discuss our findings in Chapter 6 and finally, we conclude the thesis in Chapter 7.

1.4. List of publications

Roya Haratian, Richard Twycross-Lewis, Tijana Timotijevic, and Chris Phillips, "Towards Flexibility in Sensor Placement for Motion Capture Systems: A Signal Processing Approach", *IEEE Sensors Journal*, vol. 14, issue 3, pp. 701-709, 2014.

Roya Haratian, Tijana Timotijevic, and Chris Phillips "A PCA-based technique for compensating the effect of sensor position changes in motion data" in *6th International IEEE conference on Intelligent Systems,* pp. 126-131, Sofia, Bulgaria, 2012.

Roya Haratian, Tijana Timotijevic, and Chris Phillips “A data-driven functional PCA filter for compensating the effect of sensor position changes in motion data,” *7th International ACM Conference on Body Area Networks*, pp 5-8, Oslo, Norway, 2012.

2. State of the Art Review

On-body sensors capture quantitative data from variety of bio-signals on a subject's body with applications in health, sports and entertainment. With the increase in health costs, a need has arisen to monitor a patient's condition out of hospital in a cost effective way. In healthcare applications on-body sensing systems can provide feedback information about one's health condition either to the user or to a medical centre. They can also be used for managing and monitoring chronic disease, elderly people, and rehabilitation patients. In rehabilitation applications, intelligent garments can be used to capture patient movement and monitor progress, or provide feedback to enhance patients' motor learning and increase rehabilitation effectiveness.

One of the major goals of rehabilitation is to make measurable improvements in daily motor function in order to improve the quality of life. Virtual environments are a powerful tool for various forms of rehabilitation and provide a unique medium suited to the achievement of several requirements for effective rehabilitation intervention [22]. Both therapists and users benefit from the ability to readily grade and document the therapeutic intervention using various systems. The successful integration of virtual reality into multiple aspects of rehabilitation has demonstrated the potential for the technology to be integrated with motion capture [23], especially in applications incorporating biofeedback.

Human motion capture systems are expected to generate motion data through several techniques that dynamically represent the posture changes of a human body based on motion sensor technologies. In motion analysis, the human body is typically modelled as a system of rigid links connected by rotary joints. Measurement protocols define landmarks on the rigid body model where sensors or markers are placed. Movement of sensors is described within a reference coordinate system and from their position and orientation motion data are derived in a post processing stage. In this thesis we note that most of the motion capture techniques are highly dependent on accurate positioning of sensors and require calibration before measurement [24].

There are several sensor technologies and techniques for motion capture. Motion sensors involve accurate identification, tracking and post-processing of movement. Visual based sensor technologies like optical systems and non-visual based sensor technologies like inertial systems use different techniques to capture human body motion. In this chapter after describing body models and their approximation by link-segment models, we introduce kinematics and inverse kinematics problems for determining motion. Different sensor technologies and related motion capture systems are then discussed. It is shown how motion data is derived from position and orientation for the different motion capture technologies. Considering their limitations, we review the wearability challenges of these systems. Their drawbacks will be considered in terms of portability: portable motion capture systems should be less sensitive in accurate positioning of sensors and have more battery life time or less power consumption for their wider adoption as an assisted rehabilitation platform.

2.1. Human body modelling for motion capture

Motion capture attempts to approximate human motion by a rigid-body model with a limited number of rotational degrees of freedom (DOF). A rigid body is an idealization of a solid body of finite size in which deformation is neglected. The degree of freedom of a mechanical system is the number of independent parameters that define its configuration. In motion capture, an articulated figure is often modelled as a set of rigid segments connected by joints which are constraints on the geometric relationship between two adjacent segments.

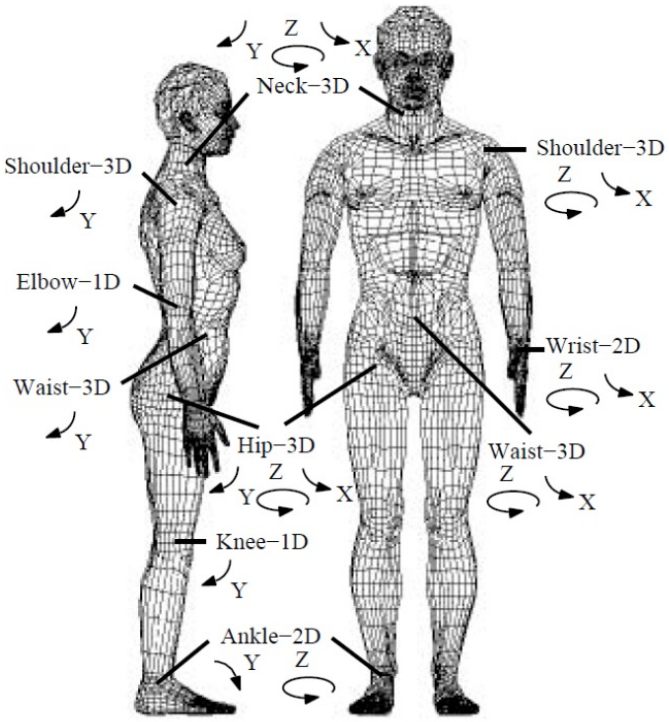

Figure 2.1, The controlled degree of freedom of human model [29]

This relationship is expressed with parameters called joint angles measured in a number of planes. With careful selection of joints so that, for example, segments are connected to form a tree structure, a collection of the joint angles of all the joints corresponds exactly to a configuration of a figure. This correspondence provides an

immediate computer representation of an articulated figure as shown in figure 2.1; it is straightforward to compute the corresponding configuration [25]. Human motion capture techniques may be categorized according to the intended degree of abstraction imposed between the subject and the animated figure. Efforts to accurately represent human motion depend on limiting the degree of abstraction to a feasible minimum. Human body motion modelled by a rigid body model typically is approximated with a limited number of rotational degrees of freedom [26].

The general name for two rigid bodies is a kinematic pair, which can move with respect to each other via a mechanical constraint (joint) between the two bodies, with one or more degrees of freedom. A kinematic chain is the assembly of several kinematic pairs connecting rigid body segments. The process of determining the parameters of a kinematic chain in order to achieve a desired pose is inverse kinematics. Describing body motion without consideration of forces is a branch of classical mechanics.

In general, a rigid body in d dimensions has $d(d + 1)/2$ degrees of freedom, i.e. d translations and $d(d - 1)/2$ rotations. This comes from the following: that rotational freedom is the same as fixing a coordinate frame. The first axis of the new frame is unrestricted, except that it has to have the same scale as the original frame, so it has (d-1) degrees of freedom. The second axis has to be orthogonal to the first, so it has (d-2) DOFs. Proceeding in this way, we get $d(d\text{-}1)/2$ rotational DOFs in d dimensions. In one, two and three dimensions then, we have one, three, and six degrees of freedom.

A non-rigid or deformable body may be thought of as a collection of many particles (infinite number of DOFs); this is often approximated by a finite DOF system. When motion involving large displacements is the main objective of a study, a deformable body may be approximated as a rigid body (or even a particle) in order to simplify the analysis. In three dimensions, the six DOFs of a rigid body are sometimes

described using these nautical names: 1. moving up and down (heaving); 2. moving left and right (swaying); 3. moving forward and backward (surging); 4. tilting forward and backward (pitching); 6. turning left and right (yawing); 6. tilting side to side (rolling) [27].

In motion analysis, modelling techniques determine the positions of bones of the subject or fitting of the skeleton. Depending on which activities are going to be modelled, there are several body segment representations of human motion [28]. Also if we assume that nearly all parts in the human body can move, it means that all movements of the human body are coordinated movements of the joints, and all movements can start independently from any one joint [29]. A local coordinate system is established at the ends of the inboard bone centre, which is located near the body mass centre, for each joint. The movement of the outboard bone is represented as an orientation with respect to this local coordinate system creating a hierarchical structure. All the joints are organized in a hierarchical tree structure with the root node located at the lower back especially in gait analysis [30].

In general, there are two kinds of modelling technique: dependent and independent of sensor or marker placement. In modelling techniques that are dependent on marker placement, marker placement should be precise. In modelling techniques that are independent of marker placement, there is no need for the precise marker set-up, but they require a calibration process, which takes time.

In modelling techniques, which are dependent on marker placement, data may be acquired unilaterally or bilaterally for the calculation of internal joint centres, e.g. for the hip, knee, and ankle joints in case of modelling gait. Their 3D internal rotations can be calculated in addition to the 3D orientations of the pelvis and foot. This process can be done by using a special marker set which includes a pelvic frame, thigh wands and

shank wands. Additional data is required for the calculation of internal joint centres and for the inverse dynamics calculation of joint moments and powers. This can be acquired from subject data and includes subject age and weight, joint widths, and leg-segment data (segment length, mass-ratio, centre-of-mass position, radius of gyration) [24].

Modelling techniques independent from marker placement are decomposed into three stages: partitioning the markers into rigid segment sets, estimating the position of joints, and deriving the corresponding skeleton dimensions respectively [31]. In the first stage it needs to be specified which marker belongs to which segment. This can be done manually by reference to the anatomic skeleton and making associations, or automatically. In the automatic method, an algorithm computes the distances between markers. It selects the biggest sets of markers in which all distance variations between all pairs of markers are under a certain threshold. This condition defines a rigid segment set [31].

The markers that are attached onto adjacent segments theoretically move in a sphere centred on the joint that links the two segments. The position and orientation of a segment in space is completely defined by three points because a segment is modelled as a surface. Afterwards, we can compute the movement of the markers on adjacent segments defined by these markers in the reference model, and we can estimate their centres of rotation. The centres of rotations correspond to the joints. From their position in space we can compute the lengths of the segments as the distances between them. The joint positions are estimated as the centres of rotation weighted by the associated marker weight and the radius of the sphere.

By applying the previously described procedures, the position of a set of joints can be estimated. The next step is to compute the length of each bone in the anatomical skeleton of the subject. One trivial approach is to estimate the length as the average

distance between the estimated joints. A more elaborated one is to compute the length that minimizes the square of deviations. A global adjustment of the lengths can be used that minimizes the distance between the joints of a model and the estimated joints in each frame, adjusting in the same step all the other degrees of freedom of the model.

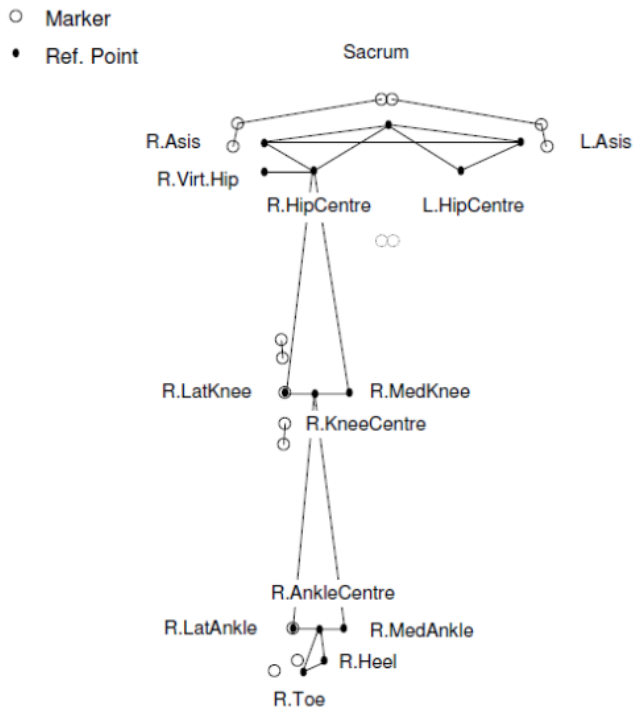

Figure 2.2, Marker position and reference points derived from the marker positions [24].

The geometrical properties of each body segment are derived, generally speaking, from three non-collinear points bearing particular anatomical relationships to the given segment. Body reference points are rigid model anatomical sites calculated from the marker positions in conjunction with information about patient data joint information as shown in figure 2.2. The skeleton of the user is obtained automatically from centre of joints locations, the measured joints' range of motion, and using 3 coordinates of reference points [24].

After determining the position of joints in the human body model, joint angles should be calculated. The problem of finding a set of joint angles is referred to as the

inverse kinematics problem. In solving the inverse kinematics problem, the main concern is finding a set of joint angles that corresponds to a given configuration. We need the angles which the body segments make relative to each other to quantify the movements of the joint which connect them and therefore the human motion of interest. In inverse kinematics we know position of body and we attempt to find angles of joints. Conversely in forward kinematics, we know joint angles of a body and we try to compute the body configuration or position. So motion data is derived from different techniques depending on which sensor technologies are used for body sensing.

2.2. Sensor technologies for motion capture

Body area sensing systems can capture bio-signals like electrocardiogram, blood pressure, body temperature, respiration rate, oxygen saturation, heart rate, skin conductivity, electromyogram, electroencephalogram, and body movement. The sensors can be skin electrodes, temperature probes, piezoelectric sensors, galvanic skin response sensors, pulse oximeters, gyroscopes, and accelerometers [1]. A wearable system may have a wide variety of components other than sensors like wearable components, smart textiles, processing units and advanced algorithms for data extraction and decision making.

There are two categories of sensor technologies for motion capture: visual and non-visual. Visual technologies can be marker-based or markerless, while non-visual tracking sensors are inertial, magnetic, ultrasonic and electromechanical [32], (see figure 2.3). In this section we review these technologies, their advantages and disadvantages and we discuss their potential for wider adoption in home-based rehabilitation systems.

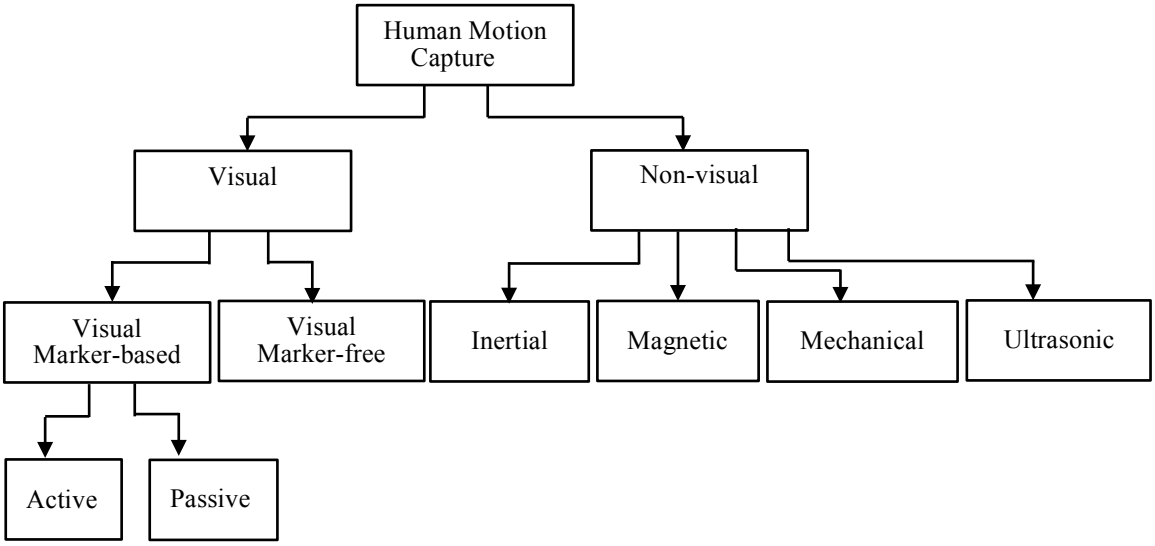

Figure 2.3, Motion capture systems using different sensor technologies

Two classes of visual tracking systems are visual marker-based and marker-free, depending on whether or not sensors or markers need to be attached to body parts. In visual marker-based tracking systems, cameras are applied to track human movements with markers that act as identifiers of the rigid body model landmarks. Marker-based systems are used because of the accuracy of marker position information. They can be active or passive; active marker-based systems use light emitting markers, while passive ones use markers made of reflective material that do not require a power supply. One of the active visual tracking systems is *Codamotion* which is for 3 dimensional (3D) measurements. Its measurements have been commonly used as ground truth to evaluate motion measurements [24]. Although measurements of these systems are highly accurate with position resolution of about 0.05 mm, they need to be performed in a laboratory and cannot be used in home-based rehabilitation.

Passive motion capture systems usually consist of 1–16 cameras, each emitting a beam of infrared light. Small reflective markers are placed on an object to be tracked. Infrared light emitted by the cameras is reflected back and picked up by the cameras.

The system then computes a 3D position of the reflective target, by combining 2D data from several cameras [32]. The two common widely used passive visual motion capture system are *Qualisys* and *VICON*. These systems are designed to be used in virtual and immersive environments, and in medical science. Marker-based tracking systems are more accurate in comparison to other motion capture technologies, although they need precise calibration before each motion capture process and it should be performed in laboratory.

Marker-free systems exploit optical sensors to measure movements of the human body without any sensor on the human body. Human body motion can be tracked by cameras and is mainly concerned with the boundaries or features of human body on the images. Image based systems use computer vision techniques to obtain motion parameters directly from video footage without the use of special markers [33]. By using a proper camera set-up, including a single camera or a distributed-camera configuration, motion capture can be performed. A single camera readily suffers occlusion from a human body, due to its fixed viewing angle. Thus, a distributed-camera strategy is a better option for minimizing such a risk. In comparison to marker-based tracking systems, which are a less restricted to limited degrees of freedom due to mounted markers, marker-less based systems are a less restrictive motion capture technology but still the motion capture process are not convenient to be used in home based rehabilitation as they need camera set-up in the motion capture environment.

Non-visual sensors such as inertial and electromechanical sensors are used in non-visual tracking systems. They enable motion capture without the need for external emitters and cameras. These sensors can be fitted in a garment or attached directly to the body. The advantage of non-visual tracking systems over visual tracking systems is that there can be ambulatory motion tracking, which means motion tracking by a

portable motion tracking system outside the laboratory to capture daily activities, so they are applicable in home-based rehabilitation and there is no need for doing the experiments in special laboratories.

Miniature inertial sensors, which are small, relatively cheap and have low energy consumption, are categorized into accelerometers and gyroscopes. Accelerometers measure acceleration and gyroscopes measure angular velocity. By integration and double integration of gyroscope and accelerometer signals, respectively, one obtains some measure of orientation and position [14]. By knowing the initial position and orientation, we can find sensor orientation and position changes [34]. The position and angle of an inertial sensor cannot be correctly determined, due to the fluctuation of offsets and measurement noise, which lead to integration drift. Therefore designing drift free inertial systems is a challenge. On the other hand, these sensors can be used in home-based rehabilitation as there is no need for cameras to be set up.

Mechanical sensors provide joint angle data to determine body posture. A goniometer is a sensor with attachments to the proximal and distal limb segments that span a joint to be measured. The sensor operates on the assumption that the attachment surfaces move with (track) the midline of the limb segment onto which they are attached and thereby measures the actual angular change at the joint. These devices provide an output voltage proportional to the angular change between the two attachment surfaces. Mechanical sensor accuracy should be carefully evaluated by testing them on individuals of various statures. Attachment and positioning of goniometers present several problems; in addition alignment of the goniometers with body joints is difficult [35] so it needs experts for system set-up in home-based rehabilitation.

Strain and stress sensors have been developed for fabrics from piezo-electric to polyvinylidene fluoride (PVDF) polymer films. These sensors can be integrated within textiles, or securely attached to them. Most are based on the principles that the electrical resistance of the flexible sensor changes during stretching. Many of the developed flexible strain sensors are based on using coated fabric technology [4]. The limitations of these kinds of sensors are their sensitivity to temperature and electromagnetic interference, tensile stiffness and transient output signals, which preclude their use in wearable garments.

Motion capture data such as position and orientation of sensors can be generated from magnetic sensors as well. Magnetic motion tracking systems have been widely used for tracking user movements in virtual reality, due to their size, high sampling rate, and lack of occlusion. One of the common motion tracking systems with electromagnetic sensors is *MotionStar* by *Ascension Technology Corporation*. The system detects the position and orientation of the sensors by the magnetic field (either the Earth's magnetic field or the field generated by a large coil). These systems offer good accuracy with no line of sight problems, so are more applicable for home-based rehabilitation. However, they are expensive, have high power consumption, and are sensitive to the presence of metallic objects in the environment [26].

Acoustic systems collect signals by transmitting and sensing sound waves, where the flight duration of a brief ultrasonic pulse is timed and calculated. These systems are used in medical applications, but have not been used in motion tracking. This is due to the drawbacks such as; (a) the efficiency of an acoustic transducer is proportional to the active surface area, so large devices are desirable; and (b) to improve the detected range, the frequency of ultrasonic waves must be low (e.g. 10 Hz), but this affects system latency in continuous measurement. In addition, acoustic systems require

a line of sight between emitters and receivers [14], which is not suitable in assisted home-based rehabilitation.

For home-based rehabilitation the reviewed sensor technologies have their own advantages and disadvantages. Visual marker-based technologies have high accuracy but they need camera set up in a motion capture environment which is not suitable for home-based rehabilitation. Similarly, magnetic and acoustic systems need transmitters and receivers, which should be set up in the environment. On the other hand, inertial and mechanical sensors do not need external set up in the environment; however they need precise alignment on the subject's body.

2.3. Derivation of motion data from sensors' signals

As explained in Section 2.2, different sensor technologies are used for motion capture. Depending on which of these sensors categories are used, there are different techniques to derive angles of joints on the modelled human body. Some sensor technologies like visual marker, magnetic and ultrasonic based systems derive the position of sensors and other ones like inertial and mechanical systems derive the orientation of sensors. Techniques for motion capture try to solve the inverse kinematics problem to find the angles of joints from position of sensors or to solve the kinematics problem to find the posture of body segments from the position of sensors. In Section 2.3.1 we explain how angles of joints can be derived from sensors' position and orientation.

2.3.1. Deriving motion data from the position of sensors

Motion capture systems which derive position of sensors in space, like optical, magnetic and ultrasound systems use similar techniques to determine the angles of joints and therefore kinematic parameters. As explained in Section 2.1, a skeletal model

is built or adjusted by using a special calibration motion that highlights all the necessary degrees of mobility once per session [36]- [37]. Then the model is used to derive the motion trajectories of all the captured motions. Finally angular data are adjusted to adapt the motion to a virtual character. The process can be described in the following pipeline: calibration and capturing, knowing positions of cameras and markers, skeleton estimation, inverse kinematics processing, and determining the angle of joints.

After installing the cameras, attaching markers to the subject is the second step. To obtain accurate results, markers should be positioned on the subject at specific anatomical locations. The cameras capture the movement of the markers rather than the body to which they are attached. Determining the skeleton of a subject means to find the 3D positions of joints from the 3D marker locations and therefore determine the 3D positions of the bones of the subject.

After deriving the 3D position of segments and joints from marker placements, finding the set of joint angles is the next step. The problem of finding a set of joint angles that corresponds to a given configuration is referred to as the inverse kinematics problem. We need the angles which the body segments make relative to each other to quantify the movements of the joint which connects them. A single marker can represent no more than a single point on a body segment as its motion is tracked. A pair of markers mounted upon a rigid segment presents sufficient information to describe both translational and rotational movement, though not fully, as rotations about axis joining the two markers remain undefined.

The arrangement is typical of a simple stick-figure description of the human form where limb segments are indicated as straight lines between markers placed over joints. Though not very sophisticated, it is obviously far better than representing each

limb segment by a single marker bearing no spatial relationship to markers on adjacent segments.

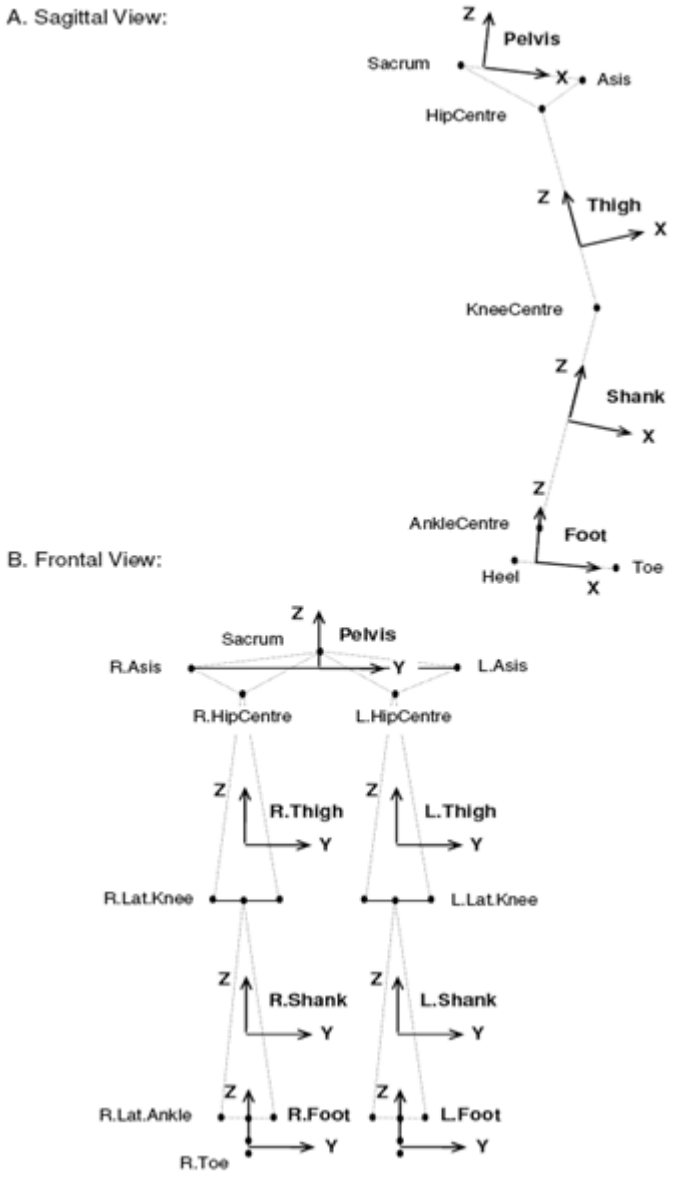

Figure 2.4, Segment embedded coordinate frames for capturing gait [24]

In every case, the dynamic representation of a segment follows from vector reconstructions based on a minimum set of three points. For the pelvis the orientation of the local co-ordinate frame from the available marker set and its reference points using local offsets will be obtained. For the remaining limb segments the reference points will be obtained by vector constructions, then the local co-ordinate frames are derived

from those as shown in figure 2.4. The co-ordinate frames are required for the subsequent calculation of Euler angles. The longitudinal axis of a limb segment usually becomes the local Z axis, the medio-lateral the Y axis, and the antero-posterior the X axis, all mutually orthogonal.

To calculate the angles which the body segments make relative to each other, a rotation matrix is used which describes the orientation of the moving coordinate system on each body segment in comparison to a fixed coordinate system. The rotation matrix will translate movement from the fixed coordinate systems to the moving local coordinate system associated with the signals. This allows the angle between two segments to be calculated. So the rotation matrix between the coordinate systems of a proximal segment and the coordinate system of distal segment relative to the proximal segment can be achieved by producing the corresponding rotation matrix of the two segments coordinates [38].

To calculate the orientation of a segment and its embedded coordinate frame, Euler angles are used. Euler angles are set of angles corresponding to rotations about given axes, usually orthogonal axes. The meaning and validity of the derived anatomical angles are determined by the choice of axes and rotation sequence. In order for limb segment angles to be clinically relevant we can define the orientation of the distal segment relative to the proximal segment by comparing the corresponding axes of the segment-embedded co-ordinate frames [39]. There are many ways of doing this.

Euler angles are readily calculated (requiring no joint centre model), and correspond to relevant axes which are generally orthogonal and therefore kinetically useful. [40]. A single rotation through a given angle about a given (proximal) axis may be represented by a rotation matrix.

Rotation through θ about X axis:

$$\mathbf{R_x} = \begin{bmatrix} 1 & 0 & 0 \\ 0 & \cos\theta & -\sin\theta \\ 0 & \sin\theta & \cos\theta \end{bmatrix} \quad (2\text{-}1)$$

Rotation through Φ about Y axis:

$$\mathbf{R_y} = \begin{bmatrix} \cos\phi & 0 & \sin\phi \\ 0 & 1 & 0 \\ -\sin\phi & 0 & \cos\phi \end{bmatrix} \quad (2\text{-}2)$$

Rotation through Ψ about Z axis:

$$\mathbf{R_z} = \begin{bmatrix} \cos\psi & -\sin\psi & 0 \\ \sin\psi & \cos\psi & 0 \\ 0 & 0 & 1 \end{bmatrix} \quad (2\text{-}3)$$

Non-cummulative matrix multiplication in the order Z,Y,X results in the decomposition matrix,

$$\mathbf{R}_{zyx} = \mathbf{R}_x\mathbf{R}_y\mathbf{R}_z \quad (2\text{-}4)$$

$$\mathbf{R}_{zyx} = \begin{bmatrix} 1 & 0 & 0 \\ 0 & \cos\theta & -\sin\theta \\ 0 & \sin\theta & \cos\theta \end{bmatrix} \times \begin{bmatrix} \cos\phi & 0 & \sin\phi \\ 0 & 1 & 0 \\ -\sin\phi & 0 & \cos\phi \end{bmatrix} \times \begin{bmatrix} \cos\psi & -\sin\psi & 0 \\ \sin\psi & \cos\psi & 0 \\ 0 & 0 & 1 \end{bmatrix}$$

By obtaining the orientation of the local co-ordinate frame, referred to as the Embedded Vector Basis (EVB), Euler angles can be derived. By calculating the Euler angles for lower limbs (from the pelvis down), the following relations apply: hip joint angles: thigh EVB (distal) relative to pelvis EVB (proximal); knee joint angles: shank EVB relative to thigh EVB; ankle joint angles: foot EVB relative to shank EVB; pelvic rotations: pelvis EVB (distal) relative to global laboratory frame (proximal); foot rotations: foot EVB relative to the laboratory frame.

2.3.2. Deriving motion data from the orientation of sensors

Each body segment's orientation and position can be estimated by integrating the gyroscope data and double integrating the accelerometer data in time. By using the calculated orientations of individual body segments and the knowledge of the segment lengths, rotations between segments can be estimated and the position of the segments can be derived under strict assumptions of a linked kinematic chain [41]. This process may have drift because of gyroscope offset, measurement noise, integration and so forth. Although these sensors give some measure of orientation, it is stated in [42]- [43] that inertial sensing cannot be used on its own to estimate relative position and orientation of sensors with respect to each other. The estimation of displacement and relative distances between sensors need to be determined using different methods.

In [14], relative distances between sensors were measured by acoustic signals. In this work each unit consists of inertial sensors and miniature microphones, which are used to record distances between pairs of sensors on the body. These distance measurements reduce the drift in purely inertial systems. The reconstruction algorithm estimates body posture by combining inertial and distance measurements with an extended Kalman filter that incorporates estimation of the body's joint structure and poses.

The filter evaluates the system dynamics to evolve the system state until the next observation, and then uses the observation to improve its estimate of system state. The body structure provides constraints that aid the recovery of its joint configuration, or pose. The pose of an articulated body is specified by the joint angles that describe the configuration of the body joints. By using a single vector to assemble all joint angles in

the body, the forward kinematic equation, which is used to compute the position and orientation of each body segment, can be determined.

Another way of measuring the relative distance between sensors is using magnetic sensors. By combining inertial sensors with magnetic sensors, an ambulatory 6 degrees of freedom human motion tracking system has been designed in [44]. The magnetic system consists of three orthogonal coils with a magnetic field source fixed to the body and 3D magnetic sensors, which measure the fields generated by the source. Based on the measured signals, a processor calculates the relative positions and orientations between the source and sensor. Since accelerometers and gyroscopes can only measure changes in position and orientation and suffer from integration drift, an improved solution for position and orientation estimation is obtainable by combining measurements from both systems in a filtering structure [44] - [45]. In this method a 3D source of magnetic signals is used which can consist of one [42] or three [46]- [47] circular coils that are mounted orthogonally with respect to each other [48].

The MVN motion capture system, which is fully ambulatory and consists of body worn sensors, was introduced in [34]. Body segment orientation and position changes are estimated by integration of gyroscope and accelerometer signals which are continually updated by using a biomechanical model of the human body. Using this method dynamic motion can be tracked as shown in figure 2.5. By facilitating the constraints of the model, the kinematics of body segments is corrected for drift and other errors. To correct rotation errors about the vertical axis a magnetic sensor is used as a heading-aiding sensor in each accelerometer and gyroscope unit worn on each body segment. A patent has been published which shows that heading and, via the calculation of the relative orientation of segments, the 3D orientation of the subject segments

relative to one another can be estimated [49] without requiring a magnetic field as a reference, so there is no need to measure the distance between the sensors.

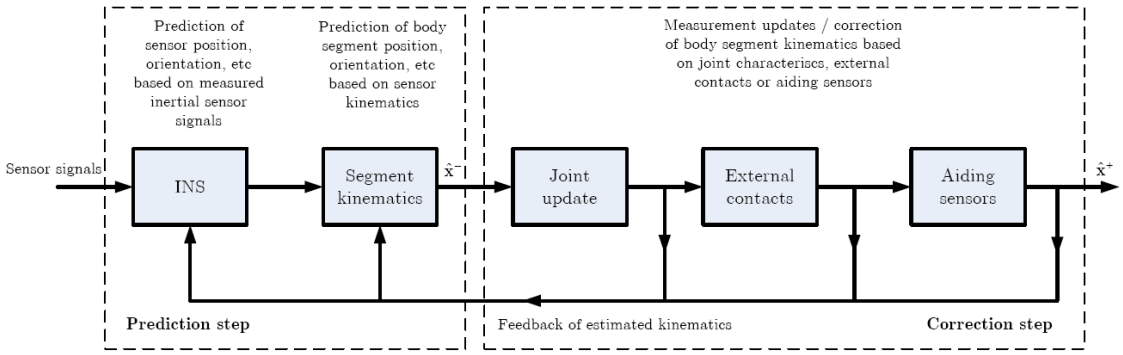

Figure 2.5, Sensor fusion scheme [34].

Since the sensor signals and the biomechanical model can be described in a stochastic manner, in this full ambulatory motion capture system, it can be divided into the sensor fusion scheme with a prediction and correction step. In the prediction step, all sensor signals are processed using so-called inertial navigation system (INS) algorithms. This is followed by the prediction of the segment kinematics using a known sensor to align the real body and a biomechanical model of the body.

The correction step includes updates based on biomechanical characteristics of the human body, notably joints, detection of contact points of the body with an external world which constrains the global position and velocity, and, optionally, other aiding sensors. Estimated kinematics is fed back to the INS algorithms and the segment kinematics step to be used in the next time frame. These kinematics data are translated to body segment kinematics using a biomechanical model which assumes that a subject's body includes body segments linked by joints and that the sensors are attached to the subject's body segments. The sensor fusion scheme calculates the position, velocity, acceleration, orientation, angular velocity and angular acceleration of each body segment with respect to a global (earth-fixed) reference coordinate system.

In a number of other research papers, for example [50] - [51], upper-limb orientation estimation using accelerometers and gyroscopes have been proposed. In [50] the orientation of an upper-limb has been derived by focusing on a design that minimizes the number of sensors. In [51] an upper limb motion estimation method was proposed using three types of micro sensors, namely, a 3D accelerometer, a gyroscope, and a magnetometer, for elbow joint abduction/adduction distortion free motion. They propose a method to model the upper limb skeleton structure as a link structure with 5 DOF. Within the framework of the dynamic system, the forward kinematic equations are derived as the sensor measurements model.

2.4. Activity recognition techniques

In another category of studies, researchers have already prototyped on-body sensors systems with application in wearable computer systems that use acceleration, audio, video, and other sensors to recognize user activity. Activity recognition aims to recognize the actions and goals of a subject from a series of observations of the subject's actions. Sensor-based activity recognition integrates the emerging area of sensor networks with novel data mining and machine learning techniques to model a wide range of human activities. Several algorithms are developed and evaluated to detect physical activities from data acquired using sensors worn simultaneously on different parts of the body.

Accelerometers have been used for gait analysis in [52] to derive gait parameters like cadence, speed, asymmetry and irregularity. Activity recognition of assembly tasks has been introduced in [53] by using microphones and accelerometers. Classification techniques have been used on sound and acceleration signals to perform activity recognition. By using classifiers and five small biaxial accelerometers worn simultaneously on different parts of the body, everyday activities can be recognized

with an overall accuracy of 84% [54]. Recognition of hand movements has been done in [55] using classification techniques and accelerometers worn simultaneously on different parts of the hand.

In [56] a posture recognition system has been introduced as a smart shirt. This smart shirt, which is called SMASH, has a hierarchical architecture which allows the overall system weight to be improved by minimizing weight at the limbs. At the first layer sensor data are acquired and pre-processed by terminals which are distributed in the garment. Features are computed by gateways that fuse sensor data at the second layer. Recognition tasks are performed at the third layer. Results show that exercise postures can be discriminated using acceleration terminals attached to the system. The ability to discriminate postures was enabled by classification using acceleration patterns recorded by the terminals.

A miniature heading reference system, named ETHOS, which uses Xsense off-the-shelf technologies, was introduced in [57]. ETHOS has a unit which contains processing resources consisting of inertial sensors and accelerometers to estimate its orientation online. A Kalman and a complementary filter are used to estimate orientation. Results show that this system functions with sufficient accuracy in estimation of human movement in real-life conditions using an arm rehabilitation robot. In the paper a therapist performs a series of six rehabilitation exercises by guiding the patient's arms, while the robot records the motion path. Subsequently, the subject repeats the motion five times, while the robot supervises and supports the execution.

Wearable systems and algorithms for long term monitoring of physical activity and gait analysis for the estimation of the 3D joint kinematics and kinetics are covered in literature as well. A data logger which holds a 3D accelerometer and gyroscope has been introduced in [58]- [59]. In this study a highly sensitive scheme for the detection

of basic body postures such as sitting, standing, lying, and walking has been proposed. By calculating kinematics features of the body movements during the transitions between different postures, and using statistics and fuzzy classifiers, different body postures can be determined.

In [60] a signal processing technique based on data obtained using a new body area sensor network has been introduced to improve robustness and feature extraction for gait classification. A sensor node which consists of a 3D gyroscope and 3D accelerometer was affixed at the right ankle and subjects were instructed to walk 10 meters. In the study a precise binary classification was executed using artificial neural networks to accurately differentiate between the shuffle gait and normal gait data.

A Support Vector Machine (SVM) classifier has been implemented in [61] to estimate the severity of some movement diseases by using inertial sensor signals. Inertial sensors positioned on the upper and lower limbs were used to gather movement data whilst performing of a series of motor tasks. The accelerometer time series were segmented using a rectangular window randomly positioned through the recording gathered during performance of each motor task. Five different types of features were estimated from the accelerometer data. These features were identified because they were sensitive to changes in the severity of motor impairment and could capture movement characteristics associated with the studied disease.

2.5. Variability in motion data

Variability in movement patterns plays a fundamental role in motion analysis. Inconsistencies due to placement errors of on-body sensors can come from three primary sources: human error in the process of sensor/marker placement, the

measurement system, and the subject under evaluation [62]. Variability is defined by the sum of variances from each independent source [63]. Sensor placement variation among technicians is the largest source of unwanted variability [13]. Inaccurate sensor placement causes measurement variability, which is a key impediment to the wider adoption of home-based assistive rehabilitation. Particular care should be taken to ensure that sweating, rapid movements and the placement of markers on the subject's body during different trials and sessions do not affect sensor/marker positioning specified by the marker placement guidelines.

This issue arises with intelligent textile technologies for applications in wearable computing and health monitoring, smart human–machine interface, and so forth [64]. Silicon flexible skins have been introduced to address flexibility in sensing garments [65]. While such techniques try to develop a new technology for intelligent sensing, in our research we explore techniques that can permit current commercial off-the-shelf technologies to be used more effectively. We devise a signal processing technique as an alternative to smart sensing.

The reliability of measurements is directly affected by the sensor placement during different sessions. If experimental errors conceal important motion deviations, meaningful information will be lost. On the other hand, if the limitations of the motion capture methods are not understood, small deviations may be considered meaningful, thereby leading to over interpolation [66]. Every time that a subject tries to carry out the same movement, a certain amount of variation may be registered between different sessions of marker wearing. Variability between sessions was found to be much higher than within-session variability because of the high probability of differences in the marker placement that arise [63].

Sensor misplacement and consequent anatomical landmark mislocation have a substantial effect on measured joint kinematics and angles. Sensitivity of joint kinematics variables to anatomical landmark misplacement has been reviewed in [67]. Human movement analysis requires the definition of a system of axes; this can be defined from body surface marker positions and anatomical landmark positions [68]-[69]- [70]. One of the main concerns in motion capture is identification of anatomical landmarks and reconstruction of their position in a selected set of axes. Therefore precision and accuracy of determination of landmarks have an influence on joint kinematics variables [71].

In [72] it was shown that there are substantial differences in determining anatomical landmark locations between experts and self-marking operators. In the research they asked the subject under examination to perform anatomical landmark identification and calibration on his/her own body. The study estimated the precision of anatomical landmark identification performed by experts and subjects under experiment. The accuracy of the self-marking procedure provided interesting information. The greater trochanter location was more than 20 mm apart between the two groups of operators, and all pelvic anatomical landmarks were determined with more than 10 mm difference.

In [73] the problem studied was how the errors in estimating the hip joint centre location propagate to the hip and knee kinematics and hence to gait analysis results. It was shown that hip joint centre mislocation of 30 mm in the anterior-posterior direction generates a mean error on the flexion/extension moment of 22% of its value, and hence affects gait analysis results. Angles of hip and knee joints were calculated for five able-bodied subjects during level walking. Angles were calculated after errors in range of

$\pm$ 30 mm were added to the hip joint centre coordinates. It is shown that angles of both hip and knee joints were affected by hip joint centre mislocation.

It is shown in [74] that anatomical landmark position uncertainties result in the observation of physiological knee motions such as the screw-home mechanism even when such motion did not occur. In the study, the motions of two different two-segment mechanical linkages were examined to study the effect of kinematic cross-talk, that is, one joint rotation being interpreted as another. Kinematic cross-talk results from the chosen joint coordinate system being misaligned with the axes about which the rotations are assumed to occur. These uncertainties in motion capture process can lead to erroneous clinical interpretation of the estimation, so they need to be reduced.

Sensitivity of the knee flexion-extension moment patterns to the variation in the estimation of the knee centre location was studied in [75]. Tests were performed on 18 healthy adults who were asked to walk at five different speeds using three different knee centre locations that varied by plus or minus 10 mm in anteropostrerior direction. It is shown that when the magnitudes of the knee moments are less than or equal to the knee centre location variation effect, it was not possible to confidently interpret them as representing either a net flexion or extension of the knee.

Given the clinical relevance of variability in motion capture measurements, it is critical that we summarize and compare motion data in a way that reflects the true nature of motion variability [62]- [76]. To measure variability among gait curves, some distance based measures have been used in literature, including the mean distance from all curves to the mean curve in raw 3-dimensional spatial data [77], the point-by-point intercurve ranges averaged across the gait cycle [78], and the norm of the difference between coordinate vectors representing upper and lower standard deviation curves in a vector space spanned by a polynomial basis [79]. In this thesis to show variability in

motion capture measurements, we use variance and variation terms which are introduced in Chapter 6.

2.6. Energy efficiency

The importance of body sensing systems to monitor patients over a prolonged period of time has increased with an advance of home healthcare applications. Wearable medical devices could eliminate patients' dependence on clinical environments and allow monitoring at home. Body sensing platforms for monitoring of various biological and physiological signals face the challenge of how to achieve low power consumption as well as mentioned sensor placement challenge. The overall size of the electronic part of wearable systems is generally dominated by the size of the batteries. Hence to have less bulky systems, sensors need to operate with low power consumption.

Power management in emerging wearable medical devices, intended to continuously monitor physiological signals, is one of crucial design issues [80]. Sensor nodes need to operate with very low power consumption. In recent years the design trade-off of performance versus power consumption has received much attention because of the large number of mobile systems being developed that need to provide services with the energy releasable by a battery of limited weight and size [81]. Energy-efficient design requires reducing power dissipation in all parts of the system. Typically, an electronic system consists of a hardware platform, and application software.

When considering the hardware platform, we can distinguish three major constituents consuming significant energy: computation units, communication units, and storage units. In body sensing systems the computation unit is usually centralized and far from the human body and signals can be sent via the communication units to the computation unit. Biological and physiological signals are usually saved in the centralized unit which can be connected to sources of power with fewer power

restrictions in comparison to the sensors' batteries. Therefore our focus for energy efficiency is on the communication units. Energy efficiency of the communication units depends on the hardware and the protocols which are used to capture the biological signals and send them to the central computing units.

In the communication units transmission of data in wearable systems can be achieved by communicating the collected signals from the biosensors to the system's central node; or sending aggregated measurements from the wearable system to a remote station. Short-range transmission can be used either by wires or by multiple wireless links. However, the user's mobility and comfort can be impeded by the use of wires, and the risk of system failure in this case is high [5].

Optimising the design of the system to achieve low power consumption has been studied by several research groups [82]- [83]. Resource management based on runtime estimation of memory, storage, hardware, and bandwidth is required to achieve low-power performance. Techniques in algorithm development, communications, hardware architecture and circuit design to achieve the necessary power saving are described in [84]. In [85] a low power transceiver has been described for wearable medical healthcare systems. A power management microsystem for body sensing composed of a rectifier as a regulator has been presented in [86].

In [87] power reduction is achieved by introducing rest and common mode feedback circuit techniques while the system is switched between different operational modes like *sleep*, *low power* and *high resolution*. In [88] system level energy power optimization techniques have been used on a body sensing system powered by solar cells using energy harvesting. Harvesting of energy from the environment like solar power, thermal energy, energy from human movement has been reviewed in [89]. It is

important for body sensing systems to achieve both low power consumption and small size without jeopardizing performance and reliability.

Communication technologies have a significant effect on energy efficiency of ambulatory body sensing systems [90]. Cooperative communication as a power allocation strategy to minimize energy consumption in body area networks has been investigated in [91]. A flexible protocol that offers better performance and energy saving has been introduced in [92]. Using body channel communication that is using the human body as a signal transmission medium, energy consumption can be reduced, increasing energy efficiency of body sensing systems [93].

Changing the sampling rate has already been used as a technique for reducing power consumption. Adaptive sampling is established as a practical method to reduce the sample data volume and thus increase energy efficiency [94]. In [95] a low-power analogue system is proposed, which adjusts the converter clock rate to perform a peak-picking algorithm on the second derivative of the input signal. The presented circuit contains only basic circuit blocks, allowing for a low-power and small-size implementation that can ultimately be integrated as a part of a body-area network sensor.

A context aware sensing scheme known as episodic sampling for wearable sensor technologies was introduced in [96]. It requires a trade-off between energy reduction and accuracy of the system. The effect of the reduction in sampling rate for a wearable posture recognition system was studied in [97]. The results showed that performance of posture classification was insensitive to a reduction in sampling rate from 100Hz to 10 Hz for inertial sensors. A power efficient biomedical acquisition portable system using variable resolution with a sigma delta modulator for converting analogue signals to digital was introduced in [98].

Decreasing the sampling rate combined with decomposition techniques is another way of achieving power savings [99]- [100]. Compressive sampling (CS) has great potential for low power pulse rate detection, since by reducing data sampling rate, less energy is consumed. Compressive sampling is an emerging technology, known as a novel sensing paradigm that goes against the common wisdom in data acquisition. It asserts that one can recover certain signals from far fewer samples or measurements than traditional methods. This technique helps to save more power by reducing the power consumption [101]. The CS protocol samples data at a low rate and later uses computational power for reconstruction. Obviously the higher the CS rate, the lower the power consumption and the greater the measurement inaccuracies.

Compressive sampling, also known as compressed sensing, is a simple and efficient signal acquisition protocol which samples - in a signal independent fashion - at a low rate and uses computational power for reconstruction from what appears to be an incomplete set of measurements [102]. CS relies on the two basic principles: sparsity and incoherence. Sparsity expresses the idea that the information rate of a continuous time signal maybe much smaller than suggested by its bandwidth, or that a discrete time signal depends on a number of degrees of freedom which is comparably much smaller than its finite-length. Incoherence extends the duality between time and frequency and expresses the idea that objects that have a sparse representation must be spread out in the domain in which they are acquired.

Common approaches to sampling signals or images follow Shannon's theorem. The sampling rate must be at least twice the maximum frequency present in the signal, which is called Nyquist rate. This principle underlies nearly all signal acquisition protocols used in consumer audio and visual electronics, medical imaging devices, radio receivers, and so on. For some signals, such as images that are not naturally band-

limited, the sampling rate is dictated not by the Shannon theorem but by the desired temporal or spatial resolution. However, it is common in such systems to use an antialiasing low-pass filter to band-limit the signal before sampling, and so Shannon's theorem plays an implicit role [103]- [104].

What is most remarkable about these sampling protocols is that they allow a sensor to very efficiently capture the information in a sparse signal without trying to comprehend that signal. Further, there is a way to use numerical optimization to reconstruct the full-length signal from the small amount of collected data [105].

2.7. Summary

In this chapter after introducing human body modelling for motion capture, we reviewed sensor technologies for motion capture, and techniques to derive motion data. Motion capture systems are sensitive to exact positioning of sensors, or alternatively need a calibration procedure which is time consuming and requires training. For ambulatory motion capture and especially home-based rehabilitation, systems should be portable. Two important requirements of portable motion capture systems are tolerance to changes in the position of sensors and extended system life. Therefore, we reviewed causes and effects of variability in motion pattern, and energy efficiency of on-body sensing systems. The focus of the thesis is to solve these two issues. We explore a number of signal processing techniques that may lend themselves to overcoming these challenges.

3. Background Theory of Filtering Techniques and Signal Decomposition

Removal of undesirable signals from a superposition of source signals is one of the challenges in signal processing. Filtering strategies for suppression of unwanted source signals have traditionally involved a linear decomposition of signals. The approach is to re-express the original data along a new coordinate system such that the signal of interest can be separated from other sources in the original data while projecting along different bases. By keeping the bases describing the signal of interest and rejecting the rest, filtering can be achieved. Depending on the means by which the bases are determined, these methods can be classified into *a priori* and adaptive categories.

In *a priori* approaches the bases are defined independently of the data, like frequency based finite impulse response (FIR) or infinite impulse response (IIR) filters. Discrete Fourier transform (DFT) filtering has been widely used in clutter rejection [106]- [107]. Although DFT-based methods have been widely used, they underperform when the frequency characteristics of the unwanted signal and the signal of interest overlap. To overcome this challenge adaptive frameworks for determining basis functions have been introduced. In adaptive approaches the bases are determined adaptively from the data. ICA (Independent Component Analysis), PCA (Principal Component Analysis) and SVF (Singular Value Filter) based signal separation methods

are in the category of adaptive filtering. In these techniques the basis functions are determined adaptively from the statistical properties of the data.

The basic principles of signal decomposition can be described by first considering an observed signal, represented discretely as a row vector $\mathbf{x}$ (dim 1×*N*), which can be decomposed into a weighted sum of orthonormal basis functions,

$$\mathbf{x} = \sum_{k=1}^{N} \gamma_k \mathbf{v}_k \tag{3-1}$$

where γ_k are weighting coefficients for each of *N* orthonormal basis functions $\mathbf{v}_k$. Coefficients can be expressed as the dot product between the observed signal and each orthonormal basis vector $\gamma_k = \mathbf{x}.\mathbf{v}_k{}'$ where $\mathbf{v}_k{}'$ is the conjugate transpose of $\mathbf{v}_k$. The basis functions can be any set of vectors provided that they are mutually orthonormal.

$$\mathbf{v}_l.\mathbf{v}_k{}' = \begin{cases} 1, & \text{for} \quad l = k \\ 0, & \text{for} \quad l \neq k \end{cases} \tag{3-2}$$

The mutually orthonormal basis functions $\mathbf{v}_k$ used for linear transformation of the data can be determined either *a priori* or adaptively from the signal itself. The Fourier Transform is an example of linear signal decomposition where basis functions are defined *a priori* such that $\mathbf{v}_k$ are a set of complex exponentials of different frequencies. In adaptive methods, the set of basis functions can be formed adaptively as polynomials.

In this chapter, we review finite impulse response and infinite impulse response filters as *a priori* signal decomposition methods. Then, we study adaptive signal separation methods like principal component analysis, independent component analysis, and singular value based filtering techniques. We apply these signal separation techniques to captured sets of motion data, and compare them to the one we introduced in the next chapter.

3.1. A priori signal decomposition

The most common *a priori* filtering approach, where the bases are defined independently of the data, is discrete Fourier transform-based filters. DFT-based filtering has been widely used in signal decomposition literature [108]- [109]- [110]. To review the technique briefly, we consider a discrete time system. A discrete time system takes an input, $\mathbf{x}=[\mathrm{x}(0),\mathrm{x}(1),\dots,\mathrm{x}(N-1)]^T$, and produces an output, $\mathbf{y}=[\mathrm{y}(0),\mathrm{y}(1),\dots,\mathrm{y}(M-1)]^T$. A general linear filtering operation can be expressed by the matrix multiplication, $\mathbf{y} = \mathbf{A}\mathbf{x}$ where $\mathbf{A}$ is an $M \times N$ matrix. With the matrix element in row n and column k denoted by $a(n,k)$, the elements of output vector are given by equation (3-3).

$$y(n) = \sum_{k=0}^{N-1} a(n,k)x(k), \quad n = 0,\dots,M-1 \tag{3-3}$$

The parameters describing the frequency response of a filter are the stop-band cut-off frequency, ω_s, and pass-band cut-off frequency, ω_p. The deviation from zero in the stop-band is given by d_s, which should be as small as possible . In the pass-band, all of the frequencies should be passed through unaltered, which means that the ripple, d_p, should be minimized. Finally, the pass-band cut-off frequency, ω_p , should be as close as possible to the stop-band cut-off frequency, ω_s, to obtain a more ideal filter response. Finite impulse response and infinite impulse response filters are two key methods of signal separation in the *a priori* category, discussed next.

3.1.1. Finite impulse response filters

Digital filters with a finite duration impulse response (FIR) are also called non-recursive filters or convolutional filters. These filters are sometimes called moving

average filters from the time domain viewpoint. The impulse response duration of these filters is finite; therefore the output can be written as a finite convolution. The output of a $(K-1)^{th}$ order FIR filter can be written as the finite convolution sum;

$$y(n) = \sum_{k=0}^{k-1} h(k)x(n-k) = \sum_{k=n-K+1}^{n} h(n-k)x(k). \tag{3-4}$$

With input vector size *N*, and filter order *K*−1, the number of valid output samples is *N*−*K*−1. It can be shown that for FIR filters, the frequency response becomes $H_0(\omega) = |H(\omega)|^2$, where $H(\omega)$ is the Fourier transform of the impulse response *h*(*n*). FIR filters can be categorised as linear phase and minimum phase filters.

The frequency response of FIR linear phase filters is written as equation (3-5):

$$H(\omega) = G(\omega)e^{j(k_1+k_2\omega)} \tag{3-5}$$

where $G(\omega)$ is a real function and k_1 and k_2 are constants. The advantage of linear phase is that in the pass-band, the frequency response is $H(\omega) \approx G(\omega)e^{j(k_1+k_2\omega)}$. For a signal *x*(*n*) consisting only of frequencies in the pass-band of the filter, the spectrum of the filtered signal is $Y(\omega) \approx X(\omega)e^{j(k_1+k_2\omega)}$. This is just a constant phase shift, and the time delay of the input signal and the waveform is not distorted. A FIR filter with real coefficients has linear phase if the impulse response satisfies the symmetry constraint, $h(n) = \pm h\,(K-n-1)$.

Linear phase imposes a symmetry constraint on the impulse response. Without any phase constraints, the required order to obtain a specified amplitude response is reduced. For the case where only the amplitude response is considered, many filters with the optimum amplitude response but different phase responses exist. Among these filters, the minimum phase filter has all of the zeros inside the unit circle and has the smallest time delay. The minimum phase filter also maximizes the partial energy

$E(n) = \sum_{k=0}^{n} |h(k)|^2$ of the impulse response and, therefore, has the most asymmetric impulse response.

3.1.2. Infinite impulse response filters

A *K*th-order IIR filter is described by the difference equation:

$$y(n) = -\sum_{k=1}^{K} a_k\, y\,(n-k) + \sum_{k=0}^{K} b_k\; x(n-k) \tag{3-6}$$

where we see that each output sample depends on present and past input samples, as well as past output samples. The recursive part of the filter causes the response to an impulse input to endure forever and is the reason why such filters are called IIR filters. There are many techniques for designing IIR filters based on the steady-state magnitude response. The most common IIR filters are Butterworth, Chebyshev type I and II, and Elliptic filters. With an input signal of finite length, the transient response becomes important. The Butterworth filter has the smallest transient because among the three filter types, Butterworth filters have poles with the smallest magnitude. Butterworth filters have a wider transition region than the other filters, and there is a trade-off between transient duration and magnitude response.

As discussed in section 3.1.1 a FIR filter can have exactly linear phase. In other words, the group delay of the filter can be constant. This linear-phase property results from the symmetry of the unit-pulse response of the filter. An IIR filter has an infinite duration unit-pulse response that cannot be symmetric if it is causal. Therefore an IIR filter cannot have exactly linear phase. The required filter length *N* increases when sharp transitions between frequency bands are specified and/or large attenuation are required in the stop band. High performance linear phase filters with sharp cut-offs and

large attenuation are necessarily long and have large, though constant, delays and a large number of coefficients to be stored.

When constant delay is not required for all frequencies, better FIR filters can be designed. When the group delay is of little concern, the minimum phase FIR filters may be a good choice. An IIR filter can generally achieve a sharper transition between band edges than an FIR filter can with the same number of coefficients. Implementation of IIR filters with a recursive realization in fixed-point arithmetic is much more difficult than the direct, non-recursive implementation of an FIR filter. An IIR filter has an advantage over an FIR filter in that it generally has fewer coefficients than an FIR filter with similar magnitude characteristics, so less memory is required to store the coefficients [111].

3.2. Adaptive signal decomposition

The reviewed filtering techniques in previous part fail to achieve a signal separation when there is overlap in the frequency characteristics of the undesirable signal and the signal of interest. Moreover, the signals may change through space and time, so adaptive frameworks for determining basis functions have been proposed in filtering techniques. Common adaptive frameworks for determining basis functions are Independent Component Analysis, Principal Component Analysis, and Singular Value Filter.

Blind source separation, BSS, is a method for recovering unobserved signals or sources from several realizations of their mixture. No prior information about the signals or their combination is employed to separate the sources. Instead, BSS assumes statistical relationships between the sources, that is, assuming different physical processes generate signals with predictable relationships [112].

As BSS filters employ no prior information regarding the signals themselves, they are widely applicable to many signal structures along all dimensions. The assumed source signal statistics plays a significant role in the overall ability of BSS to separate source signals thoroughly. One approach, known as principal component analysis (PCA), assumes that the source signals are orthogonal [113]. Another method, which assumes that the source signals are independent and non-Gaussian-distributed, is known as independent components analysis (ICA) [112].

BSS-based filtering is performed by adaptively selecting either orthogonal or independent basis functions corresponding to source signals of interest. If the signal of interest is to be removed from the data, the input data matrix is projected onto the complement of the predicted signal subspace [114]. If the signal of interest is to be retained and extracted from the other signals, the input data matrix is projected onto the basis functions selected to span the desired signal subspace [115].

Independent component analysis, ICA, based filtering techniques separate unwanted sources of variation from the desired signal by maximizing the entropy of the data transformed linearly into the ICA component axes. In principal component analysis, PCA, the basis functions are determined adaptively from the covariance properties of the data. PCA finds orthogonal directions of greatest variance in the data, whereas ICA component maps may be non-orthogonal. The singular value filter, SVF, differs from PCA based approaches by incorporating a weighting function that computes non-binary filter coefficients adaptively from information contained in the singular value spectrum.

3.2.1. Independent component analysis for source separation

Independent component analysis is a linear transformation that captures the essential structure of the data in the observed signal. The goal is to find a linear

representation of non-Gaussian data so that the components are statistically independent. ICA, which is another form of BSS, is based on the assumption that source signals are not only uncorrelated but also mutually independent. ICA basis functions are extracted by maximizing the entropy in the joint probability density functions (pdf) of the basis vectors. The decomposition is then whitened, meaning that each basis function is magnitude-normalized.

ICA can achieve superior signal separation to PCA if the underlying source signals are statistically independent and non-Gaussian [112]. If, however, the source signals are not independent, ICA may not offer significant advantages over PCA for BSS-based adaptive filtering. For example, in noise filtering applications, jitter and other noise signal components are likely to be independent of the desired signals; an independent decomposition may be appropriate for BSS noise filtering [116]. A non-independent decomposition may be suitable for separating unwanted and desired signals in other cases.

Independent Component Analysis can be used to estimate the mixing coefficients, a_{ij}, based on the information of their independence, which allows separation of the original source signals $s_1(t)$, … ,$s_n(t)$ from their mixtures $x_1(t)$, … , $x_n(t)$ where parameters a_{ij} are mixing coefficients.

$$x_j = a_{j1}s_1 + a_{j2}s_2 + \cdots + a_{jn}s_n \qquad \text{for all } j \tag{3-7}$$

It is assumed that each mixture x_j , as well as each independent component s_k, is a random variable. We represent the model by **x**, a random vector whose elements are the mixtures $x_1(t)$, … , $x_n(t)$, and likewise by **s**, a random vector with elements $s_1(t)$, … ,$s_n(t)$ and by **A**, the matrix with elements a_{ij}. Using this vector–matrix

notation, the above mixing model is written as **x** = **As.** Sometimes we need the columns of matrix **A**; denoting them by a_j the model can also be written as equation (3-8).

$$\mathbf{x} = \sum_{i=1}^{n} \mathbf{a}_i \, s_i \tag{3-8}$$

For estimating the mixing matrix **A**, it is assumed that the components s_i are statistically independent and the independent components must have non-Gaussian distributions. Then, after estimating the matrix **A**, we can compute its inverse, say **W**, and obtain the independent component simply by **s** = **Wx.** By using the technique sources of variation can be separated, so in filtering application the unwanted source of variation can be removed from the signal.

The meaning of independence can be summarized as follows. Variables y_1 and y_2 are said to be independent if information on the value of y_1 does not give any information on the value of y_2, and vice versa. For ICA this is the case with the variables s_1 and s_2. Technically, independence can be defined by the probability densities. We define that y_1 and y_2 are independent if and only if the joint pdf is factorizable in the following way: $p\,(y_1, y_2) = p\,(y_1)p\,(y_2)$. This definition extends naturally for any number *n* of random variables, in which case the joint density must be a product of *n* terms. For independent random variables, given two functions, h_1 and h_2, we always have $E\,\{h_1(y_1)h_2(y_2)\} = E\,\{h_1(y_1)\}E\,\{h_2(y_2)\}$.

A weaker form of independence is uncorrelatedness. Two random variables y_1 and y_2 are said to be uncorrelated, if the following quality exists between the expected values: $E\,\{y_1y_2\}$-$E\,\{y_1\}E\,\{y_2\} = 0$. If the variables are independent, they are uncorrelated. On the other hand, uncorrelatedness does not imply independence. Since independence indicates uncorrelatedness, many ICA methods constrain the estimation

procedure so that it always gives uncorrelated estimates of the independent components. This reduces the number of free parameters, and simplifies the problem.

The important restriction in ICA is that the independent components must be non-Gaussian for ICA to be possible. In the Gaussian case the density is completely symmetric. Therefore, it does not contain any information on the directions of the columns of the mixing matrix **A**. This is why **A** cannot be estimated in this case. Intuitively speaking, the key to estimating the ICA model is non-Gaussianity. Actually, without non-Gaussianity the estimation is not possible at all [117].

The Central Limit Theorem, a classical result in probability theory, states that the distribution of a sum of independent random variables tends towards a Gaussian distribution, under certain conditions. Thus, a sum of two independent random variables usually has a distribution that is closer to Gaussian than any of the two original random variables. To estimate data vector **x** using ICA, we assume that it is a mixture of independent components, and the components have identical distributions. To estimate one of the independent components, a linear combination of the x_i is considered; we denote this by $y = \mathbf{w}^{\mathrm{T}}\mathbf{x} = \sum_i w_i x_i$, where **w** is a vector to be determined. If **w** were one of the rows of the inverse of **A**, this linear combination would actually be equal to one of the independent components [118].

It is possible to find an estimator that gives a good approximation for the ICA transform. It stems from the basic principle of ICA estimation by a change of variables, defining $\mathbf{z} = \mathbf{A}^{\mathrm{T}}\mathbf{w}$. Then we have $y = \mathbf{w}^{\mathrm{T}}\mathbf{x} = \mathbf{w}^{\mathrm{T}}\mathbf{A}\mathbf{s} = \mathbf{z}^{\mathrm{T}}\mathbf{s}$. Thus, the variable y is a linear combination of s_i, with weights given by z_i. Since a sum of even only two independent random variables is more Gaussian than any of the original variables, $\mathbf{z}^{\mathrm{T}}\mathbf{s}$ is more Gaussian than any of the s_i and becomes least Gaussian when it in fact equals one of the s_i. In this case, obviously only one of the elements z_i of **z** is non-zero.

Therefore, we could take as **w** a vector that maximizes the non-Gaussianity of $\mathbf{w}^{\mathrm{T}}\mathbf{x}$. Such a vector would necessarily correspond (in the transformed coordinate system) to a **z** which has only one non-zero component. This means that $\mathbf{w}^{\mathrm{T}}\,\mathbf{x} = \mathbf{z}^{\mathrm{T}}\,\mathbf{s}$ equals one of the independent components.

Another approach for ICA estimation inspired by information theory is minimization of mutual information. Using the concept of differential entropy, the mutual information I between m (scalar) random variables, y_i, i = 1,..., m is defined as equation (3-9):

$$I(y_1, y_2, \ldots, y_m) = \sum_{i=1}^{m} H(y_i) - H(y). \qquad (3\text{-}9)$$

Entropy H is the basic concept of information theory. The entropy of a random variable can be interpreted as the degree of information that an observation of the variable provides [119]. The more "random", i.e. unpredictable and unstructured the variable is, the larger its entropy. Entropy H is defined for a discrete random variable Y as follows, where the a_i are the possible values of Y;

$$H(Y) = -\sum_i P(Y = a_i) \log P(Y = a_i) \qquad (3\text{-}10)$$

Mutual information is a natural measure of the dependence between random variables. In fact, it is equivalent to the divergence between the joint density $f(\mathbf{y})$ and the product of its marginal densities; a very natural measure of independence. It is always nonnegative, and zero if and only if the variables are statistically independent. Thus, mutual information takes into account the whole dependence structure of the variables, and not only the covariance, like PCA and related methods.

To obtain a measure of non-Gaussianity that is zero for a Gaussian variable and always non-negative, one often uses a slightly modified version of the definition of differential entropy, called negentropy. Negentropy J is defined as $J(y) = H\left(y_{\mathrm{gauss}}\right) - H(y)$ where y_{gauss} is a Gaussian random variable of the same

covariance matrix as y. In this approach, the ICA of a random vector **x** is defined as an invertible transformation, where the matrix **W** is determined such that the mutual information of the transformed components s_i is minimized. Finding an invertible transformation **W** that minimizes the mutual information is roughly equivalent to finding directions in which the negentropy is maximized [120].

3.2.2. Principal component analysis for source separation

Principal component analysis (PCA) and the closely related Karhunen-Loeve transform are classic techniques in statistical data analysis and feature extraction. PCA is one of the most valuable techniques resulting from applied linear algebra. In multivariate measurement analysis the goal is to find a smaller set of variables with less redundancy that gives as good a representation of the original set as possible [121]. The goal is related to the goal of ICA, that is source separation. However in PCA the redundancy is measured by correlation between data elements, unlike in ICA, where a much richer concept of independence is used and the reduction in the number of variables is given less emphasises. Using only the correlations, as in PCA, has the benefit that analysis can be used on second order statistics alone and so it results in less complexity.

To perform PCA, the Karhunen–Loeve (KL) transform can be employed to decompose the input data matrix into its orthogonal basis functions with a corresponding energy signature. In this manner, the KL transform is to PCA what the Fourier transform is to spectral analysis. The KL expansion illustrates that a complex random process can be fully described by the eigenvalues and associated orthonormal eigenvectors of its autocorrelation matrix [122]. Further, an approximate expansion of

the data can be achieved by using only a subset of the eigenvalues and associated eigenvectors.

Although PCA may be useful for certain filtering applications like in [123], its general utility for adaptive regression filtering is limited. This limitation arises because orthogonality indicates that the basis functions are uncorrelated, but does not necessarily imply that the functions are statistically independent. Orthogonal basis functions are independent only if the functions are Gaussian or otherwise distributed random variables for which the second and higher order moments are zero [113]. If an orthogonal decomposition is performed, the resulting basis functions may be orthogonal but not mutually statistically independent. As a result, multiple independent source signals may project onto the same orthogonal basis vector, leading to incomplete source signal separation that makes filtering via projection operations difficult.

Considering the random vector $\mathbf{x}$ with n elements and available samples $\mathbf{x}(1), \ldots, \mathbf{x}(T)$ from this random vector, there is no explicit assumption on the probability density of the vectors in PCA as long as the first and second order statistics are known or can be estimated from the samples [124]. In PCA transformation the vector $\mathbf{x}$ is first centred by subtracting its means. Next, $\mathbf{x}$ is linearly transformed to another vector $\mathbf{y}$ with m elements, where $m < n$, so that the redundancy induced by correlations is removed. This is done by finding a rotated orthogonal coordinate system such that the elements of $\mathbf{x}$ in the new coordinate system become uncorrelated. At the same time, the variances of the projections of $\mathbf{x}$ on the new coordinate axes are maximized so that the first axis corresponds to the maximum variance, the second axis to the maximum variance in the direction orthogonal to the first axis, and so on. The PCA transformation can be achieved by either variance maximization or by minimum mean-square error compression.

Variance maximization: Consider a linear combination $y_1=\sum_{k=1}^{n} \omega_{k1}\, x_k= \boldsymbol{\omega}_1^T\, \mathbf{x}$ of the elements $x_1, \ldots, x_n$ of the vector **x**. The $\omega_{11}, \ldots, \omega_{n1}$ are scalar coefficients, or weights, of an *n*-dimensional vector $\boldsymbol{\omega}_1$ and $\boldsymbol{\omega}_1^T$ denotes the transpose of $\boldsymbol{\omega}_1$. The factor y_1 is called the first principal component of **x,** if the variance of y_1 is maximally large. Because the variance depends on both the norm and orientation of the weight vector $\boldsymbol{\omega}_1$ and grows without limits as the norm grows, it imposes the constraint that the norm of $\boldsymbol{\omega}_1$ is constant, in practice equal to 1. Thus we look for a weight vector $\boldsymbol{\omega}_1$ maximizing the PCA criterion

$$J_1^{PCA}(\boldsymbol{\omega}_1) = \mathrm{E}\{y_1^2\} = \mathrm{E}\{(\boldsymbol{\omega}_1^T\mathbf{x})^2\} = \boldsymbol{\omega}_1^T\, \mathrm{E}\{\mathbf{x}\mathbf{x}^T\}\boldsymbol{\omega}_1 = \boldsymbol{\omega}_1^T\, \mathbf{C}_\mathrm{x}\, \boldsymbol{\omega}_1 \qquad (3\text{-}11)$$

such that $\|\boldsymbol{\omega}_1\| = 1$

The norm of $\boldsymbol{\omega}_1$ is the usual Euclidean norm defined as $\|\boldsymbol{\omega}_1\| = (\boldsymbol{\omega}_1^T\boldsymbol{\omega}_1)^2$. The matrix $\mathbf{C}_\mathrm{x}$ is the $n \times n$ covariance matrix of **x** given for the zero mean vector **x** by the correlation matrix $\mathbf{C}_\mathrm{x} = \mathrm{E}\{\mathbf{x}\mathbf{x}^T\}$.

It is well known from basic linear algebra that the solution to the PCA problem is given in terms of the unit length eigenvectors $\boldsymbol{e}_1, \ldots, \boldsymbol{e}_n$ of the matrix $\mathbf{C}_\mathrm{x}$. The ordering of the eigenvectors is such that the corresponding eigenvalues $\lambda_1, \ldots, \lambda_{1_n}$ satisfy $\lambda_{1_1} \geq \ldots \geq \lambda_{1_n}$. The solution for the maximization problem is $\boldsymbol{\omega}_k = \boldsymbol{e}_k$.

Following the variance framework, a simpler and widely used approach to compute basis functions involves performing eigenvalue decomposition (EVD) on the autocorrelation matrix,

$$\mathbf{R} = \mathbf{X}'\,\mathbf{X} = \mathbf{V}\,\boldsymbol{\Lambda}\,\boldsymbol{V}' \qquad (3\text{-}12)$$

where the matrix $\boldsymbol{\Lambda}$ is a diagonal matrix with the *k*th entry being the *k*th eigenvalue. Eigenvalues are positive and real, and they are typically arranged in order of descending

value. For each eigenvalue, there is an associated eigenvector, which is contained in the columns of $\mathbf{V}$. These eigenvectors correspond to the PCA basis functions. The *k*th associated eigenvalue is proportional to the amount of variance accounted for by the *k*th eigenvector $\lambda_k = \left\|\mathbf{X}\,\mathbf{v}_{\boldsymbol{k}}'\right\|^2$.

An alternative method to eigenvalue decomposition is to perform a singular value decomposition (SVD), which finds the PCA basis functions and avoids computation of the autocorrelation matrix [125]. The SVD of $\mathbf{X} = \mathbf{U}\,\sum\mathbf{V}'$ is where columns of $\mathbf{U}$ are the singular vectors corresponding to the eigenvectors of $\mathbf{X}\,\mathbf{X}'$ and $\sum$ is a diagonal matrix of singular values σ_k with singular values arranged in order of descending value [126].

Minimum mean-square error compression: The principal components are defined as weighted sums of the element **x** with maximal variance, under the constraints that the weights are normalized and the principal components are uncorrelated with each other. It turns out that this is strongly related to minimum mean-square error compression of **x**, which is another way to pose the PCA problem [127]. In this approach we search for a set of *m* orthonormal basis vectors, spanning an *m*-dimensional subspace, such that the mean square error between **x** and its projection on the subspace is minimal. The mean square error to be minimized by the orthonormal basis $\boldsymbol{\omega}_1, \ldots, \boldsymbol{\omega}_m$ becomes as equation (3-13).

$$J_{MSE}^{PCA} = E\{||\left(\mathbf{x} - \sum_{i=1}^{m}(\boldsymbol{\omega}_i^T\mathbf{x})\,\boldsymbol{\omega}_i\right)||^2\} \tag{3-13}$$

Due to orthogonally of the vectors $\boldsymbol{\omega}_i$, this criterion can be further written as

$$J_{MSE}^{PCA} = E\left\{\left|\left|\mathbf{x}\right|\right|^2\right\} - E\left\{\left|\left|\sum_{j=1}^{m}(\boldsymbol{\omega}_i^T\mathbf{x})\,\boldsymbol{\omega}_i\right|\right|^2\right\} = \text{trace}\,(\mathbf{C}_\text{x}) - \sum_{j=1}^{m}\boldsymbol{\omega}_j^T\mathbf{C}_\text{x}\;\boldsymbol{\omega}_j. \tag{3-14}$$

It can be shown that the minimum of it under the orthonormality condition on the $\boldsymbol{\omega}_i$ is given by any orthonormal basis of the PCA subspace spanned by the *m* first eigenvectors $\boldsymbol{e}_1, \ldots, \boldsymbol{e}_m$.

As the principal component basis vectors $\boldsymbol{\omega}_i$ are eigenvectors $\boldsymbol{e}_i$ of $\mathbf{C}_\mathrm{x}$, it follows that

$$\mathrm{E}\{y_m^2\} = \mathrm{E}\{\mathbf{e}_m^T\, \mathbf{x}\mathbf{x}^T\, \mathbf{e}_m\} = \mathbf{e}_m^T\, \mathbf{C}_\mathrm{x}\, \mathbf{e}_m = d_m \,. \tag{3-15}$$

The variance of the principal components are thus directly given by the eigenvalues of $\mathbf{C}_\mathrm{x}$. Note that because the principal components have zero means, a small eigenvalue (a small variance) d_m indicates that the value of the corresponding principal component is mostly close to zero [120].

Following decomposition of the signal along a new set of basis functions, PCA-based filtering can be achieved by assigning weights to each basis function

$$\boldsymbol{y} = \sum_{\boldsymbol{k=1}}^{\boldsymbol{N}} \omega_k \gamma_k \mathbf{v}_{\boldsymbol{k}} \tag{3-16}$$

where $\boldsymbol{y}$ is the filtered output signal with the same dimensions as *x*.

In PCA-based filtering approaches, the weights are defined *a priori* based on the assumed relative amount of variance accounted for by the desired source signal. This procedure entails rejecting a number of basis functions on the assumption that unwanted source of variation has a higher or lower variance in the data. While this *a priori* strategy for defining weighting coefficients parallels standard DFT filtering design, it can be inadequate in PCA based methods since PCA basis functions are not known *a priori* as in the DFT.

3.2.3. Singular value filter for source separation

The singular value filter operates by decomposing the signal along the PCA basis functions as computed from their singular value decomposition. Filtering is then applied by assigning weights to the basis functions to achieve the filtered output. It is possible to achieve consistent filtering results when the weighting coefficients are determined adaptively from the singular values, but superior performance can be achieved when the filter coefficients are non-binary and determined as a function of the singular value spectrum of data.

In PCA-based filtering, weightings are restricted to binary numbers such that each basis function is either completely rejected or completely retained. In contrast, the SVF framework for PCA-based filtering that incorporates a weighting function created from statistical assumptions and a signal model, which computes non-binary from the singular value spectrum. Non-binary filter coefficients are demonstrated to achieve consistent and better filtering results as they effectively eliminate undesirable signal components whilst avoiding block artefacts that arise from strict thresholding.

The singular value filter is a PCA-based regression filter where filter coefficients are complex, and they are adaptively determined as a function of the singular value spectrum of

$$\omega_k = \omega_k\,(\sum) = \; 1 - \frac{1}{1 + \; e^{-\alpha\,(\Sigma - \boldsymbol{\tau})}} \tag{3-17}$$

where $\boldsymbol{\tau}$ and α are weighting function parameters that adjust the cut-off threshold and weighting function roll-off, respectively. $\sum$ is a diagonal matrix of singular values σ_k . As displayed in Fig. 3.1, as $\propto \to 0$, $\omega_k\,(\sum)$ flattens, indicating that all basis functions are retained at the same level and no filtering is obtained. At the other limit as $\propto \to \infty$, filtering is reached through strict thresholding where $\omega_k\,(\sum)$ are binary. In this instance,

basis functions are rejected if their associated singular values have a $\sum$ value above threshold $\boldsymbol{\tau}$ and retained if $\sum$ is below the threshold [128].

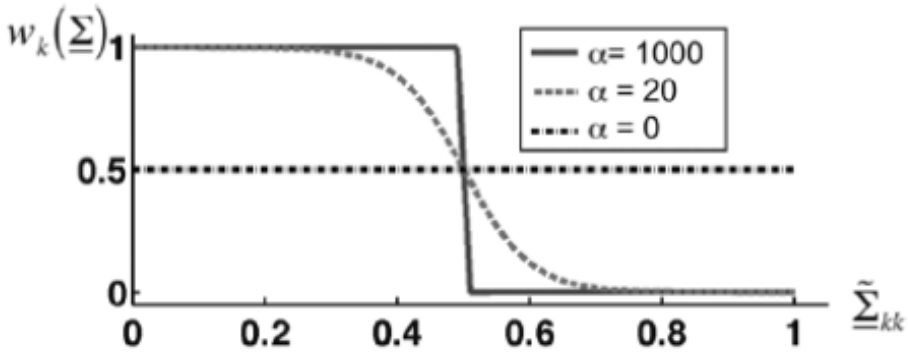

Figure 3.1, The SVF weighting function [128]

3.3. Time normalization

In motion analysis, identifying features during action sequences with different speeds or different numbers of samples in each cycle is an important issue. In such cases time normalization is necessary before or during the recognition process. Each cycle should be normalized so it is represented by the same number of samples. Linear time normalization and nonlinear time normalization using dynamic time warping are the most common techniques that can be used for this purpose [129]. Linear time normalization linearly converts the trajectory's time axis from the experimentally-recorded time units to an axis representing the gait cycle [130]. Dynamic time warping shifts the time index of each data point in a test trajectory to minimize the distance between the test and consensus trajectories [131]. In general, time-warping can be performed implicitly, i.e. by the resizing along the time axis of patterns that depict the evolution of a feature through time.

To become familiar with the principles of time-warping we can imagine two signals which can be expressed by appropriate sequence of feature vectors as shown in equation (3-18).

$$A = a_1 , a_2 , \dots , a_i , \dots , a_I \qquad (3\text{-}18)$$

$$B = b_1 , b_2 , \dots , b_j , \dots , b_J$$

The goal of time-warping is to eliminate timing differences between these two feature vectors. Considering an i - j plane, where patterns A and B are developed along the i-axis and j-axis, respectively, the timing differences between them can be depicted by a sequence of points $c = (i , j)$:

$$F = c(1), c(2), \dots , c(k), \dots , c(K) \qquad (3\text{-}19)$$

where $c(k) = (i(k) , j(k))$.

This sequence can be considered to represent a function which approximately realizes the mapping from the time axis of pattern A onto that of pattern B. Hereafter, it is called a warping function. When there is no timing difference between these patterns, the warping function coincides with the diagonal line $j = i$. It deviates further from the diagonal line as the timing difference grows.

As a measure of the difference between two feature vectors a_i and b_j , a distance

$$d\,(c) = d\,(i,j) = \left\| a_i - b_j \right\| \qquad (3\text{-}20)$$

is calculated between them. Then, the weighted summation of distances on the warping function F becomes

$$E(F) = \sum_{k=1}^{K} d\big(c(k)\big).\ w(k) \qquad (3\text{-}21)$$

where $w(k)$ is a nonnegative weighting coefficient, which is intentionally introduced to allow the $E(F)$ measure to be a flexible characteristic and is a reasonable measure for

the goodness of warping function *F*. It reaches its minimum value when warping function *F* is determined so as to optimally adjust the timing difference. This minimum residual distance value can be considered to be the distance between patterns *A* and *B,* still remaining after eliminating the timing differences between them, and is naturally expected to be stable against time-axis fluctuations. Based on these considerations the time-normalized distance between two patterns *A* and *B* is defined as follows:

$$D\ (A,B) = \text{Min}\left[\frac{\sum_{k=1}^{K} d\big(c(k)\big).\ w(k)}{\sum_{k=1}^{K} w(k)}\right] \tag{3-22}$$

where denominator $\sum w(k)$ is employed to compensate for the effect of *K* (the number of points on the warping function *F*). Equation (3-22) is no more than a fundamental definition of time-normalized distance. [129].

3.4. Statistical significance

To show that the results are statistically valid, in this thesis we use a statistical significance test. Any hypothesized relationship between two variables can be expressed in terms of a probability that the relationship exists; and how strong is the relationship. Statistical significance is one of the tools that is used to address existence and strength of the relationship [132]. They tell us what the probability is that we would be making an error if we assume that we have found an apparent relationship.

A statistical significance test is used to show if we select random samples from a population, the same relationship would exist between variables in every sample or not. The test is also used to show that if we could do a census of the population, the same relationship would exist in the population from which the sample was drawn, or whether our findings are due to random chance. Generally, we can never be 100% certain that a relationship exists between two variables. There are too many sources of

error to be controlled, for example, sampling error, researcher bias, problems with reliability and validity, simple mistakes, and so forth.

Using probability theory and the Normal curve, the probability of incorrectly concluding that a relationship exists can be estimated. If the probability of an incorrect conclusion is small, then we say that our observation of the relationship is a statistically significant finding. Statistical significance is not the same as practical significance. We can have a statistically significant finding, but the implications of that finding may have no practical application.

In testing for statistical significance we need to state the research hypothesis, the null hypothesis, then by selecting a probability of error level, we need to compute the test for statistical significance, and interpret the result. A research hypothesis states the expected relationship between two variables. It may be stated in general terms, or it may include dimensions of direction and magnitude. A null hypothesis usually states that there is no relationship between the two variables.

Researchers use a null hypothesis in research because it is easier to disprove a null hypothesis than it is to prove a research hypothesis. That is, it is easier to show that something is false once than to show that something is always true. It is easier to find disconfirming evidence against the null hypothesis than to find confirming evidence for the research hypothesis [133].

Even in the best research project, there is always a possibility (hopefully a small one) that the researcher will make a mistake regarding the relationship between the two variables. There are two possible types of mistake or error. The first is called a type I error. This occurs when the researcher assumes that a relationship exists when in fact

the evidence is that it does not. In a type I error, the researcher should accept the null hypothesis and reject the research hypothesis, but the opposite occurs.

The second is called a type II error. This occurs when the researcher assumes that a relationship does not exist when in fact the evidence is that it does. In a type II error, the researcher should reject the null hypothesis and accept the research hypothesis, but the opposite occurs. Generally, reducing the possibility of committing a Type I error increases the possibility of committing a Type II error and vice versa.

Researchers generally try to minimize type I errors, because when a researcher assumes a relationship exists when one really does not, consequences may be worse than before the conclusion was made. In type II errors, the researcher misses an opportunity to confirm that a relationship exists, resulting in no change of thinking, i.e. no action. Researchers generally specify the probability of committing a type I error that they are willing to accept. In social sciences, most researchers select it to be 0.05. This means that they are willing to accept a probability of 5% of making a type I error.

3.5. Summery

In this chapter we reviewed signal separation, time normalization and statistical significance techniques. As a conclusion to the reviewed techniques, we note that there are some important differences between PCA and ICA. Principal component analysis is not based on a generative model, although it can be derived from one. It is a linear transformation that is based either on variance maximization or minimum mean square error representation. The PCA model is invertible in the theoretical case of no compression i.e., when all principal components are retained. Once the principal components y_i have been found, the original observations can be readily expressed as either linear functions as $= \sum_{i=1}^{n} y_i \ \ \boldsymbol{\omega}_i$, and also the principal components are simply

obtained as linear functions of the observations: $y_i = \boldsymbol{\omega}_i^T \mathbf{x}$. ICA is a similar generative latent variable model, but now the independent components are assumed to be statistically independent and non-Gaussian; that is a much stronger assumption that removes the rotational redundancy.

4. Research Method

When considering the applicability of on-body sensing systems for home-based rehabilitation, we face the challenges related to wearer's comfort. As discussed in Chapter 2, these systems are bulky due to large batteries and sensitive to sensors positioning which need uncomfortable tight-fitting attachments and experts for placement/set-up. In this thesis we look at signal processing techniques to overcome the mentioned challenges. We show how we overcome these challenges by applying signal processing techniques on motion data which is gathered through a set of designed experiments,

To compensate for the effect of the random changes in the position of sensors on measured data, and to enable a more energy efficient on-body sensing system, we use source separation and filtering techniques. Finding characteristic features that represent the main patterns of motion enables on-body sensing systems to reduce variability in motion data. Our proposed way of using functional principal component analysis (fPCA) is introduced in this chapter with a brief review of its theory along with the application of PCA-based techniques reported in literature. To date this technique has not been reported as a filtering or source separation method. Its applicability in compensating for the effect of random changes in position of sensors is compared with other techniques in Chapters 5 and 6 by analysing motion data of experiments on a robot arm and human motion.

Three experimental scenarios were designed, on human subjects and a robot arm. By designing and performing experiments on robot arm we assess the validity of applying the technique that we introduce. We study and compensate for the uncertainties in the data due to sensor position changes. Experiments are designed for motion capture of a robot arm at different frequencies while random changes are introduced in position of sensors.

The superiority of the approach over the other considered techniques is shown in the third experimental scenario of experiments when reducing the sampling rate. As the sampling rate decreases, the system becomes more energy efficient. Therefore, by decreasing the sampling rate, the battery size can be reduced or there can be increase in measurement time and therefore the system lifetime. Although decreasing the sampling rate causes more variation in the captured motion data, we can use the proposed data analysis technique to compensate for this effect.

4.1. An introduction to theory

FPCA is an extension to the traditional PCA, where the principal components are represented by functions rather than vectors. It has been shown to be very effective for the study of human motion. By examining the entire waveform data, this tool can identify embedded patterns of complex movements, and more detailed pattern differences can be discriminated [134]. Principal components provide indications for identifying potentially important differences in motion curves.

4.1.1. Functional principal component analysis

Functional principal component analysis-based technique has been used in motion analysis, although it has never been used as a filtering technique in motion data analysis. Standard data analysis techniques, which determine the mean and standard

deviation of time series data, summarize motion data in single patterns that are the average behaviour and show deviations as possible errors by standard deviation bands. Such techniques severely reduce the information gleaned from the raw data, and may discard much important information.

In particular, the results do not account for the information that may be inherent in all the variations apparent in the data. When different sessions of marker wearing are averaged, information can be lost and the averaged curve does not closely resemble any of the individual curves. To facilitate analysis and present only the essential structures contained within the data, multivariate statistical analysis has been proved to be a powerful tool [135]. However, the extent of information loss when averaging data remains a matter of concern.

The basic philosophy of applying functional data analysis on human motion data is the principle that the best unit of information is the entire observed function rather than a string of numbers. It is assumed that human motion data are supposed to have an underlying functional relationship governing them [136]. A central idea in functional data analysis is smoothness which implies that adjacent values in time are linked and it is unlikely that these values will differ largely [137]. Since fPCA provides a means of identifying and examining the main source of variability of a set of curves, it is useful for analysing human movement data where variability plays a key role [138].

Among multivariate statistical techniques, linear transformations are computationally easier to perform. With linear transformations, the use of functional techniques may provide additional insight into differences in motion patterns. Treating the data as functions preserves all the information contained in the raw data. They are an effective tool for the study of human motion in modelling motion curves by identifying hidden combinations and relationships between variables [15]- [134].

We use fPCA as a filtering technique which has not been reported in literature to-date; then we test the applicability of it to motion capture data. In the first step, we fit the function to the data. To fit a function to our raw data **y**, we use a set of functional building blocks $\emptyset_k$, $k = 1, 2, \ldots, K$, called basis functions which are combined linearly (4-1). That is, a function *x* (*t*) defined in this way is expressed as follows, and called a basis function expansion.

$$x(t) = \sum_{k=1}^{K} c_k \emptyset_k \tag{4-1}$$

Parameters c_k are the coefficients of the expansion. The upper limit of the number of principal components in the multivariate case is the number of variables, while in fPCA the number of eigenfunctions is equal to the smaller of *K* and *N*, where *K* is the number of basis functions, and *N* is the number of variables [137]. To compute coefficients c_k there are two strategies [139]. Smoothing by regression analysis, and smoothing by roughness penalties. In the first approach, smoothness is achieved by defining the data fitting as the minimization of the sum of squared errors, SSE, and considering the error as follows,

$$y_j = x(t_j) + \varepsilon_j = \mathbf{c}'\, \emptyset(\mathrm{t}) + \varepsilon_j = \emptyset'(t_j)\mathbf{c} + \varepsilon_j \tag{4-2}$$

Using matrix notation let **y,** the raw data vector, contains the *n* values to be fitted, vector ε contains the corresponding true residual values, and *n* by *K* matrix $\emptyset$ contains the basis function values $\emptyset_k(t_j)$. Then we have $\boldsymbol{y} = \emptyset\mathbf{c} + \varepsilon$ **.** The least-square estimate of the coefficient vector **c** is shown in equation (4-3).

$$\hat{\mathbf{c}} = (\emptyset'\emptyset)^{-1}\emptyset'\boldsymbol{y} \tag{4-3}$$

There is no particular limitation on the number of variables *N* that we want to fit the functions into. The number of basis functions *K* should be less than or equal to the number of sampled data points, *n*. An exact representation of sampled data is achieved

when K=n in the sense that we choose the coefficients c_k to yield $x(t_j) = y_j$ for each j. A larger K provides a better fit to the data, but for smaller values the less computation is required. However, if we make K too small, we may miss some important aspects of the function that we are trying to estimate

Therefore the degree to which the data y_j are smoothed as opposed to being interpolated is determined by the number of K basis functions. Consequently we do not view a basis system defined by a fixed number K of parameters, but rather we see K itself as a parameter that we choose according to the characteristics of data. Ideally, basis functions should have features that match those known to belong to the functions being estimated. This makes it easier to achieve a satisfactory approximation using a comparatively small number K of basis functions.

The trade-off can be expressed in another way. For a larger value of K, the bias in estimating $x(t)$, which is defined as $\text{Bias}[\mathbf{x}(t)] = \mathbf{x}(t) - \text{E}[\mathbf{x}(t)]$, is small. The bias will be zero for $K = n$. The variance of the estimate which is defined as $\text{Var}[\{\mathbf{x}(t)\}] = \text{E}[\{\mathbf{x}(t) - \text{E}[\mathbf{x}(t)]\}^2]$ for $K = n$ is almost surely going to be unacceptably high. Reducing the variance leads us to look for smaller values of K, but of course not so small as to make the bias unacceptable. It is appropriate to tolerate a little bias if the result is a substantial reduction in the sampling variance.

The considerable literature on multiple regressions contains many ideas for deciding how many basis functions to use. For example, stepwise variable selection would proceed in a step wise fashion by adding basis functions one after another, testing whether the added function significantly improves the fit at each step. Conversely, variable-pruning methods are often used for high-dimensional models, and work by starting with a generous choice of K and dropping a bias function at each step that seems to not account for a substantial amount of variance. These methods all have

their limitations and there is no "gold standard" for the selection of *K*. According to the nature of human movement there are no rapid changes in the main pattern of motion that could be missed when the sampling frequency is high in comparison to movement pattern [137].

The roughness penalty approach uses a large number of basis functions and at the same time imposes smoothness by penalizing some measure of function complexity. A measure of roughness of the fitted curves can be the square of the second derivative of a function, $[D^2x(t)]^2$, at argument value *t* which is called curvature at *t*. Thus, a measure of a function's roughness is the integrated squared second derivative or total curvature,

$$\mathrm{PEN}_2(x) = \int [D^2x(t)]^2 \mathrm{d}t. \tag{4-4}$$

Therefore the roughness penalized fitting criterion can be as in (4-4), where λ is the smoothing parameter specifying the emphasis on the second term penalizing curvature relative to goodness of fit, quantified in the sum of squared residuals in the first term. Adding a penalty to the least-squares criterion, causes the following penalized sum of squared errors, $F(\mathbf{c})$,

$$F(\mathbf{c}) = \sum_j [y_j - x(t_j)]^2 + \lambda\, \mathrm{PEN}_2(x(t)). \tag{4-5}$$

In equation (4-5), λ represents a continuous tuning parameter. Larger λ causes roughness increasingly penalized, and $x(t)$ becomes smooth. Smaller λ causes penalty to be reduced. By defining the roughness penalty matrix as $\mathbf{R} = \int \emptyset(\mathrm{t})\emptyset'(t)\mathrm{d}t$, We can show the estimate of the coefficient vector **c** as follows [137],

$$\hat{\mathbf{c}} = (\emptyset'\emptyset + \lambda\mathbf{R})^{-1}\emptyset'\boldsymbol{y} \tag{4-6}$$

In this thesis we chose the regression method for finding the expansion coefficients c_k. The roughness penalty approach uses a large number of basis functions

and it requires parameter λ to be adjusted in addition to the parameters needed in regression method. In the nature of human movement there are no rapid changes in the main pattern of motion that could be missed when the sampling frequency is high in comparison to the speed of motion. So in our analysis, there is no need to select a more complex way of finding the coefficients, which is roughness penalty approach.

After calculating the coefficients and deriving the fitted functions into our data, we calculate the sample variance-covariance function, $v(s,t)$, which is defined as follows,

$$v(s,t) = N^{-1}\sum_{i}^{N} y_i(s)\, y_i(t) \tag{4-7}$$

The functional eigenequation is

$$\int v(s,t)\xi(t)dt = \rho\xi(s), \tag{4-8}$$

where ρ is eigenvalue and $\xi(\mathrm{s})$ is an eigenfunction of the variance-covariance function. The eigenfunction which is called the principal component weight function, $\xi_1(\mathrm{s})$, can be calculated by (4-9).

$$\text{Maximize } \sum_i f_{i1}^2$$

$$\text{Subject to } \int \xi_1^2(s)ds = \left\|\xi_1\right\|^2 = 1, \tag{4-9}$$

where the principal component score f_{i1} is defined as

$$f_{i1}=\int \xi_1(\mathrm{s})\, x_i(\mathrm{s})ds. \tag{4-10}$$

A non-increasing sequence of eigenvalues $\rho_1 \geq \rho_2 \geq \cdots \geq \rho_k$ can be constructed stepwise by requiring each new eigenfunction computed in (4-11), to be orthogonal to those computed in the previous steps,

$$\int \xi_j(t)\,\xi_l(t)dt = 0, \qquad j = 1, \ldots, l-1$$

$$\int \xi_l^2(t)dt = 1. \tag{4-11}$$

Solving the eigenequation for extracting functional Principal Components essentially reduces to performing Singular Value Decomposition (SVD) as shown in equation (4-12). The columns of Δ contain the eigenfunctions (fPCs) evaluated at time *t* and Λ contains the corresponding eigenvalues. The notation $\Delta^{\mathrm{T}}(t)$ is used to identify that we are dealing with functions.

$$v(s,t) = \Delta(s)\Lambda\Delta^{\mathrm{T}}(t) \tag{4-12}$$

In functional PCA, there is an eigenfunction associated with each eigenvalue, rather than an eigenvector in PCA. These eigenfuctions describe major variational components. It also permits the extraction of loadings and scores. Loadings are the correlation coefficients between variables and components. Scores are the contributions of the principal components to each individual variable. Motion data can be decorrelated by projection onto the eigenfuctions. After projection, stochastic components can be separated from deterministic components, by subtracting either one or the other from of the signal. There is a close relation between fPCA and PCA.

4.1.2. Principal component analysis

As discussed, PCA is a multivariate statistical technique that provides an orthogonal projection of the data onto a lower dimensional linear space, known as the principal subspace. PCA has been widely used for multivariate data analysis and dimension reduction. It can be used as a decorrelation technique by computing a new, much smaller set of uncorrelated variables, i.e. Principal Components (PCs). Each new

variable is a linear combination of the original ones. All the principal components are orthogonal to each other, so there is no redundant information. All remaining principal components are defined similarly, so that the lowest order components normally account for very little variance and can usually be ignored. In other words, PCA can be defined as a linear projection that minimizes the average projection cost, defined as the mean squared distance between the data points and their projections.

In comparison to fPCA, PCA allows for a separation of main and residual components within a data set in a vector-based manner rather than as a function. We can eliminate the dominant features by subtracting them from the data. For a mathematical description of the PCA-based signal processing technique, we consider the multivariate motion data in the form of *N* different real-valued, time dependent motion vectors of each joint, for a number of sessions.

Each motion vector consists of *M* time samples. So there would be *N* motion vectors for each session comprising *M* time samples for each joint. We combine these *M* dimensional vectors into a single *M*-by-*N* motion matrix. Consequently for each joint we create a *M*-by-*N* motion matrix, *X*, which is composed of various motion vectors from a specific subject as shown in (4-13).

$$\mathbf{X} = \begin{bmatrix} x_1[1] & \cdots & x_N[1] \\ \vdots & \ddots & \vdots \\ x_1[M] & \cdots & x_N[M] \end{bmatrix} \tag{4-13}$$

The data needs to be standardized, so they have zero mean and unit variance, forming a new matrix **Y** as shown in (4-14). The standardization affects the PCA results; the covariance matrix is then equal to the correlation coefficient matrix and the eigenvectors are normalized to unity. The *j*th column of **Y** forms the *M*-dimensional

vectors, which are the standardized time sequences of the *j*th column. *M* is the number of data samples and *N* is the number of each marker that is worn.

$$\mathbf{Y} = \begin{bmatrix} y_1[1] & \cdots & y_N[1] \\ \vdots & \ddots & \vdots \\ y_1[M] & \cdots & y_N[M] \end{bmatrix} \tag{4-14}$$

Principal components (PCs) are those linear combinations of the original variables that contain maximum variance. The PCs are obtained from the *N* eigenvalue-eigenvector $(\lambda_i, \vec{e_i})$ pairs of data covariance matrix Cov_{ij} which is defined as $\mathrm{Cov}_{ij} = \langle [y_i(t) - \langle y_i(t) \rangle_T][y_j(t) - \langle y_j(t) \rangle_T] \rangle_T$. $\vec{e}_i^{(n)}$ are principal components, also often called modes. *N* is the number of principal components.

The eigenvectors directly correspond with the principal modes introduced previously. Each λ_i represents a measure of the variance, deviation or spread of the data along the corresponding mode $\vec{e}^{(n)}$. Usually, the eigenvalues are ordered from the highest to lowest: $\lambda_1 > \lambda_2 \ldots \lambda_{N-1} > \lambda_N$. The total population variance is given by the sum of all eigenvalues: *Total Variance* $= \lambda_1 + \lambda_2 + \cdots + \lambda_{N-1} + \lambda_N$. The percentage of the total variance explained by the i^{th} PC is given by (4-15).

$$\textit{Explained variance}\ (i) = \frac{\lambda_i}{\lambda_1 + \lambda_2 + \cdots + \lambda_{N-1} + \lambda_N} \tag{4-15}$$

In terms of computational complexity of the algorithms, we can find the coefficients c_k and all smooth values at $x(t_j)$ in $O(n \log n)$ operations. This efficiency is possible because of the Fast Fourier Transform. This is one of the features that has made Fourier series a traditional basis of choice for long time series [137]. As the main difference between PCA and fPCA based techniques is finding the coefficients and smoothing values, the computational complexity of the fPCA based technique is $2O(n \log n)$ operations larger than the PCA based technique. We multiplied it by 2

because we first fit the function to data and smooth it, next we perform PCA on the coefficients and then, after applying the filtering technique and transferring the trajectories onto the first domain, we fit the function again to the discrete data.

If we consider the data matrix that we apply PCA on as an *n* by *m* matrix (*n* number of samples and *m* the dimensionality) to compute PCA, we need to compute the covariance matrix and then apply SVD to it. The time complexity of computing the covariance matrix is $O(\log(nm^2))$ and then computing SVD is $O(m^3)$. So in the procedure of applying the technique for the PCA part, the total time complexity is $2(O\left(\log(nm^2)\right) + O(m^3))$. Multiplication by 2 is for a similar reason that we explained in previous paragraph. Consequently for applying the fPCA based filtering technique the computational complexity is $2(O(n\log n) + O\left(\log(nm^2)\right) + O(m^3))$. Therefore the proposed signal processing approach adds processing complexity to the motion capture procedure. As on-body sensing systems usually have a central system for analysing the data located far from the body and connected to a powerful processing unit with a connection to an abundant electricity supply, processing complexity is not a challenge in this case.

4.2. Application of PCA-based techniques in literature

PCA has been shown to be a powerful tool for analysing complex gait data. PCA has already been used as an effective tool in motion analysis for extracting variation features in motion data [140]. To determine features of variation in motion patterns between unloaded and loaded conditions a PCA based technique was applied to motion capture data in [141]. In order to quantify the effect of external loads, the first principal was needed. Principal Components (PCs) were generated from lower body

joint angle data. It was shown that PCA could be used to characterize changes due to evenly distributed external loads.

In [142] a PCA based technique was used on motion data acquired by an optical system to yield a reduced dimension space where not only interpolation but also extrapolation is possible which is controlled by quantitative speed parameter values. Moreover, with proper normalization and time warping methods, walking motions with continuously varying human height and speed were presented.

In [135] the use of PCA in clinical biomechanics as an expedient, unbiased means for reducing high-dimensional data sets to a small number of modes or structures, as well as for separating invariant and variable components in such data sets was presented. The authors explained that PCA allows for a separation of main and residual components within a data set; especially when partitioning signals into deterministic and stochastic components, and can be seen as filtering the noise or the common parts.

Based on the properties of the PCs, more specifically the eigenvalues and eigenvectors of the covariance matrix of motion data, a method to analyse multi-joint coordination was proposed in [143]. A comparison between relative phase analysis and PCA shows that both provide similar and consistent results, when the latter technique's sensitivity is scored. It provides a method for automatic pattern detection as well as an index of performance for each joint within the context of the global coordination pattern.

To determine differences between normal and abnormal features of gait data, principal component analysis was used as a data reduction tool, as well as a preliminary step for further analysis in [144]. The emphasis was on a comparison with a reference or

normal gait pattern and detection of pathological deviations from this reference, as well as the pre- and post-operative changes. Principal components were extracted to determine features of variation that could be used to quantify differences in gait patterns. In this way, the original waveform data for a particular subject is transformed into a set of PC scores that measure the degree to which the shape of their waveform corresponds to each feature.

To extract biological and psychological information which is encoded in visual motion patterns a new method using PCA was proposed in [140]. From the trajectory of the 38 original markers, the locations of 15 virtual markers positioned at major joints of body were computed. Because each virtual marker's position is represented by 3 coordinates, a body posture is represented by a 45 dimensional vector. By using PCA, this high dimensional database was reduced to a low dimensional database in which walking was modelled by the temporal behaviour of the first four principal components.

In [145] principal components and eigenvalues are used to compare the similarity between multivariate time series datasets. The authors proposed a similarity measure in multivariate time series by comparing how far the principal components are apart using the aggregate eigenvalues as weights, taking into account the variance for each principal component. They applied their method on a human gait database and showed that their similarity measure outperforms other common similarity measures.

4.3. Proposed filtering strategy

In this thesis we propose the following pipeline, as shown in figure 4.1, for using fPCA as a filtering strategy to address the mentioned challenges in on-body sensing systems for home-based rehabilitation motion capture. fPCA can be used as a filtering technique, especially when partitioning signals into deterministic and stochastic components.

This is achieved by subtracting either one or other from the signal and can be regarded as filtering the noise or the common parts, respectively. The approach is to re-express the original data along a new coordinate system such that the signal of interest can be separated from other sources of variation in the original data while projecting the signal along different bases. Filtering is achieved by keeping the bases describing the signal of interest and rejecting the rest.

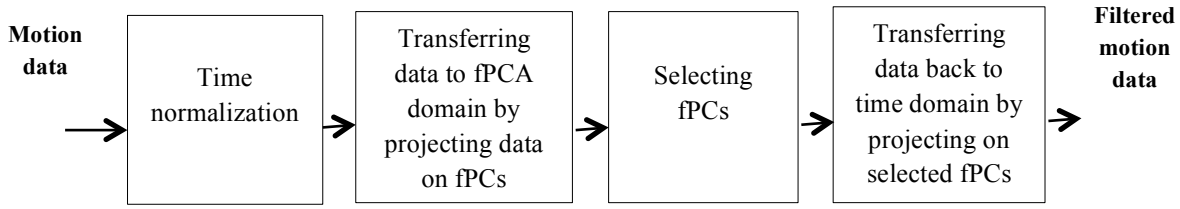

Figure 4.1, The proposed fPCA based filtering technique pipeline

The signal processing pipeline consists of several stages. Motion data needs to be normalized in the first step to ensure the same number of samples in each motion cycle. The difference in the number of samples per motion cycle is due to the different speed of performing a repetitive motion. Then we transfer the data to the fPCA domain by using the fPCA transform which is introduced in this chapter. As the effect of random changes in the position of sensors introduces a random effect on the motion data, to separate this effect from main and coherent component of movement, we partition the data into two elements, $\overrightarrow{x_i}^{(global)}$ and $\overrightarrow{x_i}^{(filtered)}$ as shown in equation (4-16);

$$\overrightarrow{x_i} = \overrightarrow{x_i}^{(global)} + \overrightarrow{x_i}^{(filtered)}$$

$$= \sum_{n=1}^{L<NE} \xi_n(\mathrm{t}) f_i^{(n)} + \sum_{n=L+1}^{NE} \xi_n(\mathrm{t}) f_i^{(n)} \qquad (4\text{-}16)$$

The sum of the dominant principal components weight functions is given by $\overrightarrow{x_i}^{(global)}$, so the filter characteristic depends on the data. The number of eigenfunctions, $\xi_n(\mathrm{t})$, that define the global pattern influences the filtered pattern. The sum of the residual components is shown by $\overrightarrow{x_i}^{(filtered)}$. In equation (4-16), principal component scores are shown by $f_i^{(n)}$. The number of eigenfunctions is shown by *NE* and the number of selected ones is shown by *L*.

After applying fPCA on our data, we filter the main source of variation in the data by keeping the signal components containing the most amount of variability or the most relevant principal component weight function or eigenfunctions and removing the rest from the fPCA domain. After this stage, the data will be returned to the first domain by projecting the data of the retained eigenfunctions and removing eigenfunctions with less variation. The dominant modes of variation in the data can be kept by considering the proportion of corresponding eigenvalues to the total variance.

To find the dominant modes of variation in the data, and to separate the deterministic and stochastic components, fPCA can be used usually after subtracting the mean from each observation. Viewing consistent features as coherent components implies that the mechanisms generating these common structures follow deterministic rules, otherwise they would not be consistent or coherent. In contrast, the residual components often contain a degree of randomness or stochasticity. We apply this data-driven filter to our experimental motion data to separate out the effect of random changes in sensor positioning from the main motion pattern.

4.4. Summary

In this chapter we proposed a signal processing approach to overcome the challenges associated with the development of portable motion capture systems aimed at assisted rehabilitation. A novel way of using functional principal component analysis (fPCA) was introduced with a brief review of the application of PCA-based techniques reported in literature along with the relevant background theory. Functional principal component analysis has never been used as a filtering technique in motion data analysis. In our approach, the main source of variation in the data is filtered by keeping the most relevant principal component weight function and removing the rest from the fPCA domain. The data will be returned to the first domain by projecting the data of the retained eigenfunctions and removing eigenfunctions with less variation.

5. Data Acquisition and Experiment Design

To describe the compensation procedure, we first explain the process of motion data acquisition. We carry out three experiments collecting motion data on human subjects and on a robot arm. The robot arm motion capture, which utilizes a more controlled movement in comparison to a human, is used to validate the experimental procedure that is used on human subjects. The motion capture system is introduced in Section 5.1. Next we explain the human motion experiment and the robot arm set-up in Section 5.2 and 5.3, respectively. The designed experiments for three motion capture scenarios are described in Section 5.4.

5.1. Motion capture system

We use a commercial optical motion capture system named *Codamotion* [24] which is available in the Human Performance Laboratory of Queen Mary University of London, shown in figure 5.1. The system is a general-purpose 3D motion tracking system. The measurement unit contains three pre-aligned solid-state cameras which track the position of a number of active markers, i.e. infra-red light emitting diodes (LEDs), in real-time. Sampling rates are selectable from 1Hz up to 200Hz, dependent on the numbers of markers in use. Each scanner unit contains three special cameras which detect infra-red pulses of light emitted by the markers and locate the marker positions with very high resolution. The cameras are rigidly mounted on the scanner

units so that the system can be pre-calibrated.

The calibrated system measures the positions of markers within a three dimensional coordinate system that is fixed in relation to the scanner unit. The active range of the capturing system is 1.5-5.2m from the scanners and follows a Gaussian distribution function so that optimal visibility occurs at a distance of approximately 3m from each scanner. The angular resolution of each camera is about 0.002 degrees; this results in a lateral position resolution of about 0.05 mm at 3 m distance (horizontally and vertically), and a distance resolution of about 0.3 mm [24]. The set-up of the motion capture system in the laboratory ensures that all experiments are carried out in this range. The process of system alignment is done by defining the X, Y, and Z axes of the reference coordinate system before performing each experiment [24].

The markers are attached to drive boxes which are positioned toward or on the mid-section of each rigid body. Each drive box acts as a battery to supply power to associated active markers. The maximum measurement time depends on a combination of the sampling rate and the total number of markers being tracked. As the number of markers decreases, the maximum measurement time can be increased proportionally for a given sampling rate. For example, with 28 markers (sampling rates of 200Hz or below), the maximum measurement times are: 100s at 200Hz, 200s at 100Hz, 400s at 50Hz, 800s at 25Hz, ... to 20000s at 1Hz. Sampling rates are selectable from 1Hz up to the upper limits for different numbers of markers in use, 100Hz for up to 56 markers, 200Hz for up to 28 markers, 400Hz for up to 12 markers, 800Hz for up to 6 markers.

Figure 5.1, Human performance lab, and motion capture environment

The markers, small infra-red light emitting diodes, are shown in figure 5.2. Their drive boxes are available in two sizes, 2-marker or 8-marker. All the drive boxes contain sophisticated circuitry which responds to infra-red synchronizing pulses sent out from the *Coda* scanner units. The circuitry flashes the markers at an appropriate point in the time multiplexed sequence which corresponds with the marker number on the box. This is how the system maintains intrinsic marker identity.

When the scanner unit is not acquiring data, very little current is being drawn from the batteries in the drive boxes. As soon as the scanner unit starts to send out control signals to the marker drive boxes, the rate of current consumption rises to about 50mA in each of the drive boxes if they have two LED markers attached. This current is principally used by the marker LEDs which are being pulsed with current pulses of 40 microseconds at up to 800Hz repetition rate. The capacity of the batteries in the drive

boxes is 30 mA hours. This is sufficient for at least 100 data acquisition runs before the batteries need to be recharged.

Figure 5.2, Markers and drive boxes of the motion capture system

5.2. Human motion experiment set-up

For human motion capture experiments, the experiments on human subjects have been approved by Queen Mary Research Ethics Committee (Appendix A). Subjects are given an information sheet explaining the procedure of the experiments before the motion capture session and a consent form was signed by each subject (Appendix B).

In the experiment the long axis of the measurement unit defines the direction of the X axis, normally a horizontal line parallel to the walkway. The perpendicular line

from the unit defines the positive Y axis, normally horizontal across the walkway. The other perpendicular (vertical) line defines the Z axis (positive up) as is shown in figure 5.3. The markers' numbers specified in figure 5.4 are the recommended sets; different numbers may be used as long as the appropriate names are assigned to the markers in the motion analysis set-up. The geometrical properties of each body segment are derived from three non-collinear points bearing particular anatomical relationships to the given segment.

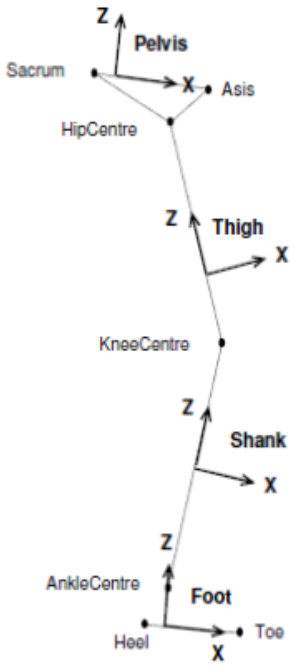

Figure 5.3, Segment embedded coordinate frames according to the gait set up of Codamotion marker-set[24]

There are several standard marker-sets for placing markers on the human body such as Cleveland Clinic, Saflo, Helen Hayes, Codamotion, and so forth. The Cleveland Clinic marker set uses a rigid triad of markers in a plane parallel to the long axis of the bone to capture the motion of the thigh and shank in 3 dimensions. The Saflo marker-set consists of a total body marker-set with 19 retro-reflective markers fixed on specific anatomic landmarks. The Helen Hayes marker set is a relatively simple set of external markers developed for time-efficient video analysis of lower extremity kinematics. All

of the named marker placement protocols are used for clinical gait analysis. For measuring bilateral gait, we use the recommended *Codamotion* marker-set comprises a total of 22 standard markers as shown in figure 5.4 for the right side of the body. Markers shown in parentheses () are optional [24]. The marker set determines ankle and knee joint centres and segment coordinate systems by means of a marker on a post or wand protruding from the anterior aspect of the thigh and shank, and by single markers placed over the lateral aspect of the joint flexion/extension axis.

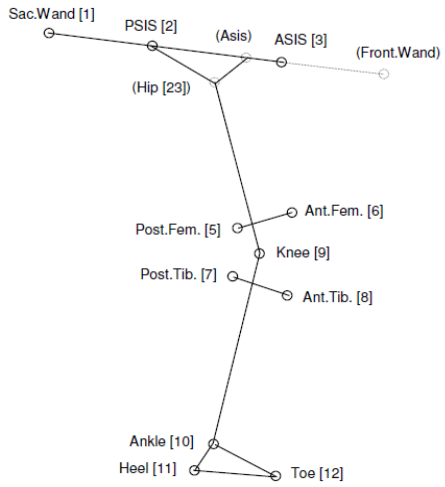

Figure 5.4, Position of markers on human body according to the gait set up of Codamotion marker-set [24]

5.3. Robot arm experiment set-up

For the purpose of the current investigation, an experiment with precisely controlled robotic arm [146] is used to measure the effect of random marker placement errors during controlled rotations of one rigid body segment with respect to another. The robot has a positional repeatability of ±0.02mm, stemming from its high precision when performing repetitive actions. The DENSO 6-axis robots provide great flexibility and improved performance [146]. Because of their increased scale of movement, they are suited to handle a wide range of applications without compromising either speed or precision. The repeatability of the robot is from ±0.02 mm, maximum speed up to

11000 mm/s, arm lengths up to 1298 mm, payloads up to 13 kg. Workspace of the robot is shown in figure 5.5. The robot includes internal wiring and air piping for maximum efficiency in restricted spaces.

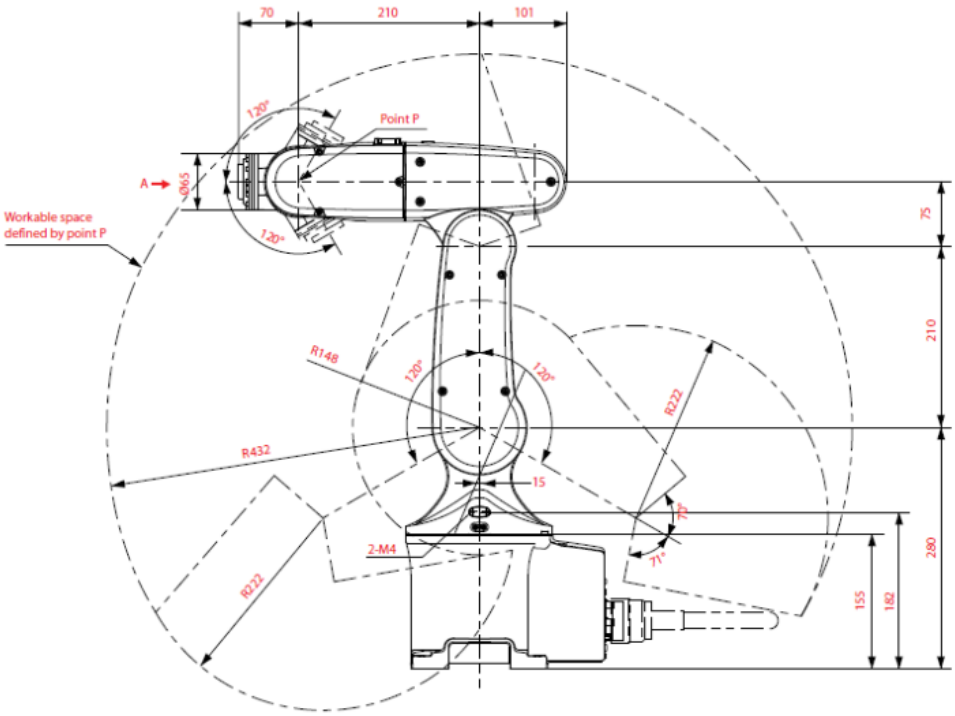

Figure 5.5, Work space of the robot arm [146]

The robot coordinate system can be defined according to the base coordinate system. The base coordinate system is a Cartesian system with the origin and the centre of the robot base. It has components X_b, Y_b, and Z_b which are identical with X, Y, and Z. Work coordinates are three dimensional Cartesian coordinates defined for each operation space of work-piece. The origin can be defined anywhere and as much as needed. It lies at a corner of the rectangular parallelepiped envelope of an object work-piece as shown below. Work coordinates are expressed by the coordinate origin (X, Y, Z) corresponding to the base coordinates and the angles of rotation (R_x, R_y, R_z) around X, Y and Z axes of base coordinates as shown in figure 5.6. If work coordinates are not defined, base coordinates go into effect.

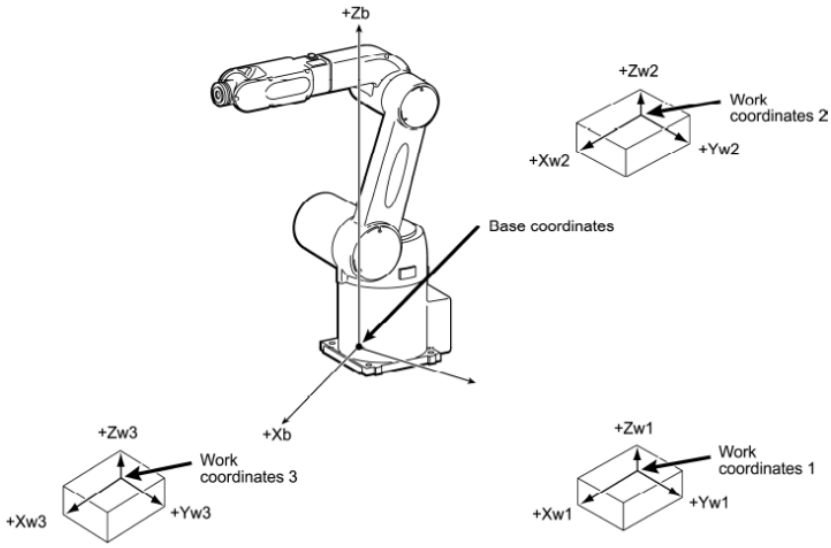

Figure 5.6, Base coordinates and work coordinates [146]

When defining rigid body segments for three dimensional kinematic analysis, a minimum of three markers is required per segment: two markers define the longitudinal axis of the segment (in our laboratory, we define the longitudinal axis as the Z axis; anterior-posterior axis is the X axis and the medio-lateral axis is the Y axis) and a third marker is placed off centre from the Z axis to define the segment as a rigid body, so that all three markers are noncolinear.

5.4. Designed experiments

Three scenarios of experiments are designed and performed in our research. In first scenario, human subjects participate in the experiments. Their motion is captured as it is explained in Section 5.4.1. In the second scenario, the robot arm movement is captured as it is explained in Section 5.4.2. The robot arm motion is captured at different sampling frequency as explained in Section 5.4.3. There are inadvertent changes in position of sensors in all scenarios to simulate effect of uncertainties in sensors positioning.

5.4.1. First scenario, motion capture of human movement

We use ten human subjects in ten sessions of marker wearing. A full analysis of an individuals' motor behaviour should involve the evaluation of an appropriate number of individual repetitions. In [136], 4 subjects are recruited for functional analysis of cyclic human motion and in [15] 7 subjects are used for walking analysis using functional PCA. Therefore in our experiments we decided to recruit 10 subjects 5 female and 5 male. Inadvertent changes are emulated in the position of markers for each session while following the standard marker set. The process of measurements in each session involves instrumenting the legs and pelvis with active markers according to the *Codamotion* marker-set (see figure 5.4 and 5.7). Ten healthy human subject, five male (weight 69 ± 7.9 kg, height 170.2 ± 3.4 cm, age 26.6 ± 1.5 years, BMI 23.8 ± 1.9) and five female subjects (weight 56.4 ± 6.9 kg, height 167.2±3.2 cm, age 25.6 ± 1.5 years, BMI 20.2 ±2.4) are recruited for the instrumented gait analysis. Detailed subjects parameters are in table 5.1.

Figure 5.7, Marker wearing on subject's body

Table 5.1, The 10 subjects' parameters who took part in the experiments

	Gender	Height (cm)	Weight (kg)	Age (years)	BMI
Subject 1	Male	168	61	26	21.6128
Subject 2	Male	171	69	25	23.5970
Subject 3	Male	166	65	27	23.5883
Subject 4	Male	175	82	29	26.7755
Subject 5	Male	171	68	26	23.2550
Subject 6	Female	169	57	24	19.9573
Subject 7	Female	165	48	26	17.6309
Subject 8	Female	163	56	25	21.0772
Subject 9	Female	168	67	28	23.7387
Subject 10	Female	171	54	25	18.3597
Mean Values		168.7	62.7	26.1	21.9592

Feigned inadvertent changes in the position of markers within the radius of 2 cm are made for each of ten sessions of marker wearing. We use a random number generator with uniform probability distribution to generate these random position displacements. We are aware, in spite of the precision in sensor placement regime, there still exists human error in placing markers whilst following the derived random position obtained from the random number generator. However, we do not consider this source of error further, believing to be relatively small. Each session consisted of six trials. In each trial the subject walks from the start point to an end point of the walkway while the motion capture system captured the subject's motion. Each trial lasts for five seconds and the sampling frequency of the system is 200 Hz. The subject is asked to walk at normal walking speed. This walking speed is maintained as far as possible whilst different marker perturbations are made across different sessions of marker wearing.

The motion capture system measures the angles of joints and provides a stick figure view for the subject under experiment as shown in figure 5.8.

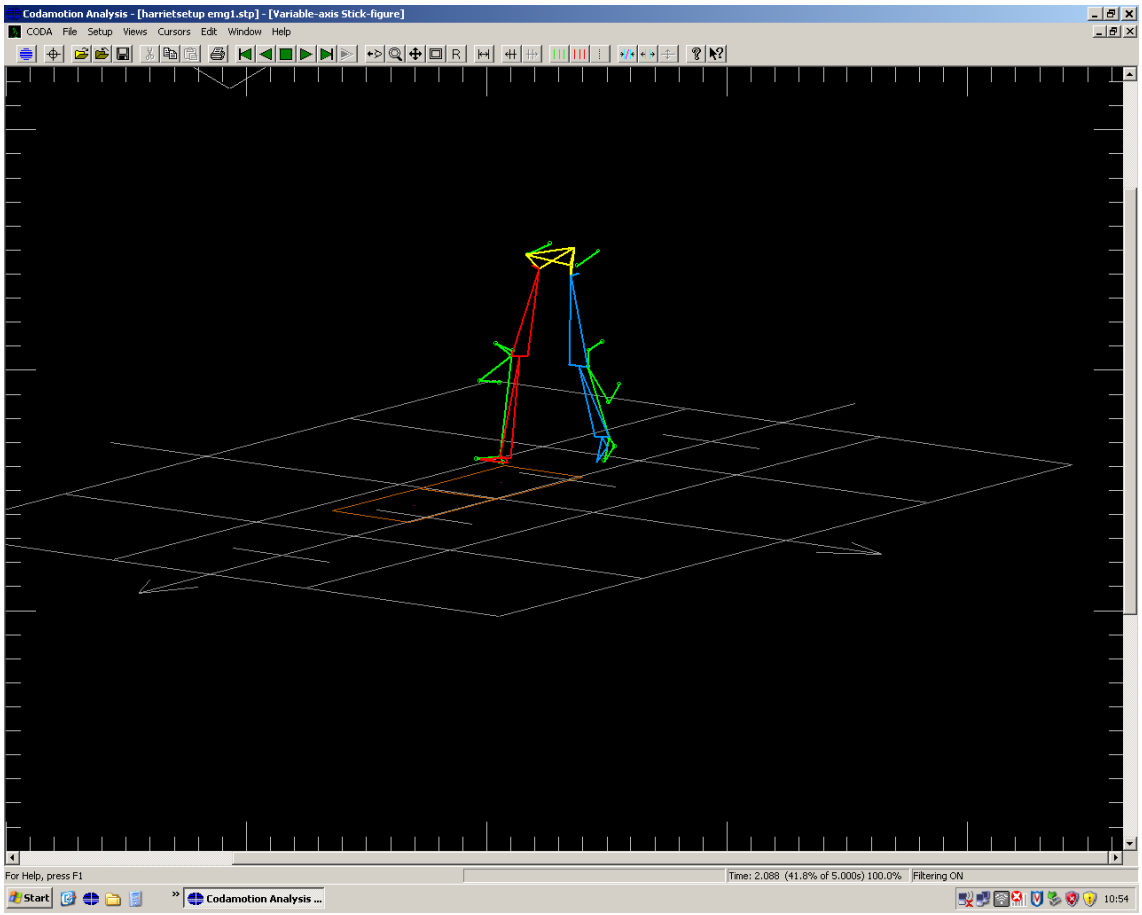

Figure 5.8, Stick figure view for the subject under experiment.

5.4.2. Second scenario, motion capture of robot arm

To test our hypothesis on a more controlled motion and validate the first experiment's results the Denso robotic arm described earlier is used. In this experiment, we measure the effect of random marker placement errors and their removal by the proposed technique during controlled rotations of one rigid body segment with respect to another. This movement is analogous to flexion-extension in the human arm. All other movements are constrained in order to reduce any measured confounding rotation from orthogonal planes to the axis of rotation that we measured.

Figure 5.9, Placement of markers which are attached to drive boxes positioned toward or on the mid-section of each rigid body.

For the motion analysis of the robot arm, it is divided into two rigid bodies: the upper segment was defined as rigid body 1 (RB1), and the lower was defined as rigid body 2 (RB2). On RB1, markers were placed at both ends of the segment, 3 cm from the end and defined the longitudinal Z axis of RB1. A marker is placed over the hinge joint between RB1 and RB2. This marker serve as the upper marker for the Z axis marker for RB2 as well as the third, off-centre, marker require to define RB1 of the local coordinate system within the software. As with RB1, RB2 is defined by two markers along the length of the segment and two further markers are used to define the RB2 segment local coordinate system as shown in figure 5.9 and 5.10.

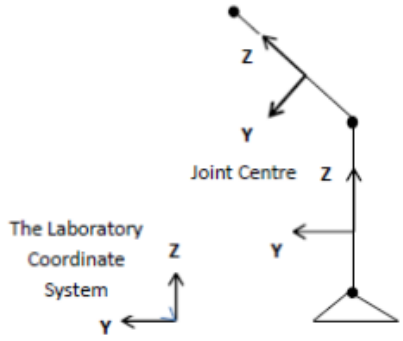

Figure 5.10, Segment embedded coordinate frames for the robot arm

The same configuration of markers was used on both sides of each segment and the local coordinate axis system for each segment is defined using a set of orthogonal axes. The arm is programmed to rotate 130 degrees. In order to control rotation data as much as possible, movement is restricted to one degree of freedom; that is, the only movement was rotation of RB1 with respect to RB2 in one fixed plane. Measurements are recorded over intervals of fifteen seconds. The motion of the robot arm is recorded while the markers are in correct positions to provide reference motion data. As the accuracy of motion capture system is high and the robot arm can perform repetitive movements with very high precision, we can define the reference motion data as our target and we can compare other motion data in this experiment with it. Next, each marker is moved in a random direction by 1 cm or 2 cm from the initial reference position within the same plane for all segments. The considered displacements are significant error within the context of marker placement [67]. A random number generator is used to generate these perturbations.

Twenty sets of data are collected: ten sets with markers randomly positioned 1 cm from the initial reference positions and ten sets of data with markers positioned randomly at a distance of 2 cm from the initial reference positions. The stick figure view of the robot arm and variation in the joint angles in *Codamotion* software view are

shown in figures 5.11 and 5.12.

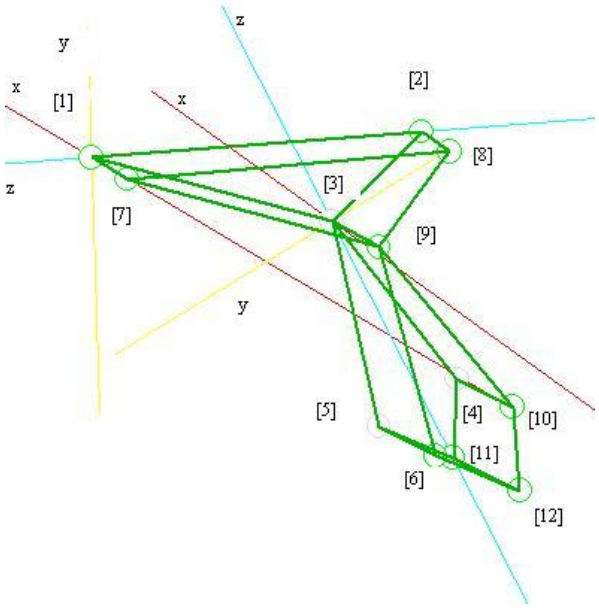

Figure 5.11, Stick figure, markers position and defined coordinate axes of the robot arm.

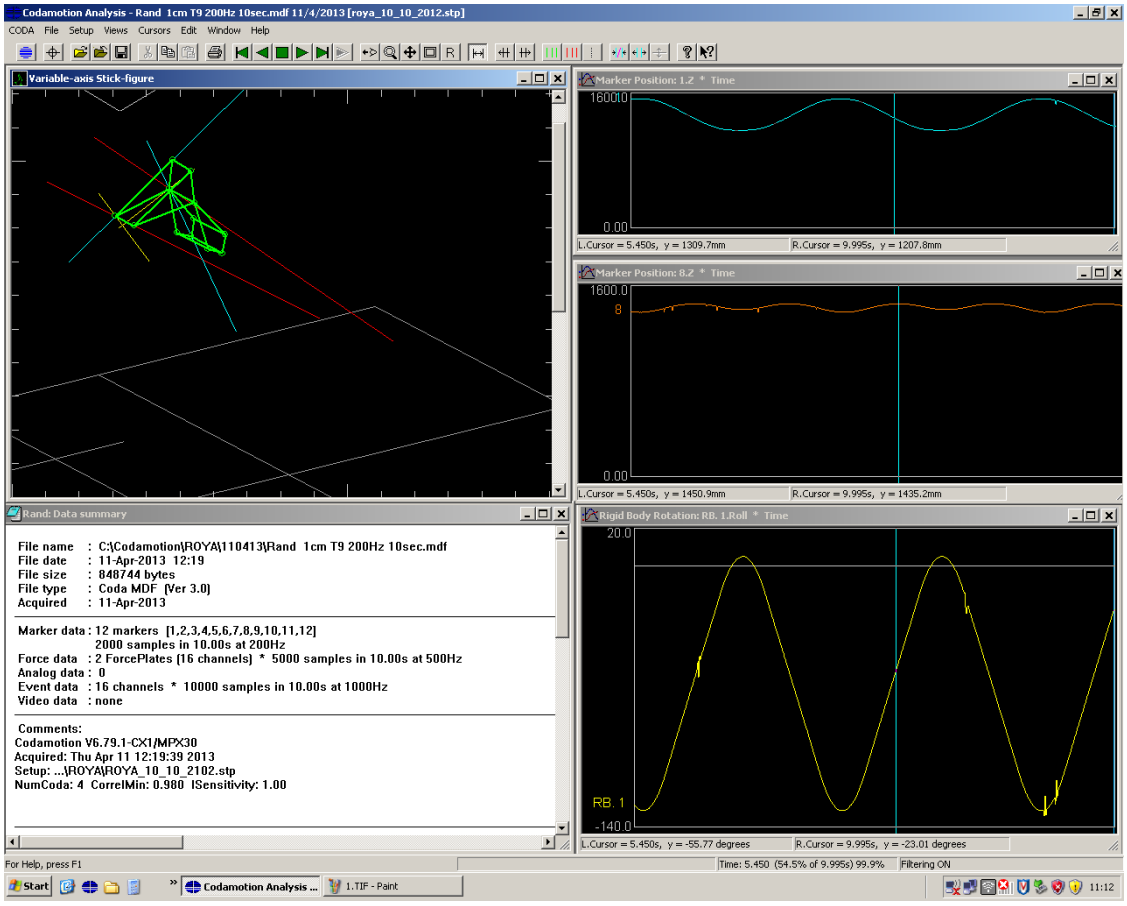

Figure 5.12, Stick figure of robot arm and the angle variation in motion capture session

5.4.3. Third scenario, motion capture of robot arm at different frequencies

To investigate the performance of the proposed signal processing technique with sampling frequency reduction, we design the third experiment. The focus of the experiment is energy efficiency, achieved by reducing sampling rate, while measurements are simultaneously affected by random changes in sensor positions. By increasing energy efficiency of the system, smaller batteries can be used in on-body sensors. Reduction in battery size is another step towards flexibility in on-body sensing systems. On the other hand, decrease in sampling rate cause greater variation in the captured motion data.

In this scenario we capture motion during ten sessions of marker wearing on the robot arm to measure the effect on the accuracy of motion capture of simultaneously reducing in sampling rate and randomly changing positions of sensors. For each perturbation of markers, we capture data in 8 available frequencies: 200, 100, 50, 25, 10, 5, 2, and 1 Hz. We have 10 random perturbations of marker positions, that is, the total of 80 trials. We use random number generator to create random positions.

The differences between data of different marker wearing sessions are the number of samples per session and the variation due to random changes in the positions of sensors. First we verify that the variation in motion data is indeed increased by decreasing sampling rate. We then apply filtering signal processing techniques to test if the variations due to both the reduction in sampling rate and the random changes in the positions of sensors can be compensated for in the single filtering step.

6. Results and Discussion

Kinematics variables are acquired for several motion capture sessions of the human body and a robot arm according to the experimental design described in Chapter 5. The position of sensors in 3D space is measured with reference to the laboratory coordinate system. The captured positions differ depending on where the subject starts to walk. Since joint angles are descriptive of motion and do not vary with the change of the position of the subject with respect to the reference point, we choose to focus on changes of derived angles. Therefore all the results of the data processing techniques refer to the joint-angle signals derived from the captured motion data. We compare the motion data and mean variance of the data before and after applying the techniques. The variance is the square of the standard deviation of each angle of motion data.

6.1. First scenario, motion capture of human movement

For experiments with the human body the kinematic variables are the angles of pelvis, hip, knee, ankle, and foot in the X, Y, and Z axes. Kinematics variables of each marker wearing session are averaged over six trials to eliminate the effect of other sources of variation that are irrelevant to differences in position of sensors in each session. The cause of these variations could be different walking speed, different ways of walking because of the tiredness of the subject and so forth.

Walking sequences are segmented into cycles. Each cycle comprises two steps.

We ask a subject to walk for a specific time interval and divide the action into cycles. Each cycle is identified as the interval from initial contact of the heel with the ground to initial contact of the following step. We use consecutive right heel contacts to separate each stride which can be determined from right heel marker position in Z direction as shown in figure 6.1.

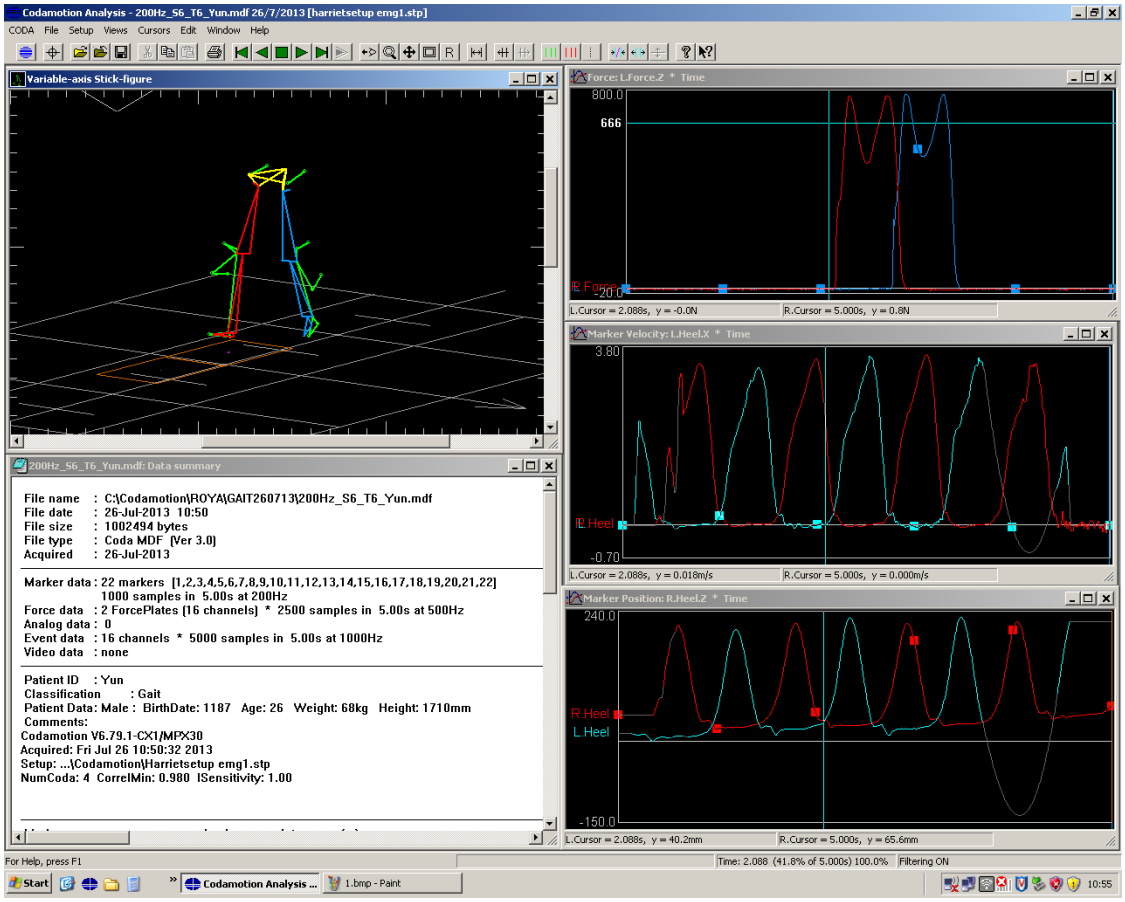

Figure 6.1, Stick figure and captured signals from force plate, left heel in X and right heel in Z direction to separate each stride.

Identifying features during action sequences with different numbers of samples in each cycle is an important challenge. Each cycle should be normalized so it is represented by the same number of samples. We use linear time normalization which linearly converts the trajectory's time axis from the experimentally-recorded time units to an axis representing the gait cycle from 0 to 100 percent.

After time normalization, we perform data standardization so that we can

compare results of different angles with each other in terms of percentage of change before and after applying the filtering techniques. In this chapter results of applying fPCA, ICA, PCA, and SVF adaptive filtering techniques and an *a priori* FFT based filtering mechanism are compared. We show how the results of second set of experiments validate the applicability of our proposed technique, and demonstrate its advantage over PCA in the results of the third set of experiments.

6.1.1. Applying fPCA

The aforementioned 15 kinematic variables for 10 marker wearing sessions are shown in figure 6.2 prior to fPCA filtering. Each plot shows one of the joint angles in 10 sessions of marker wearing, which are shown in different colours. The differences between the variables of different sessions are due to inadvertent changes in the position of sensors. Data of each session are produced and averaged over 6 trials. The placement changes are random in all directions and they were made within a radius of 2 cm from the correct position to simulate the effect of human marker placement errors between different sessions, while following the standard marker set.

Results show that random changes in the position of sensors cause additional variability in motion pattern, as expected. If the variability is not compensated for, it may cause misinterpretation. The aim of applying the filtering techniques is to explore if these variations can be compensated for. To apply fPCA based filtering, first we need to fit functions onto the data and then derive eigenfunctions. Then by rejecting the eigenfunctions with a smaller amount of variation, we project the data back to the original domain. We fit Fourier basis functions into session data considering that each matrix of data contains one of the 15 kinematic variables in a cycle for each of the 10 sessions.

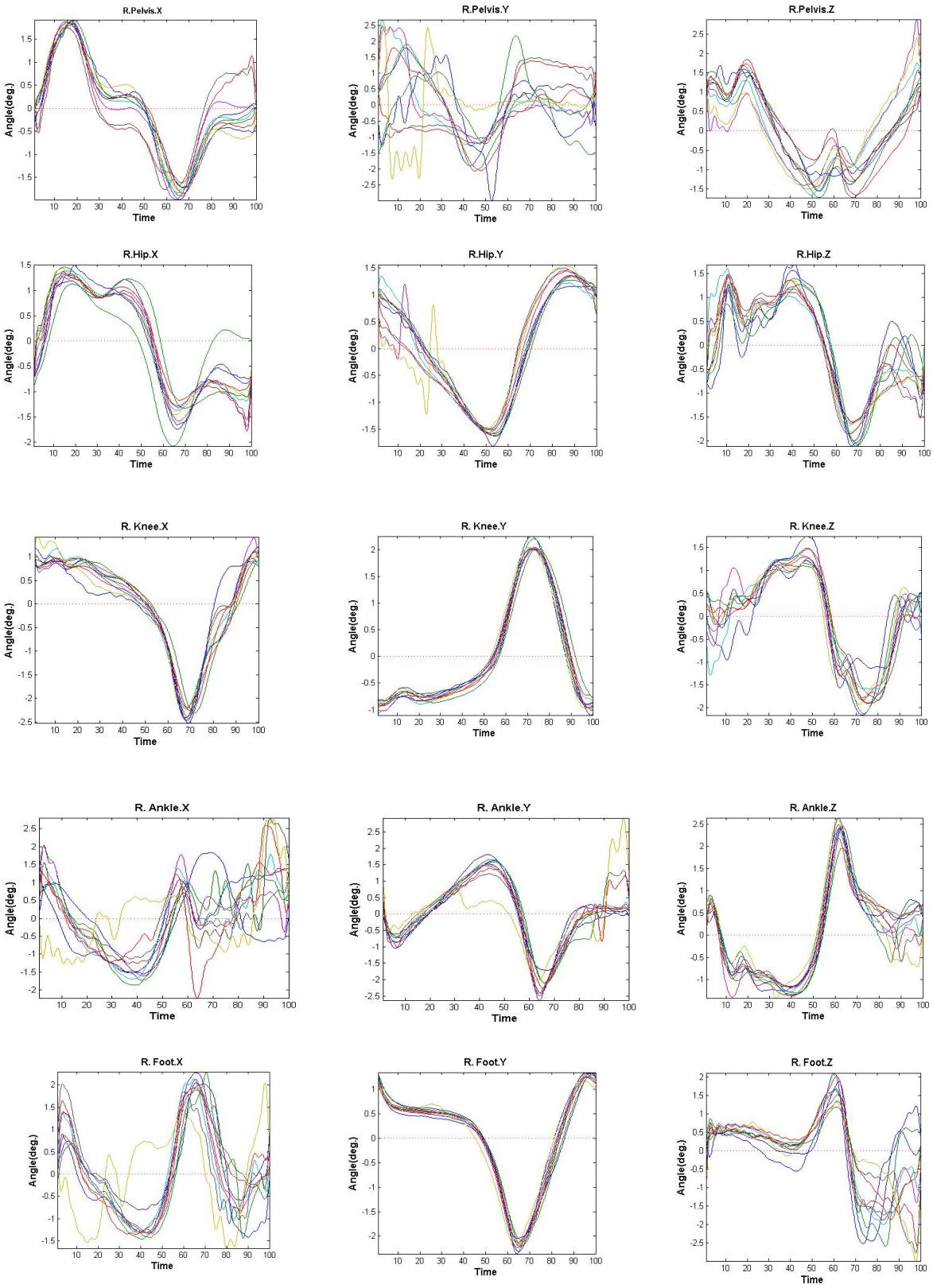

Figure 6.2, Kinematic variables of 10 marker wearing sessions. The normalized angles of the pelvis, hip, knee, ankle, and foot in X, Y, and Z planes are shown separately from each other before applying the filtering techniques.

By applying the proposed filtering technique on data, we obtain the functional principal component functions for each kinematic variable. The most dominant mode of variation is retained, and the remainder is eliminated, thus preserving the principle variations in the data and eliminating the effect of inadvertent changes in the position of the sensors. Finally, after deleting the non-dominant mode of variation, the principal component functions are returned into initial domain by using the inverse fPCA transform. The dominant mode of variation is contained by fPCs which carry 90 percentage of variation. It can be calculated as a proportion of relevant eigenvalues of corresponding fPCs with respect to the sum of all eigenvalues as shown in equation (4-15).

Figure 6.3 shows motion data averaged over 6 trials of 10 sessions for each joint angle on a human subject data after fPCA filtering. Using the technique on the motion data of ten subjects, with ten sessions of marker wearing for each one, shows the mean variance between curves typically decreases by 95.76%. The minimum averaged improvement is 88.15% for pelvic angle in Y direction and the maximum is 99.59% for knee angle in Y direction. It can be readily determined that fPCA filtering reduces variability associated with marker placement error.

It could be claimed that these variation can be from other sources such as not walking in the same way throughout the session. We therefore apply this technique on a robot arm such that we can be sure the variation is only due to random changes in the position of sensors. We see that the second set of experiments using robot arm confirms the efficacy of the technique.

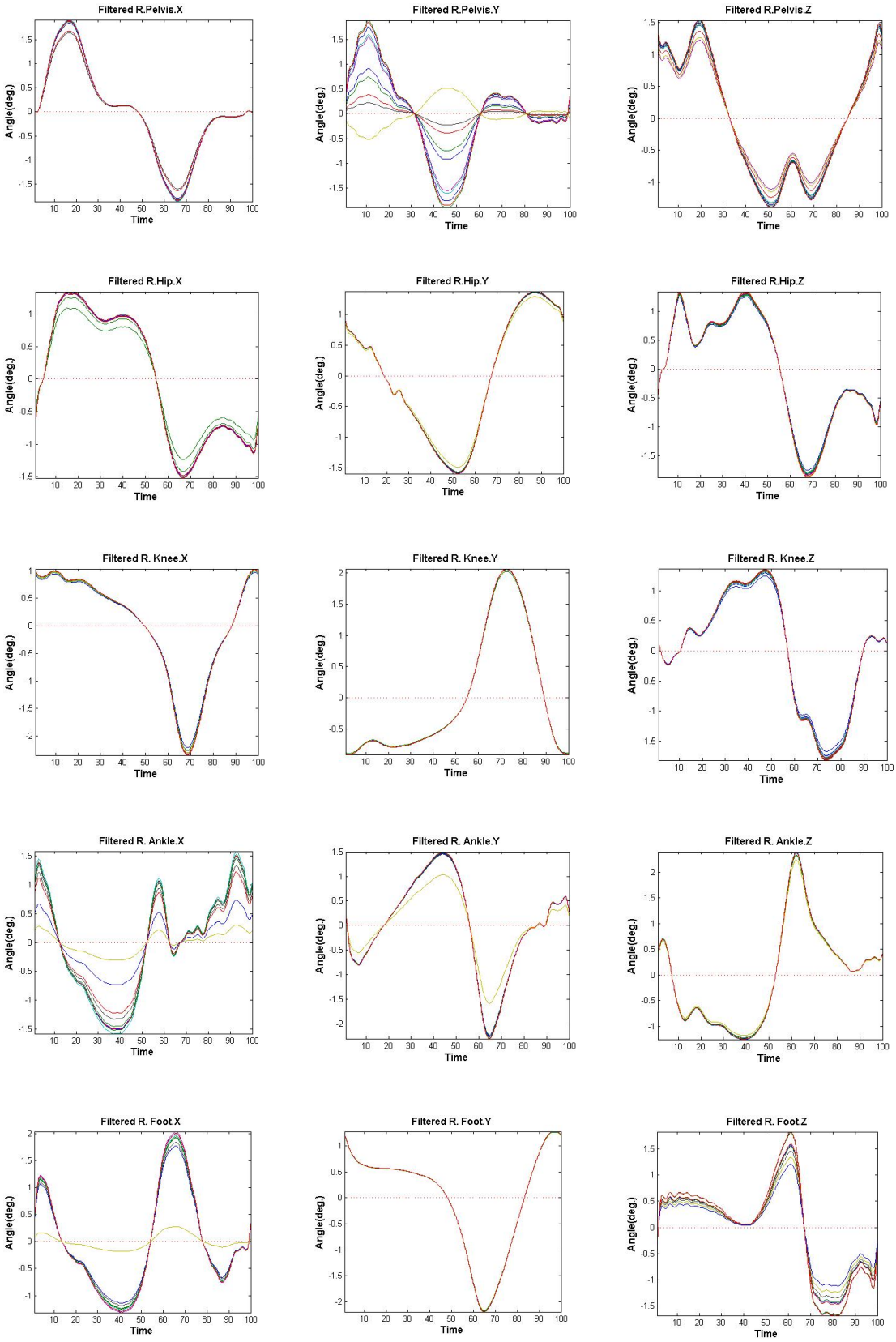

Figure 6.3, Kinematic variables of 10 marker wearing sessions. The normalized angles of the pelvis, hip, knee, ankle, and foot in X, Y, and Z planes are shown separately from each other after applying the filtering technique.

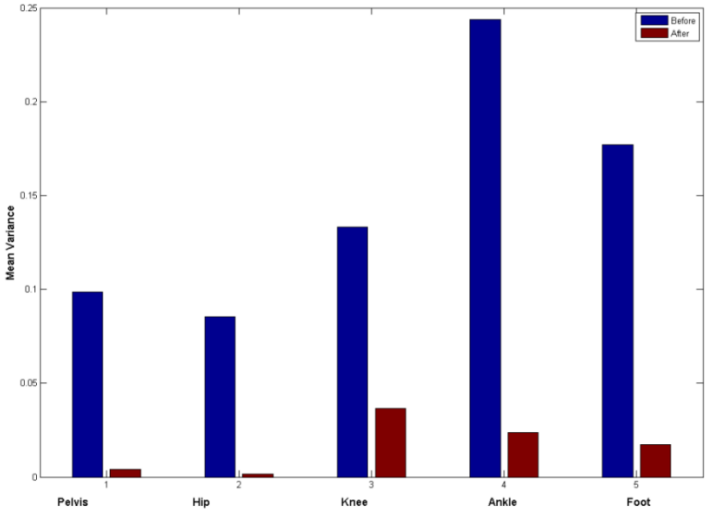

Figure 6.4, Mean variance changes before and after applying the technique for the pelvis, hip, knee, ankle and foot in the X direction

Mean variance changes before and after applying the technique for the pelvis, hip, knee, ankle and foot in the X, Y and Z directions are shown in figures 6.4, 6.5, and 6.6 respectively. We see that the mean variance is decreased in all 3 directions after applying the technique. To see if the changes are statistically significant, we use analysis of variance. Analysis of variance (ANOVA) provides a statistical test to compare the means of two or more data sets, where each data set contains an independent sample of mutually independent observations [147].

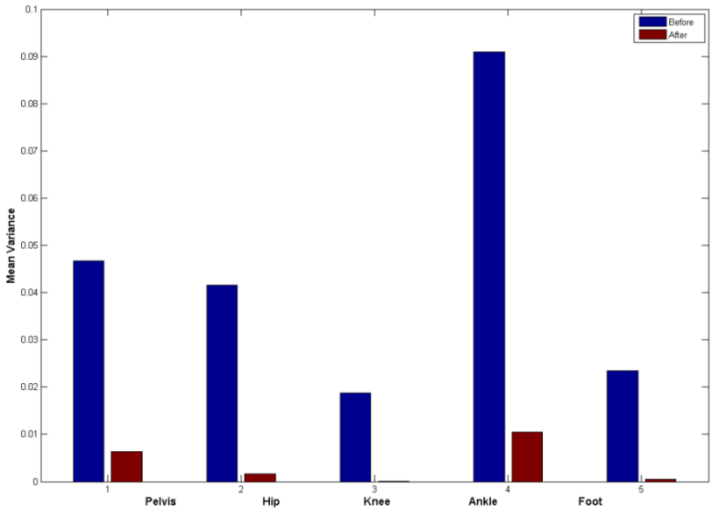

Figure 6.5, Mean variance changes before and after applying the technique for the pelvis, hip, knee, ankle and foot in the Y direction

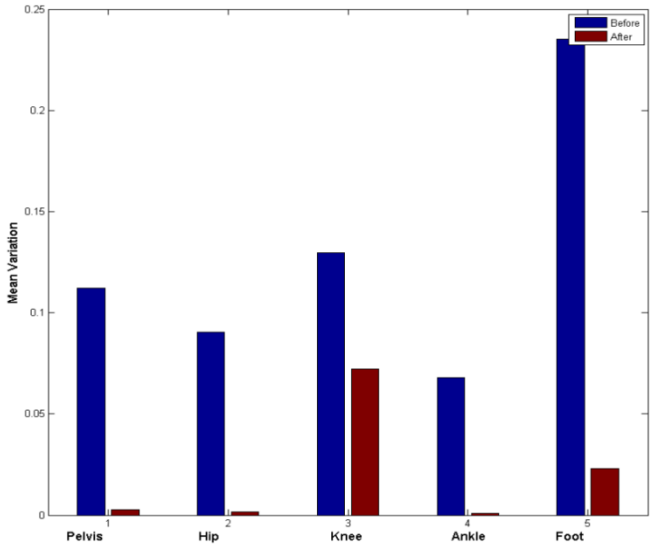

Figure 6.6, Mean variance changes before and after applying the technique for the pelvis, hip, knee, ankle and foot in the Z direction

Analysis of variance (ANOVA) is a procedure for assigning sample variance to different sources and deciding whether the variation arises within or among different population groups. Samples are described in terms of variation around group means and variation of group means around an overall mean [148]. The purpose of ANOVA is to determine whether the groups are actually different in the measured characteristic.

In analysis of variance the null hypothesis is a statement about a population that we would like to test. As introduced in Section 3.4, tests for statistical significance tell us what the probability is that the relationship we think we have found is due only to random chance. The *p* value of a test is the probability, under the null hypothesis, of obtaining a value of the test statistic as extreme or more extreme than the value computed from the sample. The *p* value depends on assumptions about the random disturbances in the model equation. For the *p* value to be valid, these disturbances need to be independent, normally distributed, and have constant variance [133].

In this experiment our research hypothesis is that there is a significant difference between mean variance of angles before and after applying the filtering technique. Thus the null hypothesis is that there are no significant differences between the mean variance of angles before and after applying the technique. The test for statistical significance was computed, using Matlab ANOVA. The *p* value for each of the angles was derived and shows (Figure 6.7) that our null hypothesis has been rejected, i.e. the results are statistically significant.

When the *p* value is very small it causes doubt regarding the null hypothesis and proposes that at least one mean of one of the samples is significantly different from the other sample means. Commonly used significance levels for the *p* value are less than 0.05. The *p* values for the pelvis, hip, knee, ankle and foot in X, Y and Z directions are calculated. They are all of the order smaller than 10^(-9). The *p* value obtained for each variable shows that the null hypothesis is rejected.

The box-plots of data for analysis of variance of each angle before and after applying the technique are shown in figure 6.7. As we compare the mean variance before and after applying the filtering technique, we have an individual matrix for each 15 kinematic variables separately. Therefore we have 15 box-plots, and there are two boxes for each kinematic variable before and after applying the technique, respectively. On each box, the central mark is the median, the edges of the box are the 25th and 75th percentiles, the whiskers extend to the most extreme data points not considered outliers, and outliers are plotted individually [148]. Results in box-plots give a visualization of the statistics of mean variance before and after applying the technique to have a better understanding of statistical changes in the data.

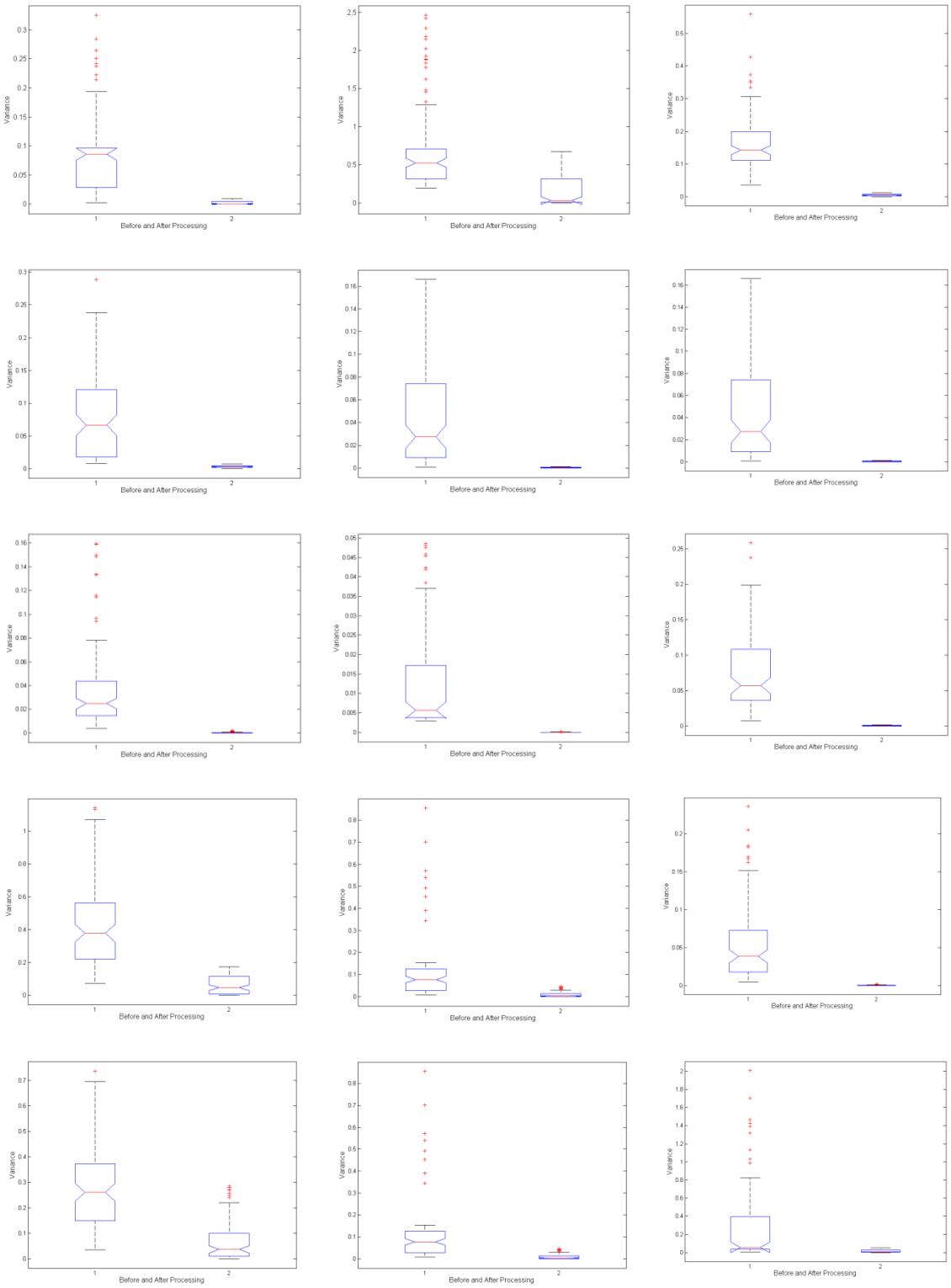

Figure 6.7, Analysis of variance for the pelvis, hip, knee, Ankle, and foot in the X, Y, and Z planes respectively

6.1.2. Applying ICA

Independent component analysis is applied to the data as a signal separation technique. We use two algorithms, Independent Component Analysis based on Maximum Likelihood (ICA ML) and ICA Molgedy and Schuster (MS). For data analysis, the rows of the input matrix **x** are the joint angles data, the rows of the output data matrix $\mathbf{u} = \mathbf{W}\,\mathbf{x}$ are projection of input on the ICA components, and the columns of the inverse matrix $\mathbf{W}^{-1}$ give the projection strengths of the respective components. Corrected motion data can then be derived as $\mathbf{x}' = \mathbf{W}^{-1}\mathbf{u}'$, where $\mathbf{u}'$ is the matrix of the activation waveforms with rows representing artefact components set to zero.

A square mixing matrix is used for ICA ML, which is a self-organizing learning algorithm that maximizes the information transferred in a network of nonlinear units. The information maximization algorithm does not assume any knowledge of the input distributions and is used for true redundancy reduction between units in the output representation. This enables the network to separate statistically independent components in the inputs as a higher-order generalization of principal components analysis [149]- [150].

ICA MS uses the Molgedey and Schuster de-correlation algorithm, having a square mixing matrix [151]- [152]. The source separation problem can be formulated as a likelihood formulation. The likelihood approach allows for direct adaptation of the plethora of powerful schemes for parameter optimization, regularization, and evaluation of supervised learning algorithms.

Results in figure 6.8 and 6.9 show the signals after applying ICA ML and ICA MS filtering algorithms. We can see that these techniques cannot eliminate the random patterns in the data. After applying the techniques we see some new ripples in the data

that are unrelated to the motion patterns. As ICA works on non-Gaussian distributed data [120], we cannot obtain appropriate results after applying this signal separation technique on our data. The variation in data is due to random changes in the position of sensors. Randomness in the position of sensors is generated using a discrete uniform distribution, which has a symmetric probability distribution. It causes Gaussian distribution of sampled motion data.

Mean variance before and after applying the techniques has been calculated for each of the angles. Table 6.1 shows the results and percentages of change before and after applying the technique. We can see that the mean percentage of change for ICA ML is 88.78% and for ICA MS is 86.17%. Although the percentage of change is high in both cases, we see new patterns of variation in the signal which shows that independent component analysis filtering based techniques are not applicable to this type of data.

Table 6.1, Mean Variance before and after applying ICA ML and MS filtering

	Mean Variance Before	Mean Variance After ICA ML	Percentage of change	Mean Variance After ICA MS	Percentage of change
Pelvis X Angle	0.0638	0.0083	87.0156	0.0029	95.4528
Pelvis Y Angle	0.6291	0.0517	91.781	0.0577	90.8344
Pelvis Z Angle	0.3253	0.0092	97.1859	0.1179	63.7649
Hip X Angle	0.0843	0.0093	88.9328	0.0055	93.4869
Hip Y Angle	0.0896	0.0039	95.667	0.0096	89.279
Hip Z Angle	0.1475	0.0064	95.6847	0.0112	92.3766
Knee X Angle	0.0508	0.0034	93.3104	0.0159	68.7341
Knee Y Angle	0.0135	0.0008	93.7439	0.0023	83.0264
Knee Z Angle	0.1873	0.0159	91.4962	0.0208	88.8901
Ankle X Angle	0.2947	0.1143	61.2125	0.035	88.1125
Ankle Y Angle	0.0201	0.0024	88.0157	0.003	84.9202
Ankle Z Angle	0.0537	0.0056	89.6315	0.0065	87.8444
Foot X Angle	0.2249	0.0318	85.8835	0.0098	95.6491
Foot Y Angle	0.008	0.0015	81.2256	0.0013	84.0055
Foot Z Angle	0.2748	0.0248	90.9858	0.0214	92.2106

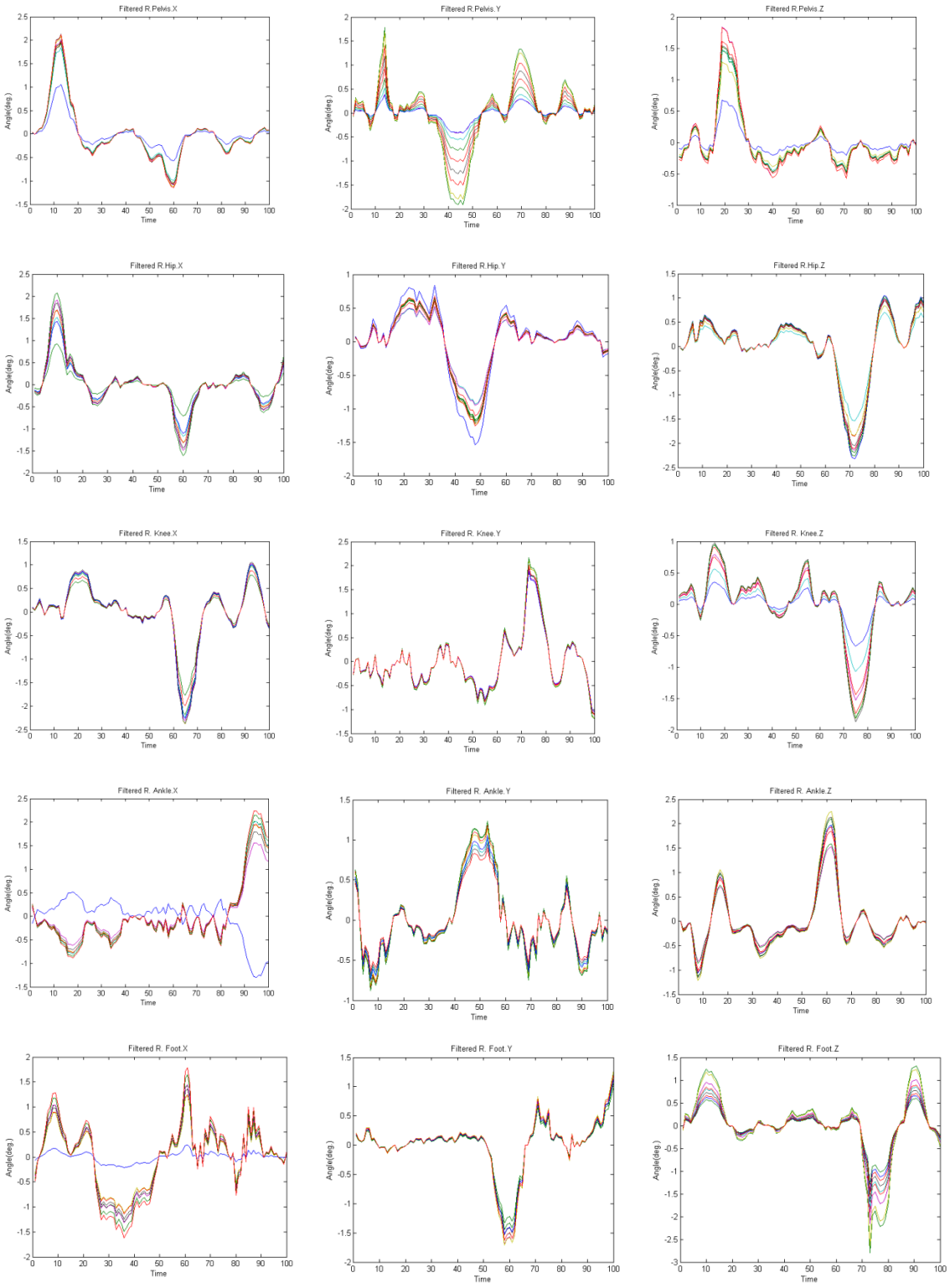

Figure 6.8, Kinematic variables of 10 marker wearing sessions. The normalized angles of the pelvis, hip, knee, ankle, and foot in the X, Y, and Z planes are shown separately after applying the ICA ML filtering technique.

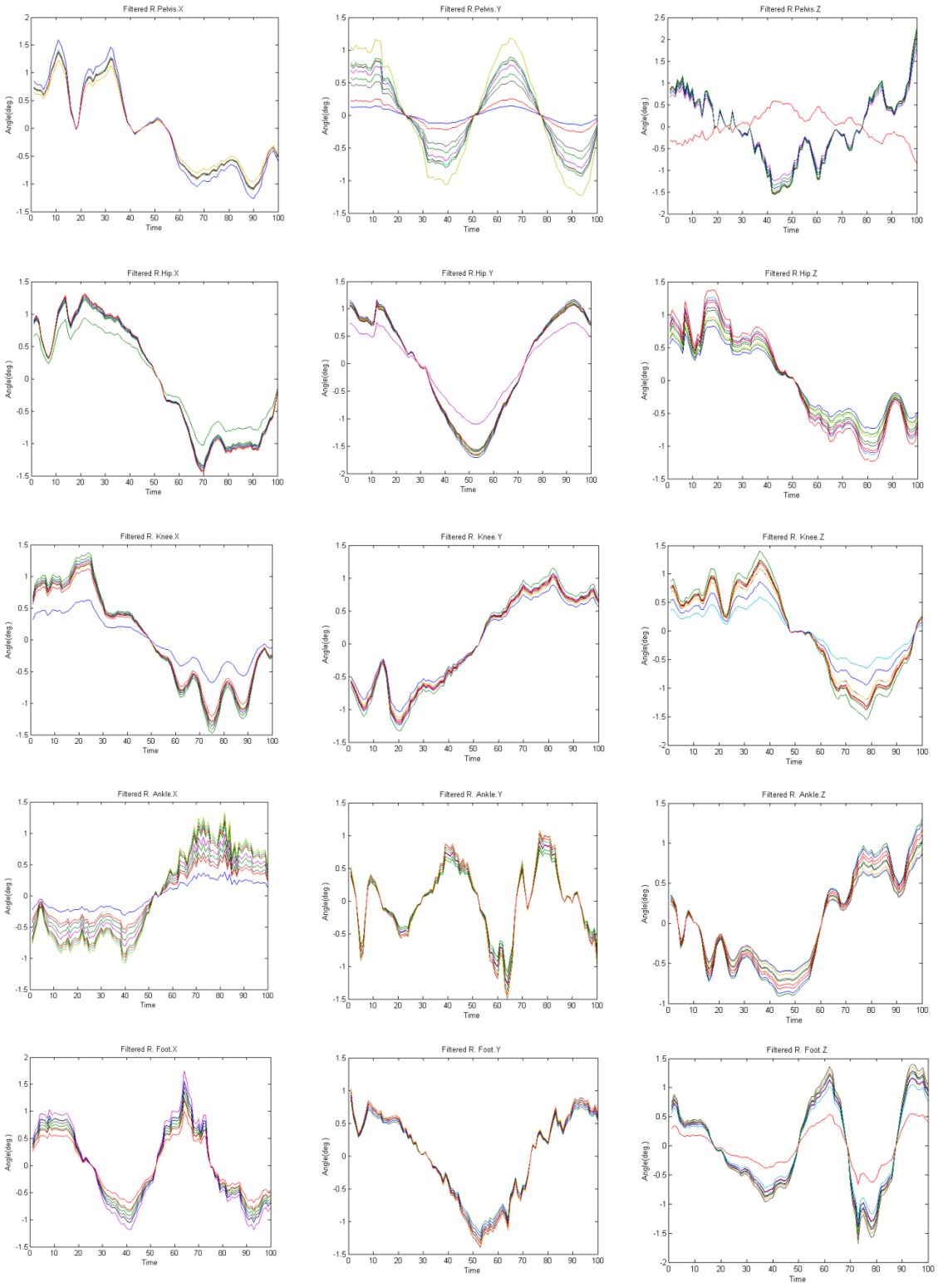

Figure 6.9, Kinematic variables of 10 marker wearing sessions. The normalized angles of the pelvis, hip, knee, ankle, and foot in the X, Y, and Z planes are shown separately after applying the ICA MS filtering technique.

6.1.3. Applying PCA

Results of applying the PCA-based filtering techniques on experimental motion data are shown in figure 6.10. It shows that the technique works properly to reduce random patterns in the data. Mean data variance before and after applying the technique is shown in table 6.2 as well as the percentage of improvement. The values in this table are for normalized data. The mean percentage change in both PCA and fPCA is 94%.

Results show that the performance of PCA and fPCA is similar in this experiment. This can be explained in terms of sampling frequency. In this experiment the sampling rate is 200 Hz while the movement pattern bandwidth is around 10 Hz according to the normal walking speed of subjects and movement patterns in data. Therefore, the sampling frequency of this experiment is high and fitting the function into highly sampled data does not have significant effect. Therefore, in highly sampled data it suggest the use of PCA instead of fPCA as it is easier to perform and it needs less calculation.

Table 6.2, Comparison of PCA and fPCA for 200Hz

	Mean Variance Before	Mean Variance After PCA	Percentage of change	Mean Variance After fPCA	Percentage of change
Pelvis X Angle	0.0886	0.0024	97.19680	0.0025	97.0640
Pelvis Y Angle	0.7301	0.1827	74.97702	0.1779	74.6841
Pelvis Z Angle	0.1713	0.0043	97.45896	0.0052	96.8486
Hip X Angle	0.0808	0.0034	95.72904	0.0032	95.9264
Hip Y Angle	0.0496	0.0003	99.24085	0.0003	99.2778
Hip Z Angle	0.0884	0.0004	99.51141	0.0004	99.5557
Knee X Angle	0.0388	0.0003	99.16443	0.0004	99.0565
Knee Y Angle	0.0123	0.0004	99.66164	0.0001	99.6883
Knee Z Angle	0.0787	0.0005	99.31882	0.0005	99.2939
Ankle X Angle	0.4393	0.0663	84.90152	0.0648	84.6287
Ankle Y Angle	0.1162	0.0080	93.05514	0.0086	92.0554
Ankle Z Angle	0.0575	0.0003	99.36345	0.0004	99.3311
Foot X Angle	0.2817	0.0676	75.99602	0.0657	75.7708
Foot Y Angle	0.0122	2.4957	99.79646	0 .0001	99.7851
Foot Z Angle	0.2786	0.0145	94.76457	0.0138	94.7488

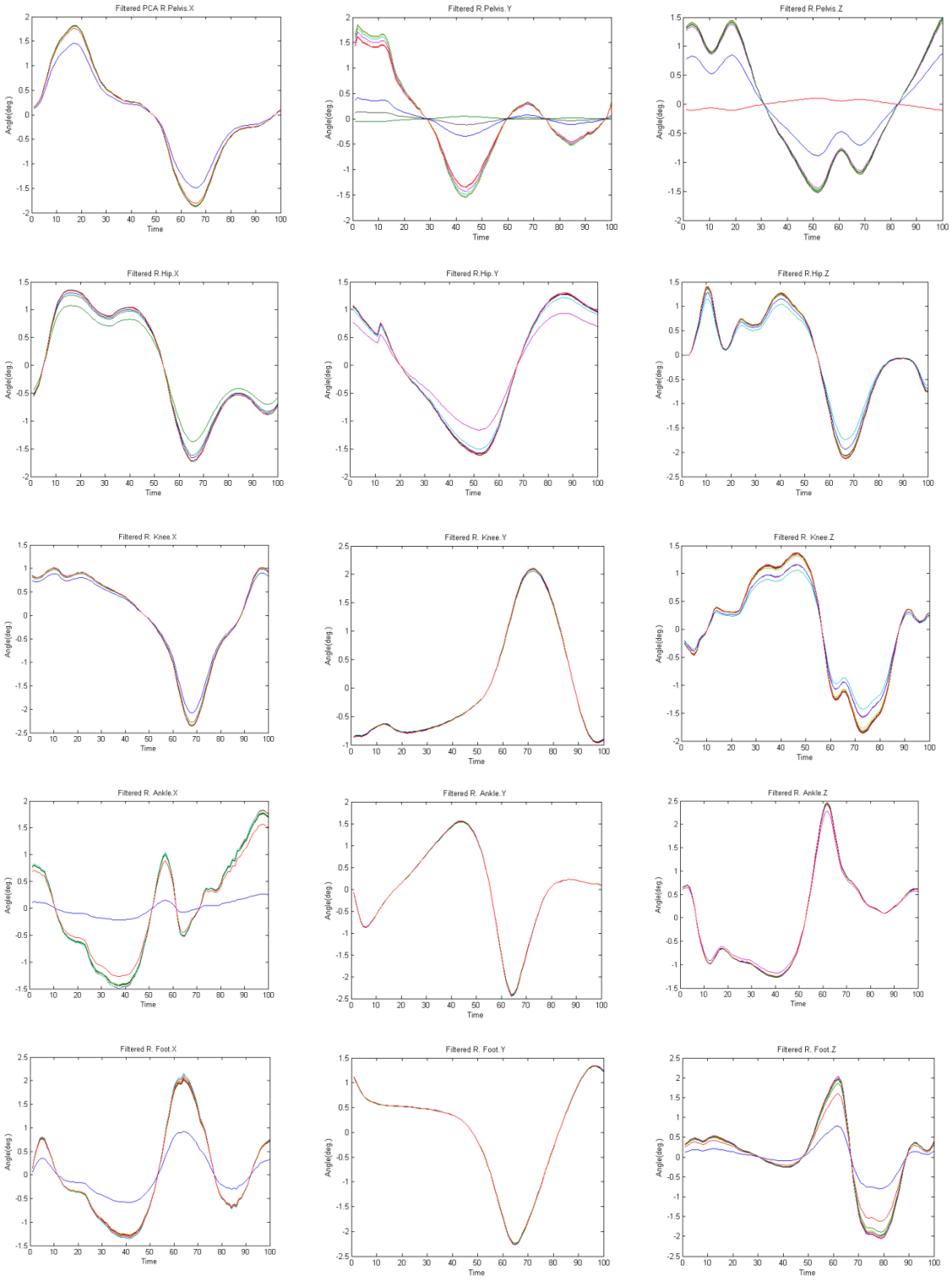

Figure 6.10, Kinematic variables of 10 marker wearing sessions. The normalized angles of the pelvis, hip, knee, ankle and foot in the X, Y, and Z planes are shown separately after applying the PCA filtering technique.

6.1.4. Applying SVF

Singular value filtering is applied on the data to examine its applicability to derived motion data. As explained in the background theory, Section 3.2.3, SVF is a PCA-based filter where the filter coefficients ω_k are adaptively determined as a function of a singular value spectrum of data. Filter design in SVF involves the construction of a weighting function that relates the singular value spectrum to the weighting coefficients. In the filter design the goal is to retain the main pattern of variation. In comparison to other filtering techniques there is no sharp cut-off threshold in SVF filtering. Therefore there is a sigmoid function to determine the selection of the PCs which are kept and those which are rejected. Results in figure 6.11 and table 6.3 show that fPCA outperforms SVF when considering mean variance after applying the technique, which in this case is 68.41 % on average.

Table 6.3, Comparison of SVF and fPCA for 200Hz

	Mean Variance Before	Mean Variance After SVF	Percentage of change	Mean Variance After fPCA	Percentage of change
Pelvis X Angle	0.0886	0.0190	70.4606	0.0025	97.0640
Pelvis Y Angle	0.7301	0.2640	58.4483	0.1779	74.6841
Pelvis Z Angle	0.1713	0.1695	48.4054	0.0052	96.8486
Hip X Angle	0.0808	0.0244	71.3214	0.0032	95.9264
Hip Y Angle	0.0496	0.0283	68.7315	0.0003	99.2778
Hip Z Angle	0.0884	0.0396	73.4604	0.0004	99.5557
Knee X Angle	0.0388	0.0138	73.0747	0.0004	99.0565
Knee Y Angle	0.0123	0.0034	74.7318	0.0001	99.6883
Knee Z Angle	0.0787	0.0521	72.4677	0.0005	99.2939
Ankle X Angle	0.4393	0.1225	58.8497	0.0648	84.6287
Ankle Y Angle	0.1162	0.0051	74.9150	0.0086	92.0554
Ankle Z Angle	0.0575	0.0139	74.3613	0.0004	99.3311
Foot X Angle	0.2817	0.0773	65.9965	0.0657	75.7708
Foot Y Angle	0.0122	0.0020	74.8733	0 .0001	99.7851
Foot Z Angle	0.2786	0.0940	66.1154	0.0138	94.7488

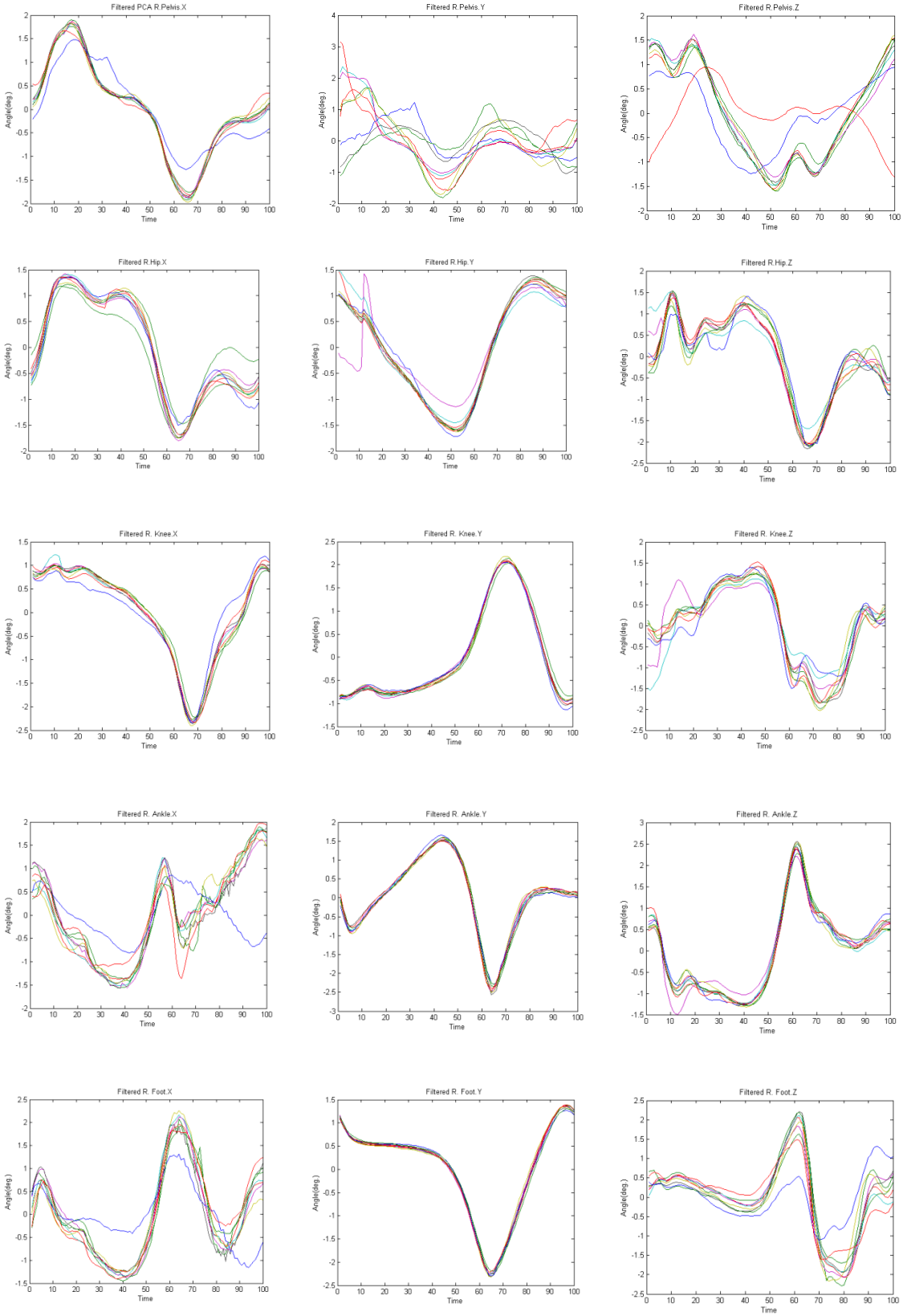

Figure 6.11, Kinematic variables of 10 marker wearing sessions. The normalized angles of the pelvis, hip, knee, ankle, and foot in the X, Y, and Z planes are shown separately after applying the SVF filtering technique.

6.1.5. Applying a priori-based signal separation

Among *a priori* based filters, we select the Butterworth IIR filter as a simple frequency based filter which is commonly used as a baseline for comparison in literature [128]. We use a second order low-pass digital Butterworth filter with normalized cut-off frequency of 0.1 Hz. Normalized cut-off frequencies take a variable in range of 0 to 1, where 1 corresponds to the Nyquist frequency.

Results in figure 6.12 show that FFT-based filtering techniques perform poorly on the motion data of our experiments, as expected. Frequency-based filtering techniques separate frequency components in the signal, which is not our concern. Our goal is to use a signal separation technique to separate the main pattern of variation in the data from residual components. Since FFT based filtering projects signals onto frequency components, then rejects some of them before returning back to the first domain, it cannot separate the main pattern of variation in the signal from the random variations, which is in the same frequency domain.

Table 6.4, Comparison of FFT-based and fPCA for 200Hz

	Mean Variance Before	Mean Variance After FFT	Percentage of change	Mean Variance After fPCA	Percentage of change
Pelvis X Angle	0.0886	0.0507	21.3747	0.0025	97.0640
Pelvis Y Angle	0.7301	0.5066	20.2806	0.1779	74.6841
Pelvis Z Angle	0.1713	0.2477	24.6207	0.0052	96.8486
Hip X Angle	0.0808	0.0731	14.1141	0.0032	95.9264
Hip Y Angle	0.0496	0.0617	31.8853	0.0003	99.2778
Hip Z Angle	0.0884	0.1078	27.6577	0.0004	99.5557
Knee X Angle	0.0388	0.0439	14.4604	0.0004	99.0565
Knee Y Angle	0.0123	0.0116	14.6224	0.0001	99.6883
Knee Z Angle	0.0787	0.1393	28.0419	0.0005	99.2939
Ankle X Angle	0.4393	0.2120	28.0419	0.0648	84.6287
Ankle Y Angle	0.1162	0.0167	18.0059	0.0086	92.0554
Ankle Z Angle	0.0575	0.0416	23.4541	0.0004	99.3311
Foot X Angle	0.2817	0.1540	32.2104	0.0657	75.7708
Foot Y Angle	0.0122	0.0072	10.3805	0 .0001	99.7851
Foot Z Angle	0.2786	0.2219	20.0677	0.0138	94.7488

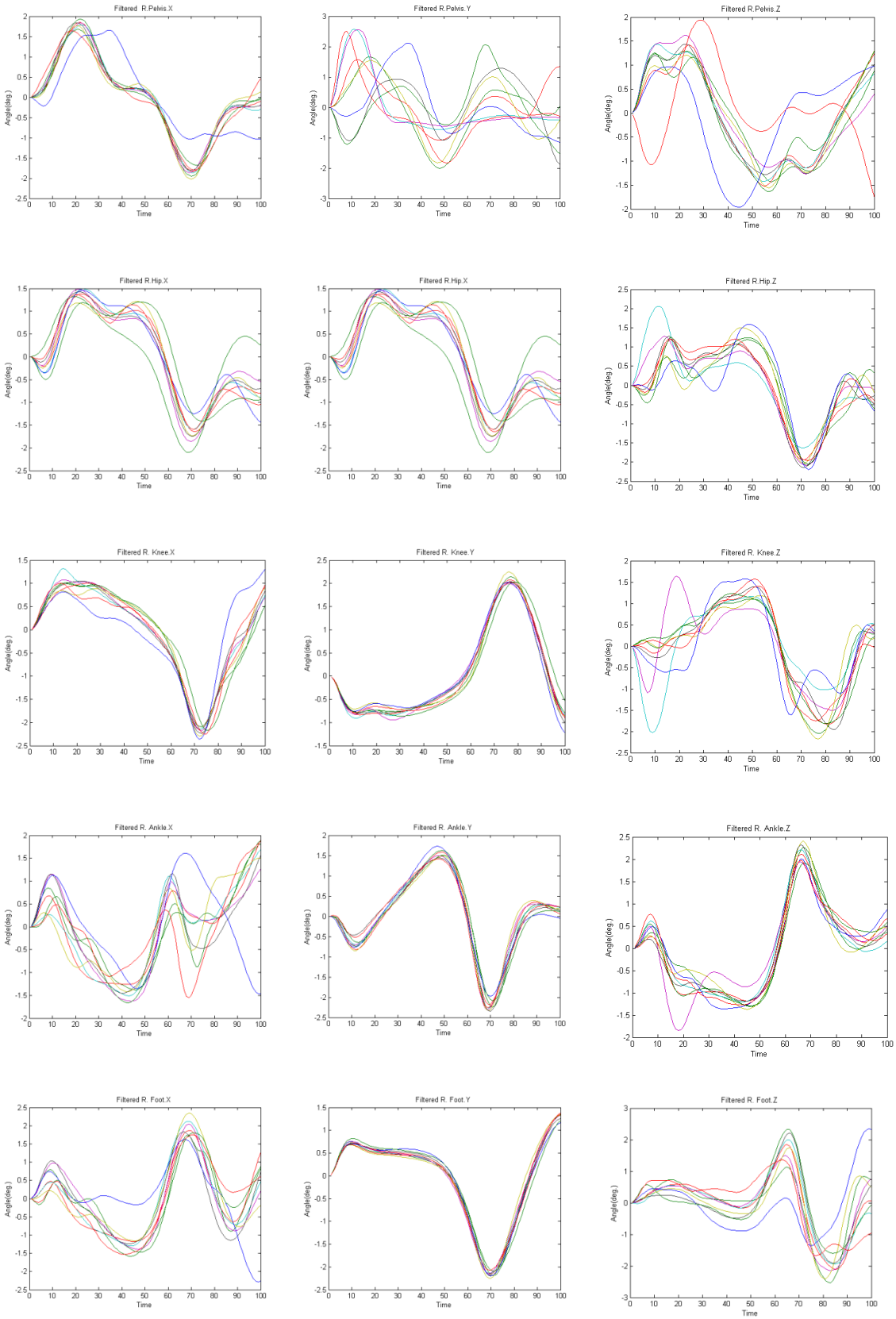

Figure 6.12, Kinematic variables of 10 marker wearing sessions. The normalized angles of the pelvis, hip, knee, ankle and foot in the X, Y, and Z planes are shown separately after applying the FFT-based filtering technique.

As it is shown in table 6.4, the mean percentage of change in motion data variance before and after applying the technique is 21.94%. In comparison to the fPCA filtering based technique, which has up to 93.85% variance reduction, performance of Butterworth IIR filter as one of *a priori* based techniques is poor. Figure 6.12 shows that the frequency based filtering technique removes high frequency components in the signal, which does not necessarily mean separating the main pattern of variation in the signals.

6.1.6. Comparison of applied signal separation techniques on the motion data

The percentage of mean improvement after applying different techniques is listed in table 6.5. The values in this table are for normalized data. Our goal is to separate out the effect of random changes in position of sensors from the main pattern of variation, in order to produce a more robust motion capture system in terms of sensors positioning. Results show that as random changes in the position of sensors are introduced, variation in motion data increases. Therefore we considered improvement as a percentage of variance changes in the data before and after applying the filtering techniques. Figure 6.13, 6.14 and 6.15 show the mean percentage of improvement in the X, Y and Z direction separately.

We can see that the performance of fPCA and PCA is similar. Other techniques perform worse, especially FFT-based filtering as it just removes the high frequency patterns in the data, and thus is unable to separate stochastic patterns from the deterministic one. The ICA based filtering technique causes more ripple in the data so it cannot separate the dominant mean of variation in derived angle motion data. The SVF-based filter perform worse than fPCA since the dominant mode of variance in the data in fPCA-based filtering is reflected in the first few principal components.

Table 6.5, Comparison of applied techniques on the data

	Percentage of change fPCA	Percentage of change PCA	Percentage of change ICA ML	Percentage of change ICA MS	Percentage of change SVF	Percentage of change FFT-based
Pelvis X Angle	97.0640	97.19680	87.0156	95.4528	70.4606	21.3747
Pelvis Y Angle	74.6841	74.97702	91.781	90.8344	58.4483	20.2806
Pelvis Z Angle	96.8486	97.45896	97.1859	63.7649	48.4054	24.6207
Hip X Angle	95.9264	95.72904	88.9328	93.4869	71.3214	14.1141
Hip Y Angle	99.2778	99.24085	95.667	89.279	68.7315	31.8853
Hip Z Angle	99.5557	99.51141	95.6847	92.3766	73.4604	27.6577
Knee X Angle	99.0565	99.16443	93.3104	68.7341	73.0747	14.4604
Knee Y Angle	99.6883	99.66164	93.7439	83.0264	74.7318	14.6224
Knee Z Angle	99.2939	99.31882	91.4962	88.8901	72.4677	28.0419
Ankle X Angle	84.6287	84.90152	61.2125	88.1125	58.8497	28.0419
Ankle Y Angle	92.0554	93.05514	88.0157	84.9202	74.9150	18.0059
Ankle Z Angle	99.3311	99.36345	89.6315	87.8444	74.3613	23.4541
Foot X Angle	75.7708	75.99602	85.8835	95.6491	65.9965	32.2104
Foot Y Angle	99.7851	99.79646	81.2256	84.0055	74.8733	10.3805
Foot Z Angle	94.7488	94.76457	90.9858	92.2106	66.1154	20.0677

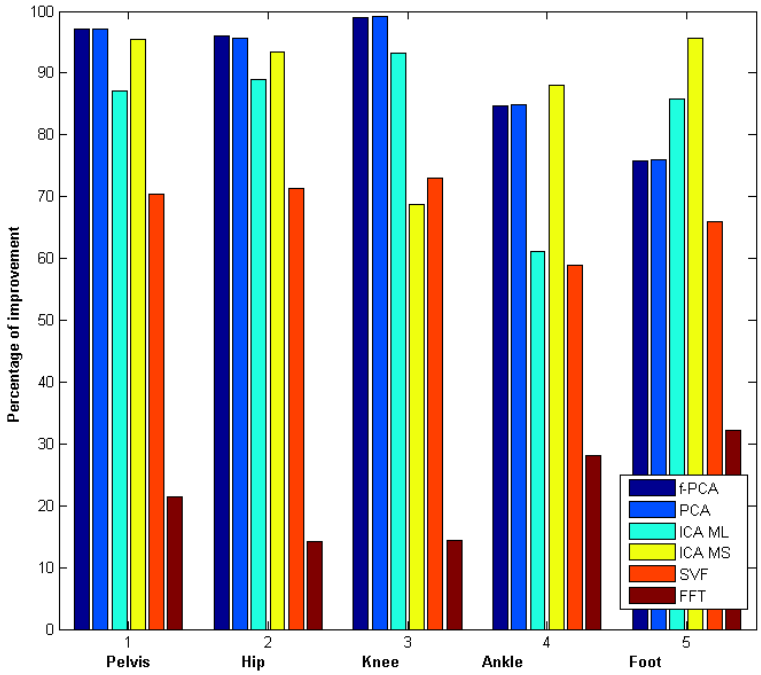

Figure 6.13, Mean percentage of improvement in the X direction

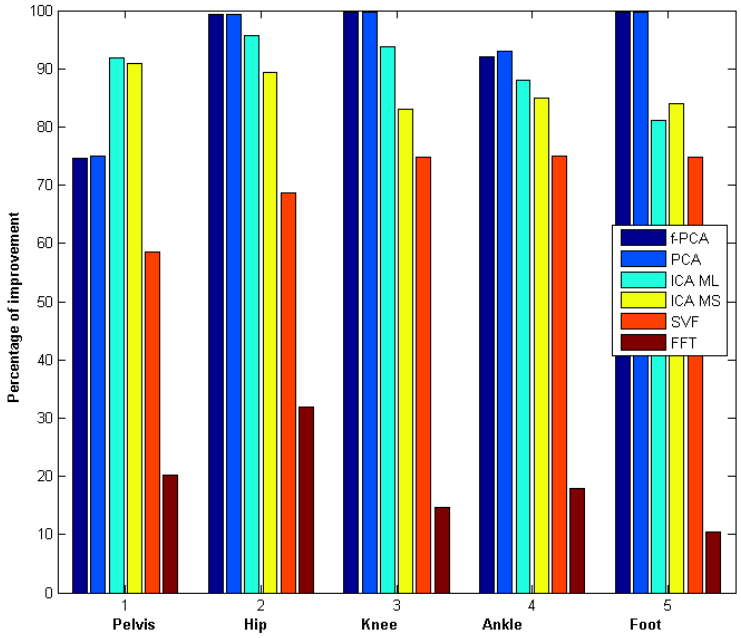

Figure 6.14, Mean percentage of improvement in the Y direction

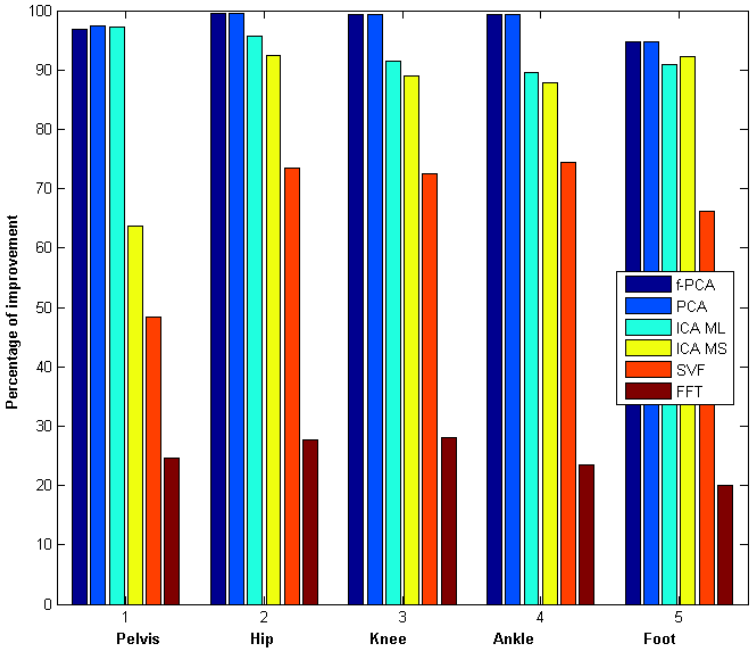

Figure 6.15, Mean percentage of improvement in the Z direction

The effect of applying the filtering techniques (fPCA, PCA, ICA ML, ICA MS, SVF and FFT based) on the right hip angle in the X direction for 10 subjects is shown in Fig 6.16 and Fig 6.17. We can see that for each subject fPCA and PCA schemes are better at separating the main pattern of variation in the motion data than other techniques. The figures confirm consistency in performance of the proposed signal separation technique in compensating for positional uncertainties for the all participants in our experiments. Our results indicate that for a 200 Hz sampling rate there is no discernible difference between fPCA and PCA. The mean change of variance across all joint angles in both cases is 94%. The results of the third experiment show the advantage of fPCA over PCA when the sampling rate is reduced. The experiments on the robot arm, set in a more controlled environment, are designed in second scenario to verify the findings measured in the first experiment. Results of the experiment are discussed in Section 6.2.

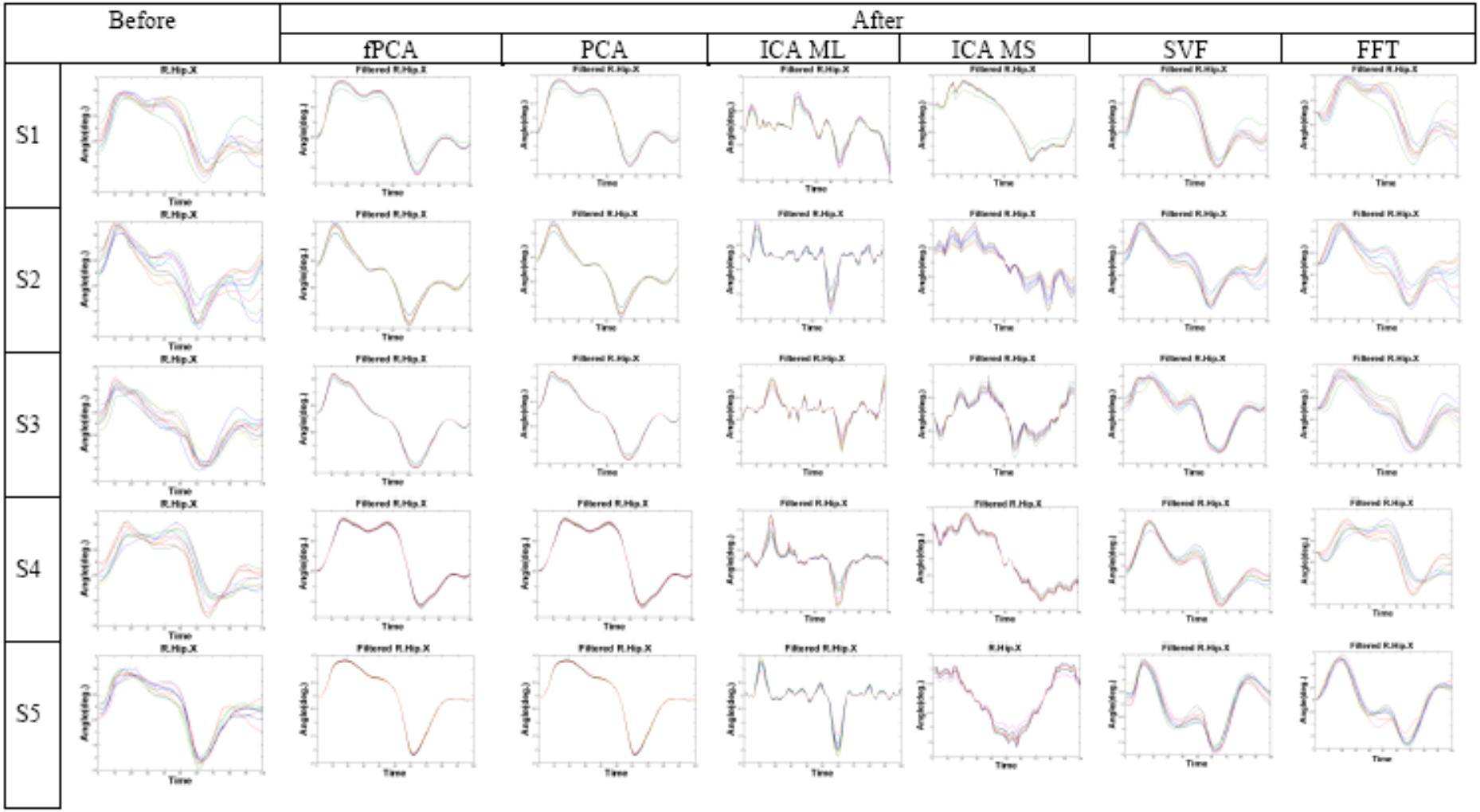

Figure 6.16, Right hip angle in X direction before and after applying fPCA, PCA, ICA ML, ICA MS, SVF and FFT for subject 1 (S1), 2(S2), 3(S3), 4(S4), and 5(S5) respectively.

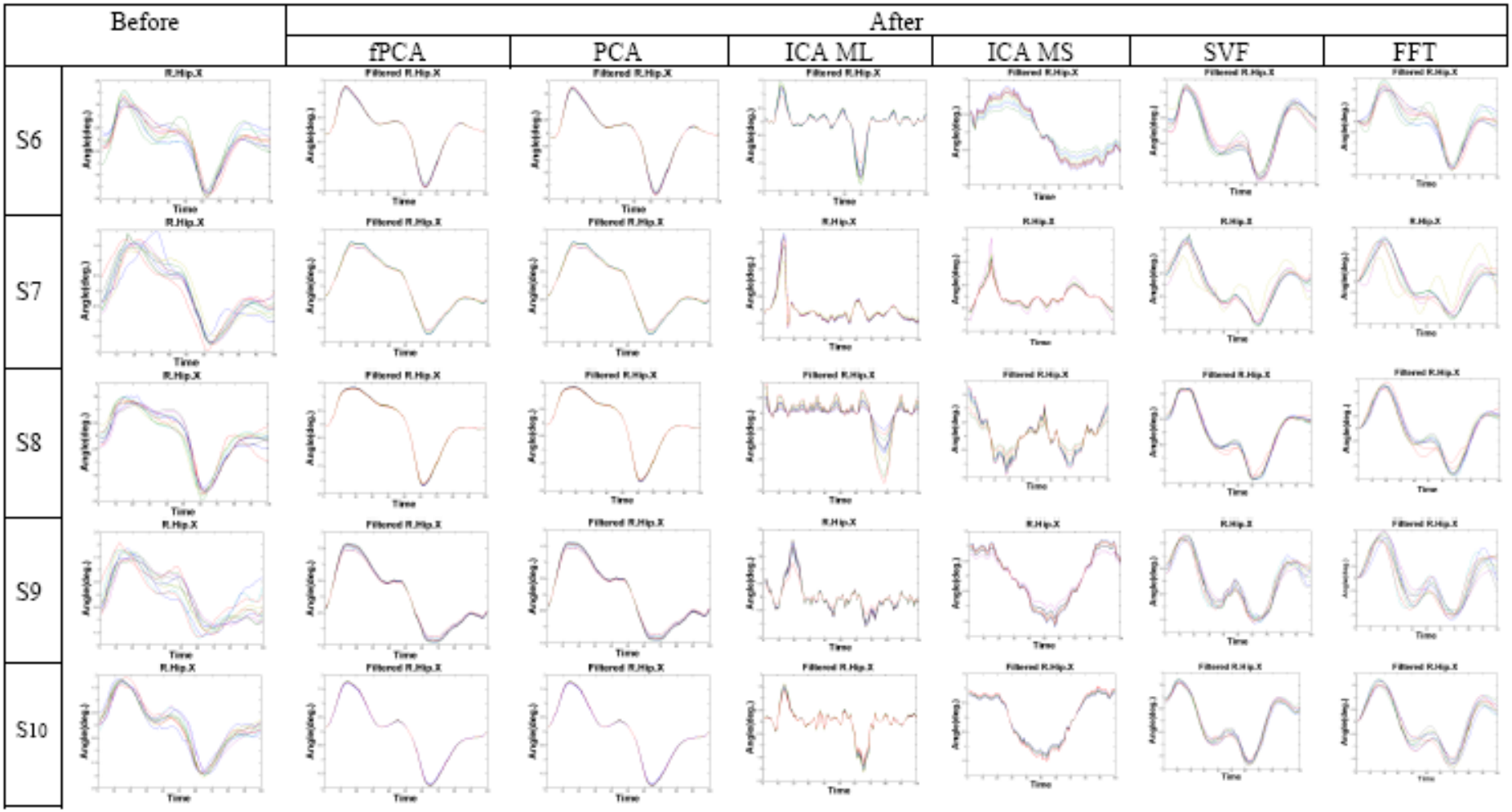

Figure 6.17, Right hip angle in X direction before and after applying fPCA, PCA, ICA ML, ICA MS, SVF and FFT for subject 6 (S6), 7(S7),8(S8), 9(S9), and 10(S10) respectively.

6.2. Second scenario, motion capture of the robot arm

To validate the applicability of fPCA as a technique for signal separation and compensation of the effect of random changes in sensors positioning, a second set of experiments was designed with a robot arm. The robot arm motion is captured in ten sessions of different marker wearing while randomly changing the position of sensors. In this experiment, all joints with the exception of the flexion-extension joint of the robot arm are constrained; therefore, our experiment considers a controlled movement with one degree of freedom.

We collect data from the cyclic movement of the robot arm whereby each cycle is identified as the interval from maximal flexion to the following maximal flexion of the unconstrained joint. Data cycles can be identified by using the Z axis position changes of Marker #1 which is the proximal marker to the grabber. Segmenting motion data into cycles almost always results in data cycles of different lengths due to differences in motion speed. We use a time normalization technique to obtain the same number of samples for all sessions.

In addition to the ten sessions of random marker position changes in a radius of 1 and 2cm from reference points, a marker wearing session was captured where markers are placed correctly on the reference points, exactly at the centre of joint rotation. The data collected from this session from target or reference motion data. We compare the captured data in the ten other motion wearing sessions to the reference motion data to measure the effect of inadvertent changes in the position of sensors on motion data.

We use variation from reference data as a comparison. Variation is calculated as summation of differences between data of motion capture sessions from the reference motion capture data, divided by the number of samples. Results show that the mean

variation of data from reference motion data due to random sensor misplacement in a radius of 1 and 2 cm are 2.02 and 5.69 degrees, respectively. Because of high accuracy of the robot arm we are sure that the variation in data from the reference motion data is only due to random changes in the position of sensors.

Table 6.6, Variation around the reference action with 1 and 2 cm random changes in the position of sensors before and after applying the technique.

	1 cm Random Changes	2 cm Random Changes
Variation before applying the technique(deg.)	2.02	5.69
Variation after applying the technique(deg.)	0.76	2.10

Results show that as the radius of the random changes in the position of sensors is increased, the variation in motion data from the reference data also increases, both before and after filtering, as shown in table 6.6. After applying the fPCA filtering technique we can see that the effect of random changes in position of sensors in the captured data is significantly reduced. The variation is reduced by 63% to 0.76 and 2.10 degrees for displacements of 1 and 2 cm, respectively. It is clear that despite the benefits of filtering, variation still increases with increased marker displacement, as expected.

6.3. Third scenario, motion capture of the robot arm at different frequencies

The third scenario is designed to examine the performance of functional principal component analysis over PCA whilst reducing the sampling rate of motion capture sessions. Reduction in the sampling rate has a benefit in lowering energy consumption and thus allowing for smaller sensor packaging. In our experiments, the

markers tracked by the scanner units are small infra-red light emitting diodes. The markers are powered from small drive units that contain sophisticated circuitry and respond to infra-red synchronising pulses sent out from the scanner units. When scanner unit starts to send out control signals to the marker drive units, the rate of current consumption rises to about 50mA in each unit. The capacity of the batteries in each of the drive unit is around 30mA hours.

The maximum measurement time depends on the sampling rate. For example, with 28 markers, the maximum measurement times are: 100s at 200Hz, 200s at 100Hz, 400s at 50Hz, 800s at 25Hz, ..., to 20000s at 1Hz [24]. That is, as the sampling rate reduces, the maximum measurement time increases. It means the marker drive unit battery can be used for a longer time by reducing sampling rate.

The life of a battery can be given either as the number of charge and discharge cycles that can be delivered or as the total lifetime in years. Factors which affect the battery life are the operating temperature, the discharge depth, and the charging regime. When the average current drain on the battery is lower, the discharge time or service life to the end of the battery life is longer [153]. The average current (I_{avg}) can be calculated by following equation.

$$I_{avg} = \frac{t_0 I_0 + t_1 I_1 + \cdots + t_n I_n}{t_0 + t_1 + \cdots + t_n} \tag{6-1}$$

In this equation $t_0, t_1, \ldots, t_n$ shows the time intervals that the battery provides current, $I_0, I_1, \ldots, I_n$, for the connected circuit. If the time intervals during which the battery provides current to the circuit are of a shorter duration, the battery can provide power for motion capture sessions over a longer period. It means that when there is a reduction in sampling rate of markers attached to the batteries, the total time during which the current will be needed will decrease. The smaller current requirement will enable longer motion capture intervals between battery recharging.

We consider different motion capture frequencies by $f_1, f_2, \dots, f_m$ where $f_1 < f_2 < \cdots < f_m$ where the time period of each frequency is shown by $T_1, T_2, \dots, T_m$. A period, $T_i = \frac{1}{f_i}$, is the time it takes for a signal to complete an on-and-off cycle. The duty cycle of each signal, which is the percentage of one period in which a signal is active, and where the batteries provide current for the sensor/marker circuit is given by $D_1, D_2, \dots, D_m$. The time that the signal is active in a period is shown by $t_1, t_2, \dots, t_m$. Therefore we can write: $D_i = \frac{t_i}{T_i} * 100$. Duty cycles can be used to describe the percentage time an electrical device is active.

In a system with different sampling frequencies, $f_1 < f_2 < \dots, < f_m$, as the sampling frequency decreases, the time period, $T_1, > T_2 > \dots > T_m$, increases. Considering the time that the signal is active in a period, is equal for all frequencies, $t_1 = t_2 = \dots = t_m$, increases in the time period reduce duty cycle, $D_1 < D_2 < \dots < D_m$. It means the percentage time of activity decreases. In a motion capture application where sensors send pulses to the detectors around them, when the percentage time of activity decreases, the total possible time of sending pulses from sensors attached to batteries will be increased. Therefore motion capture sessions can be performed for longer.

Assuming a specific time interval for motion capture in different sampling rates, and equal active time in each period for all frequencies, $t_i = t$, the total time that each sensor drain current from batteries is calculated by: $\sum_{i=0}^{K_i} t$. In a specific time interval of motion capture, for higher frequencies the number of active time slots, K_i, is higher. It can be written as $f_1 < f_2 < \dots < f_m$, then $K_1 < K_2 < \dots < K_m$. Therefore:

$$\sum_{i=1}^{K_i} t \quad < \sum_{j=1}^{K_j} t \quad \text{for} \quad K_i < K_j \tag{6-2}$$

which means the total time that the sensors drain current from batteries is greater in higher frequencies. According to equation (6-1) the service life of the battery or discharge time, which is dependant on average current drain, will be increased by decreasing the sampling rate.

In our experiment, we have ten sessions of marker wearing on the robot arm. In each of the sessions, the positions of sensors are randomly changed within a 2 cm radius from the landmarks. Motion data are captured using different frequencies for each marker wearing session. The variances of unprocessed and processed captured motion data sampled at different frequency rates are shown in table 6.7.

Table 6.7, Variance changes before and after applying PCA and fPCA

Frequency (Hz)	Before	After		Percentage of change (%)	
		PCA	fPCA	PCA	fPCA
200	7.6601	6.9826	4.8996	8.84	36.04
100	6.7113	6.1446	4.1501	8.44	38.16
50	6.1156	5.5804	3.6543	8.75	40.25
25	6.0807	5.0608	3.2224	16.77	47.01
10	10.8290	4.1176	2.6794	61.98	75.26
5	16.1705	7.8966	5.8977	51.17	63.53
2	41.5028	6.6151	4.7679	84.06	88.51
1	273.5735	25.4157	17.7664	90.71	93.51

Data variance of ten marker wearing sessions for each sampling frequency is calculated as the square of the standard deviation of each joint angle motion signal. As expected, the reduction in sampling rate increases the variance. Results show that above the Nyquist frequency the variance of in the same order of magnitude. Although there is an increase in the magnitude of variance from 100 Hz to 200 Hz, this is an insignificant

amount which could be due to high frequency noise. In motion capture, using a low pass filter usually compensates for these kinds of noise.

Further reduction below the Nyquist frequency causes a significant increase in the variance. However, applying the filtering technique compensates for the increase in the variance. The results show that fPCA outperforms PCA in terms of data variance (see graph in figure 6.17). Clearly, by applying the fPCA and PCA techniques we can compensate for the effect of random sensor positioning errors within the measured motion data, while achieving greater power efficiency.

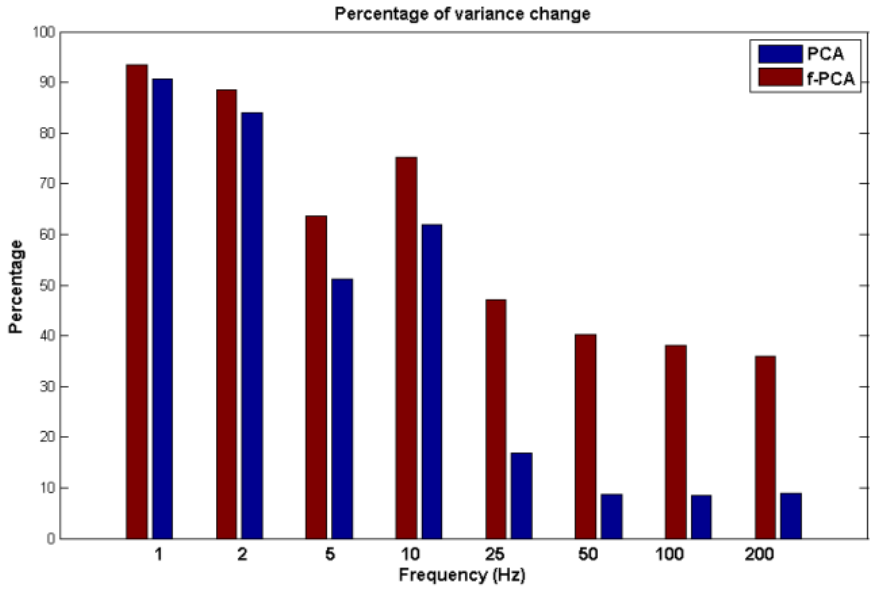

Figure 6.18, Percentage of variance change for different frequencies before and after applying PCA and fPCA based signal separation techniques.

It is shown in figure 6.17 that as the sampling rate reduces, the achievable improvement is increased. But by comparing PCA and fPCA filtering results we see that fPCA can better compensate for the variation due to random sensor displacements than PCA, and outperforms it. The advantage of fPCA over PCA is more obvious at higher frequency sampling rates. Figures 6.18 shows that fPCA works better than PCA,

although we see a change in trend of relative improvement below 25 Hz, which is due to sampling below the Nyquist frequency. The sampling rate must be at least twice the maximum frequency present in the signal (Nyquist rate), which is 20 Hz for motion data. This explains the reduction in relative improvement below 25 Hz. Taking all these results together, it is clear that the functional PCA-based signal separation techniques can be useful in removing unwanted variation in motion data and enable a more flexible assisted rehabilitation system for sensor-based motion capture.

7. Conclusion

In this thesis our focus is on flexibility of on-body sensing systems. Body sensing systems are used in wearable systems to capture different kinds of body parameters. Our main concern was on-body sensing systems for motion capture. Motion capture is the process of recording joint angles while a subject performs an action. Motion capture systems are widely used in animation, sports and rehabilitation. These systems are very sensitive to sensor positioning and they have bulky attachments to the user's body because of their large battery size. To have an ambulatory motion capture system we need to reduce the sensitivity of sensor positioning and consider wearer's comfort. These kinds of systems can then be used more easily in a home environment for the purpose of rehabilitation without expert supervision.

To reduce the sensitivity of these systems on sensor positioning, we studied the motion capture procedure of different on-body sensing systems. Undesirable variability challenge in motion data was reviewed as well. Specifically, the variability of kinematic measurements due to inadvertent sensor placement changes was discussed in this thesis. A literature review reveals that there is measurement variability due to the failure to place sensors accurately even when following the same placement protocol for each session. The variability can conceal important motion deviations and meaningful information can be lost. For the first time, a functional PCA-based technique has been applied on data from the designed experiment as a signal separation technique. The goal

is to compensate for the effects of sensor position changes and allow for a more robust set-up in terms of sensor placement.

Results show differences between similar repetitive actions with random marker position changes and how these variations can be compensated for by the proposed approach. By keeping the most dominant mode of variation, the salient motion pattern can be extracted from motion data of several marker-wearing sessions. By using a data driven filter, we can realistically derive accurate movement patterns, regardless of random errors associated with marker placement. Other signal separation techniques such as ICA, PCA, SVF and *a priori* filtering are applied on the data obtained from the experiments.

We have studied the technical challenges related to the portability of on-body sensing systems specifically in regard to motion capture applications. The motion of a robot arm was captured whilst "random" changes were made to the position of sensors for different sampling frequencies. Results show that despite the inherent accuracy of both the motion capture system and the repetitive robot arm movements, significant variation in the motion data can be introduced by relatively small random changes in the position of sensors as well as by the variation in the sampling frequency.

The overall size of the electronic component of wearable systems is generally dominated by the size of the batteries. Hence to have less bulky systems, sensors need to operate with low-power consumption. Reducing the sampling rate has the benefit of lowering the power consumption and therefore permits the use of smaller batteries. However, as the sampling frequency decreases, the variation in patterns of motion increases. Nevertheless we have shown that after applying fPCA signal processing techniques these variations as well as the variations due to errors in marker positioning,

can be substantially reduced, thus providing a step towards robust and flexible assisted rehabilitation.

In the first set of experiments ten subjects were recruited to take part in ten sessions of marker wearing each, during which the position of sensors are randomly changed to emulate variability present in the protocol execution. Results demonstrate the variation in the motion pattern of different marker wearing sessions due to the variation in sensor positioning. Results show the mean variance between curves typically decreases by 95.76%. The minimum averaged improvement is 88.15% for pelvic angle in the Y direction and the maximum improvement is 99.59% for knee angle in the Y direction. It can be readily determined that fPCA reduces variability associated with marker placement error. This was confirmed in the second experiment using robot arm. After applying the proposed filtering technique we show how these uncertainties could be compensated for in the human motion data.

It is shown that the percentage mean improvement after applying different filtering techniques is 93.9.0 %, 94.0%, 88.8%, 86.6%, 68.4%, and 21.9% for fPCA, PCA, ICA ML, ICA MS, SVF, FFT based filtering approach, respectively. We consider the improvement as a percentage of the variance changes before and after applying filtering. In the experiment, it is shown that the performance of fPCA and PCA is similar and for other techniques the performance is worse especially FFT based filtering. ICA based filtering causes more ripple in the data so it cannot separate out the dominant variation in the motion data.

In the second set of experiments, we validate the results obtained in the experiments on human subjects, using a robot arm. Results show that although both the motion capture system and the robot arm are very accurate in their operation, variation

in motion data exists when random sensor position changes are introduced. By applying fPCA based filtering technique we then show how these uncertainties can be compensated for. Variability in marker placement error was reduced by 63% in both 1 cm and 2 cm random marker placement error experiments.

In the third set of experiments the robot arm motion is captured at different frequencies simultaneously with sensor random displacement to investigate the advantage of the introduced signal separation technique when lowering the sampling frequency. Ten marker wearing sessions of the robot arm were captured at different frequencies. Results show that as the sampling frequency decreases, variations in the motion pattern increase. However, after applying the signal processing technique, the variations are significantly reduced from 30.04% for 200Hz to 93.51% for 1 Hz.

The proposed signal processing approach adds processing complexity to the motion capture procedure of the order of $2(O(n\log n) + O\left(\log(nm^2)\right) + O(m^3))$ as discussed in Chapter4. However, since on-body sensing systems usually have a central system for analysing the data that is located far from the body and connected to a powerful processing unit with a connection to an abundant electricity supply, processing complexity is not a challenge in this case.

We used a robot arm as well as human subject movements to generate motion data, which are captured by an active marker-based motion capture system. The reason for selecting them is that both the motion capture system and the fact that the robot arm is very accurate in its operation. Marker based motion capture is considered as the “gold standard” of motion capture technologies. We consider joint angles as motion data in our analysis. It has the benefit of making the results independent from the technology used to measure motion. Nevertheless, the proposed approach can be generalized for

other motion capture technologies and it can be applied to motion data of other kinds. The analysis is also independent from where the reference coordinate system is, so the subject can move anywhere within the range of the motion capture system.

The suggested signal processing approach is used as a post-processing technique. It can be used in motion capture laboratories for analysing the data and then passing the data filtered of undesirable variations to clinicians to decide about the treatment and for their clinical records. It also can be used for motion capture systems at home for the purpose of rehabilitation. After applying the technique on captured data, results can be sent to the clinicians to assess whether there has been any genuine improvement in the patient's movement.

This thesis provides a step towards flexibility of body sensing systems by using signal processing techniques. Flexible systems can be deployed for ambulatory motion capture, such as within a context of home-based rehabilitation where the potential for placement errors is greater, which in turn can affect the way that movement is interpreted and feedback given to the user.

7.1. Future work

As we did not have access to other motion capture systems, our investigations are thus limited to the active marker-based *Codamotion*. Going forward, the next step would be to test the introduced technique on other motion capture technologies to validate the generality of this filtering approach.

The proposed technique is computationally intensive and as such is potentially limited to offline processing. This is a limitation for applicability of the proposed approach in applications which require real-time feedback to the user, for example, in

real-time motor-training applications with biofeedback. Implementing the technique for online applications remains another step for the future work.

In this thesis, the motion capture focus was on human gait and a robot arm movement. As the robot arm motion was analogous to flexion-extension of a human joint, we can generalize our findings for other human body joints' motion. We suggest applying and investigating the introduced signal processing approach for other movements to validate its applicability for these situations.

The effects of "smoothing" on pathological motion data may require further investigation into the technique's applicability in broader clinical scenarios. This would require studies on patients. The experiments need several participants to validate the applicability of the technique. We did not have access to patients to take part in our experiments, so the next step could be to validate the approach on patients with known pathological characteristics rather than healthy subjects.

Exploring potential applicability of the proposed approach in other fields where the signals are mixed with unwanted sources of variation can be another step for future work. For example wireless channel response measurements need to be cleaned from effect of unwanted variation in data due to scattering in measurement environment (see Appendix C). The propose approach does not need explicit knowledge of the probability density of the data as long as the first and second order statistics are known or can be estimated from the samples. Therefore it can be widely used in adaptive filtering applications to remove unwanted variation in data or separate different sources of variation provided that the sources are uncorrelated.

In summary, the proposed post-processing technique can compensate for uncertainties due to sensor positional changes, whilst allowing greater energy efficiency

of the sensors, thus enabling improved flexibility and usability of on-body sensing. The results of applying the proposed post-processing technique on the motion data from designed experiments validate its benefit and applicability.

8. References

[1] A. Pantelopoulos and N. Bourbakis, "A survey on wearable sensor-based systems for health monitoring and prognosis," *IEEE Transactions on Systems, Man, and Cybernetics,* vol. 40, no. 1, pp. 1-12, 2010.

[2] P. Bonato, "Wearable sensors/systems and their impact on biomedical engineering," *IEEE Engineering in Medicine and Biology Magazine,* pp. 18-20, 2003.

[3] M. A. Hanson, H. Powell Jr and A. T. Barth, "Body area sensor networks: challenges and opportunities," *Computer,* pp. 58-65, January 2009.

[4] S. Tang, "Recent developments in flexible wearable electronics for monitoring applications," *Transactions of the Institute of Measurement and Control,* vol. 29, pp. 283-300, 2007.

[5] B. Latre, B. Braem, I. Moerman, C. Blondia and P. Demeester, "A survey on wireless body area networks," *Wireless Networks,* vol. 17, pp. 1-18, 2011.

[6] M. Chen, S. Gonzalez, A. Vasilakos, H. Cao and V. Leung, "Body area networks: a survey," *Mobile Networks and Applications,* vol. 16, no. 2, pp. 171-193, 2010.

[7] D. Cook and W. Song, "Ambient intelligence and wearable computing: Sensors on the body, in the home,and beyond," *Journal of Ambient Intelligence and Smart Environments,* vol. 1, pp. 1-4, 2009.

[8] D. Curtis, J. Bailey, E. Pino, T. Stair and S. Vinterbo, "Using ambient intelligence for physiological monitoring," *Journal of Ambient Intelligence and Smart Envirnments,* vol. 1, pp. 129-142, 2009.

[9] S. Park and S. Jayaraman, "Wearable sensor network: a framework for harnessing ambient intelligence," *Journal of Ambient Intelligence and Smart Envirnment,* vol. 1, pp. 117-128, 2009.

[10] A. Yang, R. Jafari, S. Sastry and R. Bajcsy, "Distributed recognition of human actions using wearable motion sensor network," *Journal of Ambient Intelligence and Smart Envirnment,* vol. 1, pp. 1-5, 2009.

[11] H. Huang, S. Wolf and J. He, "Recent developments in biofeedback for neuromotor rehabilitation," *Journal of NeuroEngineering and rehabilitation,* pp. 3-11, 2006.

[12] D. Wade and B. Jong, “Recent advances in rehabilitation,” *Biomedical Journal,* vol. 320, pp. 1385-1388, 2000.

[13] R. Baker, “Gait analysis methods in rehabilitation,” *Journal of NeuroEngineering and Rehabilitation,* 2006.

[14] D. Vlasic, R. Adelsberg, G. Vannucci, J. Barnwell, M. Gross, W. Matusik and J. Popovic, “Practical Motion Capture in Everyday Surroundings,” *ACM Transactions on Graphics,* vol. 26, no. 3, pp. 1-35, 2007.

[15] G. Dona, E. Preatoni, C. Cobelli, R. Rodano and A. J. Harrison, “Application of functional principal component analysis in race walking: an emerging methodology,” *Sports Biomechanics,* pp. 284-301, 2009.

[16] H. Ghasemzadeh, V. Loseu and R. Jafari, “Wearable coach for sport training: a quantitative model to evaluate wrist-rotation in golf,” *Journal of Ambient Intelligence and Smart Envirnment,* vol. 1, pp. 173-184, 2009.

[17] E. Jovanov, C. Yang and Y. Zhang, “Body sensor networks: from theory to emerging applications,” *IEEE Transactions on Information Technology in Biomedicne,* vol. 13, no. 6, pp. 859-863, 2009.

[18] J. Knight, D. Deen-Williams, T. Arvanitis, C. Baber, S. Sotiriou, S. Anastopoulou and M. Gargalakos, “Assessing the wearability of wearable computers,” in *10th IEEE International Symposium on Wearable Computers,*, Montreux, Switzerland, 2006.

[19] H. Harms, O. Amft and G. Tröster, “Does loose fitting matter?Predicting sensor performance in smart garments,” in *Proceedings of the 7th International Conference on Body Area Networks* , Oslo, Norway, 2012.

[20] H. Harms, O. Amft and G. Troster, “Influence of a loose-fitting sensing garment on posture recognition in rehabilitation,” in *IEEE Biomedical Circuits and Systems Conference*, Baltimore, MD, 2008.

[21] R. Haratian, R. Twycross-Lewis and T. Timotijevic, “Towards felexibility in sensor placement for motion capture systems,” *IEEE Sensors Journal,* vol. 14, no. 3, pp. 701-709, 2014.

[22] H. Sveistrup, “Motor rehabilitation using virtual reality,” *Journal of NeuroEngineering and Rehabilitation,* vol. 1, pp. 1-10, 2004.

[23] R. Kenyon, J. Leigh and E. Keshner, “Considerations for the future development of virtual technology as a rehabilitation tool,” *Journal of NeuroEngineering and Rehabilitation,* vol. 1, pp. 1-13, 2004.

[24] Codamotion user guide, Charnwood Dynamics Ltd, 2005.

[25] J. Zhao and N. Badler, ““Inverse kinematics positioning using nonlinear programming for highly articulated figures,” *ACM Transactions on Graphics,* vol. 13, no. 4, pp. 313-336, 1994.

[26] B. Bodenheimer, C. Rose, S. Rosenthal and J. Pella, “The process of motion capture: dealing with the data,” *Eurographics,* 1997.

[27] P. Geffen, “Dynamic sitting,” Universiteit Twente, 2009.

[28] M. Horsman, “The twente lower extremity model, consistent dynamic simulation of human locomotor apparant,” The Netherlands, 2007.

[29] J. Hodgins, W. Wooten, D. Brogan and J. Obrien, “Animating Human Athletics,” in *22nd annual conference on Computer graphics and interactive techniques*, New York, NY, USA, 1995.

[30] J. Hamill and W. Selby, Three dimensional kinematics in Research Methods in Biomechanics, Human Kinetics, Champaign: IL, 2004.

[31] M. Silaghi, R. Plankers, R. Boulic, P. Fua and D. Thalmann, “Local and global skeleton fitting techniques for optimal motion capture,” in *IFIP CapTech, LNCS Springer Verlag Heidelberg*, Geneva, Nov. 1998.

[32] H. Zhou and H. Hu, “Human motion tracking for rehabilitation - a survey,” *Biomedical Signal Processing and Control,* vol. 3, no. 1, pp. 1-18, 2008.

[33] T. Moeslund, A. Hilton and V. Kruger, “A survey of advances in vision-based human motion capture and analysis,” *Computer Vision and Image Understanding,* vol. 104, pp. 90-126, 2006.

[34] D. Roetenberg, H. Luinge and P. Slycke, “Xsense MVN: full 6DOF human motion tracking using miniature inertial sensors,” *Xsens Technologies,* pp. 1-7, 2009.

[35] K. Aminian and B. Najafi, “Capturing human motion using body fixed sensors: outdoor measurement and clinical applications,” *Computer Animation and Virtual Worlds,* vol. 15, pp. 79-94, 2004.

[36] J. Wang and H. Lee, “Recognition of human action using motion capture data and support vector machine,” in *World Congress on Software Engineering*, 2009.

[37] V. Zorden and N. Horst, “Mapping optical motion capture data to skelal motion using a phusical model,” in *Eurographics/SIGGRAPH Symposium on Computer Annimation*, 2003.

[38] R. Bartlett, Introduction to sports biomechanics, analysing human movement patterns, New York: Routledge, 2007.

[39] G. Wu, F. Helm, H. Veeger and M. Makhdous, “ISB recommendation on definitions of joint coordinate system of various joints for the reporting of human joint motion—part I: ankle, hip, and spine,” *Journal of Biomechanics,* vol. 35, pp. 543-548, 2002.

[40] G. Wu, F. Helm, H. Veeger and M. Makhdous, “ISB recommendation on definitions of joint coordinate systems of various joints for the reporting of human joint motion—Part II: shoulder, elbow, wrist and hand,” *Journal of Biomechanics,* vol. 38, p. 981–992, 2005.

[41] M. Schepers, “Ambulatory assesment of human body kinematic and kinetics,” Universiteit Twente, 2009.

[42] H. Luing, “Inertial sensing of human movement,” PhD Thesis in Twente University Press, 2002.

[43] D. Giansanti, V. Macellari, G. Maccioni and V. Macellari, “The development and test of a device for the reconstruction of 3-D position and orientation by means of a kinematic sensor assembly with rate gyroscopes and accelerometers,” *IEEE Transactions on Biomedical Engineering,* vol. 52, no. 7, pp. 1271-1277, 2005.

[44] D. Roetenberg, P. Slycke and P. Veltink, “Ambulatory position and orientation tracking fusing magnetic and inertial sensing,” *IEEE Transactions on Biomedical Engineering,* vol. 54, no. 5, pp. 883-890, 2007.

[45] H. Fourati, N. Manamanni, L. Afilal and Y. Handrich, “A nonlinear filtering approach for the attitudeand dynamic body acceleration estimation,” *IEEE Sensors Journal,* vol. 11, no. 1, pp. 233-244, 2011.

[46] H. Schepers, D. Rotenberg and P. Veltink, “Ambulatory human motion tracking by fusion of inertial and magnetic sensing with adaptive actuation,” *Med Biol Eng,* vol. 48, pp. 27-37, 2010.

[47] H. Schepers and P. Veltink, “Stochastic magnetic measurement model for relative positions and orientation estimation,” *Measurment Science and Technooigy,* vol. 21, pp. 1-10, 2010.

[48] D. Rotenberg, “Inertial and magnetic sensing of human motion,” Ubiversity of Twente, 2006.

[49] H. Luinge, D. Rotenberg and P. Slyeke, “Inertial sensor kinematics coupling,” Patent Application Publication, 2011.

[50] R. Hyde, L. Ketteringham, S. Neild and R. Jones, “Estimation of upper-limb orientation based on accelerometer and gyroscope measurements,” *IEEE Transactions on Biomedical Engineering,* vol. 55, no. 2, pp. 746-754, 2008.

[51] Z. Zhang, W. Wong and J. Wu, “Ubiquitous human upper-limb motion estimation using wearable sensors,” *IEEE Transactions on Information Technology in Biomedicine,* vol. 15, no. 4, pp. 513-521, 2011.

[52] R. Senden, B. Grimma, I. Heyligers, H. Savelberg and K. Meijer, “Acceleration-based gait test for healthy subjects: Reliability and reference data,” *Gait and Posture,* vol. 30, pp. 192-196, 2009.

[53] J. Ward, P. Lukowicz, G. Tro¨ ster and T. Starner, “Activity Recognition of Assembly Tasks Using Body-Worn Microphones and Accelerometers,” *IEEE Transactions on Pattern Analysis and Machine Inteligence,* vol. 28, no. 10, pp. 1553-1567, 2006.

[54] L. Bao and S. Intille, “Activity recognition from user-annotated acceleration data,” *Pervasive Computing,* vol. 3001, pp. 1-17, 2004.

[55] N. Krishnan, C. Juillard, D. Colbery and S. Panchananthan, “Recognition of hand movements using wearable accelorometer,” *Journal of Ambient Intelligence and Smart Envirnment,* vol. 1, pp. 143-155, 2009.

[56] H. Harms, O. Amft, D. Roggen and G. Troster, “Rapid prototyping of smart garments for activity-aware applications,” *Journal of Ambient Intelligence and Smart Environment,* vol. 1, pp. 1-15, 2009.

[57] H. Harms, O. Amft, R. Winkler, J. Schumn, M. Kusserow and G. Troster, “ETHOS: miniature orientation sensor for wearable human motion analysis,” in *IEEE sensors conference*, 2010.

[58] A. Salarian, H. Russmann, F. Vingerhoets, P. Burkhard and K. Aminian, “Ambulatory monitoring of physical activities in patient with Parkinson's diseas,” *IEEE Transactions on Biomedical Engineering,* vol. 54, no. 12, pp. 2296-2299, 2007.

[59] P. Jeannet, K. Aminian, C. Bloetzer, B. Najafi and A. Iobescue, “Continous monitoring and quantification of multiple parameters of daily physical activity in ambulatory Duchenne muscular dystrophy patients,” *Official Journal of the European Pediatric Neurology Society,* vol. 15, pp. 40-47, 2011.

[60] M. Hanson, H. Powell Jr, A. Barth, J. Latch and M. Pearce, “Neural network gait classification for on body inertial sensors,” in *Body Area Sensor Network*, 2009.

[61] S. Patel, K. Lorincz, R. Hughes and N. Huggins, “Monitoring Motor Fluctuations in Patients With Parkinson’s Disease Using Wearable Sensors,” *IEEE Transactions on Information Technology in Biomedicine,* vol. 13, no. 6, pp. 864-873, 2009.

[62] T. Chau, S. Young and S. Redekop, “Managing variability in the summary and comparison of gait data,” *Journal of NeuroEngineering and Rehabilitation,* 2005.

[63] G. Gorton, D. Hebert and M. Gannotti, “Assessment of the kinematic variability among 12 motion analysis laboratories,” *Gait and Posture,* vol. 29, pp. 398-402, 2009.

[64] S. William and A. Salleo, Flexible Electronics Materials and Applications, Springer, 2009.

[65] R. B. Katragadda and Y. Xu, “A novel intelligent textile technology based on silicon flexible skins,” *Sensors and Actuators,* vol. 143, pp. 169-174, 2008.

[66] M. H. Schwartz, J. P. Trost and R. A. Wervey, “Measurement and management of errors in quantitative gait data,” *Gait and Posture,* p. 196–203, 2004.

[67] U. Croce, A. Leardini, L. Chiari and A. Cappozzo, “Human movement analysis using streophotogrammetry part 4: assessment of anatomical landmark mislocation and its effect on joint kinematics,” *Gait and Posture,* vol. 21, pp. 226-237, 2005.

[68] A. Cappozzo, U. Croce, A. Leardini and L. Chiari, “Human movement analysis using streophotogrammetry part 1: theoretical background,” *Gait and Posture,* vol. 21, pp. 186-196, 2005.

[69] L. Chiari, U. Croce, A. Leardini and A. Cappozzo, “Human movement analysis using streophotogrammetry part 2: Instrumental errors,” *Gait and Posture,* vol. 21, pp. 197-211, 2005.

[70] A. Leardini, L. Chiari, U. Croce and A. Cappozzo, “Human movement analysis using streophotogrammetry part 3: soft tissue artifact assesment and compensation,” *Gait and Posture,* vol. 21, pp. 212-225, 2005.

[71] L. Lamoreu, “Errors in tight axial rotation measurment using skin mounted markers,” in *International society of Biomecbanics XIII Congress*, Sanfrancisco, USA, 1991.

[72] U. Groce, A. Cappozzo and D. Kerrigan, “Pelvis and lower limb anatomical landmark calibration precision and its propagation to bone geometry and joint angles,” *Med Biol Eng Comp,* vol. 37, pp. 1029-1034, 1999.

[73] R. Stagni, A. Leardini, A. Cappozzo, M. Bendetti and A. Cappello, “Effect of hip joint centre mislocation on gait analysis results,” *Journal of Biomechanics,* vol. 33, pp. 1479-1487, 2000.

[74] S. Piazza and P. Cavanagh, “Measurment of the screw-home motion of the knee is sensitive to

errors in axis alignment," *Journal of Biomechanics,* vol. 33, pp. 1029-1034, 2000.

[75] J. Holden and S. Stanhope, "The effect of variation in knee center location estimates on net knee joint moments," *Gait and Posture,* vol. 7, pp. 1-6, 1998.

[76] R. Baker, J. McGinleya, M. Schwartz, S. Beynon, A. Rozumalski, H. Graham and O. Tirosh, "The gait profile score and movement analysis profile," *Gait and Posture,* vol. 30, no. 3, pp. 265-269, 2009.

[77] R. Abel, M. Rupp and D. Sutherland, "Quantifying the variability of a complex motor task specifically studying the gait of dyskinetic," *Gait and Posture,* vol. 17, pp. 50-58, 2003.

[78] K. Noonan, K. Halliday, R. Browne and K. Kayes, "Interobserver variability of gait analysis in patients with serebral plasy," *Journal of Pediatric Orthopaedics,* vol. 23, no. 3, pp. 279-287, 2003.

[79] M. Kurtz and N. Stergiou, "The spanning set indicates that variabilityduring the stance period of running is affected by footwear," *Gait and Posture,* vol. 17, no. 2, pp. 132-135, 2003.

[80] G. Chen and E. Rodriguez-Villegas, "System-Level Design Trade-offs for Truly Wearable Wireless Medical Devices," in *32nd Annual International Conference of the IEEE EMBS*, Buenos Aires, Argentina, 2010.

[81] L. Beneni and G. Micheli, "System level power optimization: techniques and tools," *ACM Transactions on Design Automation of Electronic Systems,* vol. 5, no. 2, pp. 115-192, 2000.

[82] C. Figueiredo, K. Becher, K. Hoffmann and P. Mendes, "Low power wireless acquisition module for wearable health monitoring systems," in *32nd Annual International Conference of the IEEE EMBS*, Buenos Aires_Argentina, 2010.

[83] M. Altini, S. Din, S. Schachter, J. Penders and P. Bonato, "A low power multi modal body sensor network with application to epileptic seizure monitoring," in *33rd Annual International Conference of the IEEE EMBS*, Boston-USA, 2011.

[84] W. Marnane, S. Faul, C. Bleakley, R. Conway, E. Jones, E. Popovici, M. Solaz , F. Morgan and K. Patel, "Energy efficient on-sensor processing in body sensor networks," in *32nd Annual International Conference of the IEEE EMBS*, Buenos Aires - Argentina, 2010.

[85] J. Huang, L. Wang, L. Chen and Y. Zhang, "A low power wearable transceiver for human body communication," in *31st Annual International Conference of the IEEE EMBS* , Minneapolise-USA, 2009.

[86] D. Peng, J. Zhang and L. Wang, "Expremental result on wireless power management microsystem for endoscopic capsule robot," in *IEEE International Conference on Biomedical and Health Informatics*, Hong Kong-china, 2012.

[87] O. Bernal, K. Choe, P. Gopalakrishnan, H. Cheng, K. Krishna, D. Nuttman, N. Axelrod and M. Je, "A low power high performance accelerometer ASIC for high end medical motion sensing," in *32nd Annual International Conference of the IEEE EMBS* , Buenos Aires - Argentina, 2010.

[88] J. Penders, V. Pop, L. caballero, J. Molengraft, R. Schaijk, R. Vullers and C. Hoof, "Power optimization in body sensor networks: the case of an autonomous wireless EMG sensor powered by PV cells," in *32nd Annual International Conference of the IEEE EMBS*, Buenos Aires - Argentina,

2010.

[89] C. Manthuna, T. Donnell, R. Martinez-catala, J. Rohan and B. Flynn, “Energy scavenging for long-term deployable wireless sensor networks,” *The International Journal of Pure and Applied Analytical Chemistry,* vol. 75, pp. 613-623, 2008.

[90] E. Jovanov, “A survey of power efficient technologies for wireless body area networks,” in *30th Annual International Conference of the IEEE EMBS* , vancuare-Canada, 2008.

[91] A. kailas, “Power allocation strategies to minimize energy consumption in wireless body area networks,” in *33rd Annual Conference of the IEEE EMBS* , Boston - USA, 2011.

[92] B. Lamichhane, S. Mudda, F. Regazzoni and A. Puiatti, “LEXCOMM: a low energy, secure and flexible communication protocol for a heterogenouse body sensor network,” in *International Conference on Biomedical and Health Informatics*, Hong Kong-China, 2012.

[93] H. Yoo, N. Cho and J. Yoo, “Low energy werable body sensor network,” in *31st Annual International Conference of the IEEE EMBS*, Minneapolis - USA, 2009.

[94] Y. Hamouda and C. Phillips, “Adaptive sampling for energy-efficient collaborative multi-target tracking in wireless sensor networks,” *IET Wireless Sensor Systems,* vol. 1, no. 1, pp. 15-25, 2010.

[95] R. Reger and J. T. Taylor, “An adaptive sampling system for sensor nodes in body area networks,” *IEEE Transactions on Neural Systems and Relabilitation,* pp. 183-189, April 2009.

[96] L. Au, M. Batalin, T. Stathopoulos, A. Bui and W. Kiase, “Episodic sampling: towards energy efficient patient monitoring with werable sensors,” in *31st Annual International Conference of the IEEE EMBS*, Miniapolis-USA, 2009.

[97] R. Rendic, L. Gaura, J. Brusey and J. Kemp, “Wearable posture recognition systems: factors affecting performance,” in *International Conference on Biomedical and Health Informatics*, Hong Kong-China, 2012.

[98] C. Hsu, W. Wang and C. Luo, “The power efficient biomedical acquisition system by variable resolution sigma delta modulator,” in *29th Annual International Conference of the IEEE EMBS*, Lyon-France, 2007.

[99] A. Roy and J. Doherty, “Improved signal analysis performance at low sampling rates using raised cosine empirical mode decomposition,” *Electronics Letters,* vol. 46, no. 2, pp. 1-2, 2010.

[100] M. Pawlak and U. Stadtmüller, “Signal Sampling and Recovery Under Dependent Errors,” *IEEE Transactions on Information Theory,* vol. 53, no. 7, pp. 2526-2541, 2007.

[101] B. Huang, L. Wang, B. Wang, S. Lin, D. Wu and Y. Zhang, “A pilot study on low power pulse rate detection based on compressive sampling,” in *31st Annual International Conference of the IEEE EMBS* , Minneapolis-USA, 2009.

[102] E. Candes, J. Romberg and T. Tao, “Robust uncertainty principles: Exact signal reconstruction from highly incomplete frequency information,” *IEEE Transactions on Information Theory,* vol. 52, no. 2, pp. 489-509, 2006.

[103] E. Candes and M. Wakin, “An introduction to compressive sampling,” *IEEE Signal Processing*

Magazin, pp. 21-30, 2008.

[104] E. Candes and T. Tao, "Near optimal signal recovery from random projections:Universal encoding strategies?," *IEEE Transactions on Information Theory,* vol. 52, no. 12, pp. 5406-5425, 2006.

[105] D. Donho, "Compressed sensing," *IEEE Transactions on Information Theory,* vol. 52, no. 4, pp. 1298-1306, 2006.

[106] S. Bjaerum, H. Trop and K. Kristoffersen, "Clutter filter design for ultrasound color flow imaging," *IEEE Transactions on Ultrasonics Ferroelectrics and Frequency Control,* vol. 49, no. 2, pp. 204-216, 2002.

[107] A. P. Kadi and T. Loupas, "On the performance of regression and step-initialized IIR clutter filters for color doppler systems in diagnostic medical ultrasound," *IEEE Transactions on Ultrasonics Ferroelectrics and Frequency Control,* vol. 42, no. 5, pp. 927-937, 1995.

[108] R. Fletcher and D. Burlage, "An initialization techniquefor improved MTI performance in phased array radars," *Proc. IEEE,* vol. 60, pp. 1551-1552, 1972.

[109] E. Chornoboy, "Initialization for improved IIR filter performance," *IEEE Trans. Signal Processing,* vol. 40, p. 543–550, 1992.

[110] A. Kadi and T. Loupas, "On the performance of regression and step-initialized IIR clutter filters for color Doppler systems in diagnostic medical ultrasound," *IEEE Trans. Ultrason., Ferroelect.,Freq. Contr,* vol. 42, p. 927–937, 1995.

[111] T. Parks and C. Burrus, Digital Filter Design, John Wiley and Sons, 1987.

[112] J. Stone, "Independent component analysis: an introduction," *Trends in cognitive science,* vol. 6, no. 2, pp. 59-64, 2002.

[113] D. Childers, Probability and random process, New York: McGrrawHill, 1997.

[114] T. Jung, S. Makeig and C. Humpheries, "Removing electroencephalographic artifacts by blind source separation," *Psychophysiology,* vol. 37, pp. 163-178, 2000.

[115] C. Gallippi, R. Nightingale and G. Trahey, "BSS-based filtering of physiological and arfi-induced tissue and blood motion," *Ultrasound in Med. & Bio,* vol. 29, no. 11, pp. 1583-1592, 2003.

[116] T. Kolenda, L. Hansen and J. Larsen, "Signal Detection using ICA: Application to Chat Room Topic Spotting," *In proc. ICA'2001,* vol. 5, pp. 3197-3200, 2001.

[117] A. Hyva¨rinen and E. Oja, "Independent component analysis: algorithms and applications," *Neural Networks,* vol. 13, p. 411–430, 2000.

[118] M. Hayes, Statistical digital signal processing and modeling, US: John Wiley and Sons, Inc., 1996.

[119] D. MacKay, Information Theory, Inference, and Learning Algorithms, Cambridge University Press, 2005.

[120] A. Hyvarinen, J. Karhunen and E. Oja, Independant component analysis, US: John Wiley and Sons, 2001.

[121] J. Shlen, “A toturial on principal component analysis,” 2005.

[122] C. M. Bishop, Pattern recognition and machine learning, 2006, 2006.

[123] M. Negishi, M. Abilgaard, T. Nixon and R. Constable, “Removal of time-varying gradient artifacts from EEG data acquired during continuous fMRI,” *Clinical Neurophysiology,* vol. 115, p. 2181–2192, 2004.

[124] H. Hotelling, “Analysis of complex of statistical variables into principal components,” *Journal of Educational Psychology,* vol. 24, pp. 417-441, 1993.

[125] I. Jolliffe, Principal Component Analysis, Newyork: Springer, 2002.

[126] L. Trefethen and D. Bau, Numerical Linear Algebra, Philadephia, PA,: Society of Industrial and Applied Mathematics, 1997.

[127] A. Miranda, Y. Borgne and G. Bontempi, “New routs from minimal approximation error to principal components,” *Neural Process Letter,* vol. 27, no. 3, pp. 197-207, 2008.

[128] F. Mauldin Jr, D. Lin and J. Hossack, “The singular value filter: a general filter design strategy for PCA-based signal separation in medical ultrasound imaging,” *IEEE Transactions on Medical Imaging,* vol. 30, no. 11, pp. 1951-1964, 2011.

[129] H. Sakoe and S. Chiba, “Dynamic programming algorithm optimization for spoken word recognition,” *IEEE Transactions on Acoustic, Speech, and Signal Processing,* vol. 26, no. 1, pp. 43-49, 1978.

[130] N. Boulgouris, K. Plataniotis and D. Hazinakos, “Gait recognition using linear time normalization,,” *Pattern Recognition,* vol. 39, pp. 969-979, 2006.

[131] N. Boulgouris, K. Plataniotis and D. Hatzinakos, “Gait recognition using dynamic time normalization,” in *IEEE 6th Workshop on Multimedia Signal Processing*, 2006.

[132] M. Saint-Germain, “PPA 696 Research Methods,” California State University, Long Beach, [Online]. Available: http://www.csulb.edu/~msaintg/ppa696/696menu.htm. [Accessed 15 October 2013].

[133] R. Hogg and J. Ledolter, Engineering Statistics, Macmillan, 1987.

[134] O. Donoghue, A. Harrison, N. Coffey and K. Hayes, “Functional data analysis of running kinematics in chronic achilles tendon injury,” *Medicine and Science in Sports and Exercise,* vol. 40, no. 7, p. 1323–1335, 2008.

[135] A. Daffertshofer, C. Lamoth, O. Meijer and P. Beek, “PCA in studying coordination and variability: a tutorial,” *Clinical Biomechanics,* p. 415–428, 2004.

[136] D. Ormoneit, M. J. Black, T. Hastie and H. Kjellstrom, “Representing cyclic human motion using functional analysis,” *Image and Vision Computing,* pp. 1264-1276, 2005.

[137] J. Ramsy, G. Hooker and S. Graves, Functional data analysis, New York: Springer, 2005.

[138] N. Coffey, A. Harrison, O. Donoghue and K. Hayes, “Common functional principal components

analysis: a new approach to analyzing human movement," *Human Movement Science,,* vol. 30, pp. 1144-1166, 2011.

[139] J. Ramsy, G. Hooker and S. Graves, Functional Data Analysis with R and Matlab, New York: Springer, 2009.

[140] N. F. Troje, "Decomposing biological motion: a framework for analysis and synthesis of human gait pattern," *Journal of Vision,* vol. 2, pp. 371-387, 2002.

[141] M. Lee, M. Roan and B. Smith, "An application of principal component analysis for lower body kinematics between loaded and unloaded waliking," *Biomechanics,* vol. 42, pp. 2226-2230, 2009.

[142] P. Glardon, R. Boulic and D. Thalmann, "PCA-based walking engine using motion capture data," in *Computer Graphics International*, 2004.

[143] A. Forner-cordero, O. Levin, Y. Li and S. P. Swinnen, "Principal component analysis of complex multijoint coordinate movement," *Biological Cybernetics,* vol. 93, pp. 63-78, 2005.

[144] K. J. Deluzio and J. L. Astephen, "Biomechanical features of gait waveform data associated with knee asteoarthritis, an application of proncipal component analysis," *Gait and Posture,* vol. 25, pp. 86-93, 2007.

[145] K. Yang and C. Shahabi, "A PCA-based similarity measure for multivariate time series," in *2nd ACM international workshop on Multimedia databases*, 2004.

[146] Denso robot, setting-up manual, Denso wave icorporated, 2011.

[147] D. Montgomery, Statystical Quality Control, NJ: Wiley, 2009.

[148] MATLAB, version 7.11.0 (R2010b), Natick, Massachusetts: The MathWork Inc., 2010.

[149] A. Bell and T. Sejnowski, "An Information-Maximization Approach to Blind Separation and Blind Deconvolution," *Neural Computation,* vol. 7, pp. 1129-1159, 1995.

[150] H. Nielsen, "UCMINF - an Algorithm for Unconstrained, Nonlinear Optimization," IMM, Technical University of Denmark, 2001.

[151] L. Molgedey and H. Schuster, "Separation of independent Signals using Time-Delayed Correlations," *Physical Review Letters,* vol. 72, no. 23, pp. 3634-3637, 1994.

[152] L. Hansen, J. Larsen and T. Kolenda, On Independent Component Analysis for Multimedia Signals, CRC Press, 2000.

[153] D. Linden and T. Reddy, Handbook of Batteries, New York: McGraw-Hill, 2001.

[154] A. Alomainy, A. Sani, A. Rahman, J. Santas and Y. Hao, "Transient charactristics of wearable antennas and radio propagation channels for ultrawideband body-centric wireless communications," *IEEE Transactions on Antennas and Propagation,* vol. 57, no. 4, pp. 875-884, 2009.

[155] K. Joreskog, "Some contributions to maximum likelihood factor analysis," *Psychometrika,* vol. 32, no. 4, pp. 443-482, 1967.

Appendix A: Research Ethics Committee Approval

Queen Mary, University of London

Room W117
Queen's Building
Mile End Road
London
E1 4NS

Queen Mary Research Ethics Committee
Hazel Covill
Research Ethics committee Administrator
Tel: +44 (0) 20 7882 7915
Email: h.covill@qmul.ac.uk

Dr Chris Philips

Room E208
Department of Computer Science
Queen Mary University of London
Mile End Road
London

11th June 2013

To Whom It May Concern:

Re: QMREC1206 – Towards flexibility in body area sensing.

I can confirm that Ms Roya Haratian has completed a Research Ethics Questionnaire with regard to the above research.

The result of which was the conclusion that her proposed work does not present any ethical concerns; is extremely low risk; and thus does not require the scrutiny of the full Research Ethics Committee.

Yours faithfully

Ms Hazel Covill

Research Ethics Committee Administrator

Appendix B: Consent Form and Information Sheet

Queen Mary
University of London

Information Sheet

Research Study:

Towards Flexibility in Motion Capture Systems

We would like to invite you to be part of this research project. You should only agree to take part if you want to-it is entirely up to you. If you choose not to take part, there will not be any disadvantages for you and you will hear no more about it.

Please read the following information carefully before you decide to take part; this will tell you why the research is being done and what you will be asked to do if you take part.

Please ask if there is anything that is not clear if you would like more information.

If you decide to take part, you will be given this information sheet to keep and be asked to sign the attached form to say that you agree. You are still free to withdraw at any time and without giving a reason.

About this study:

Our subjects take part in a session of gait measurement in the gait lab (the Human Performance Lab, on the ground floor of Engineering Building).

The measurements will involve instrumenting of the legs and pelvis with active markers to carry out several sessions of gait motion capture. The subject will need to wear shorts or leggings. The purpose of the data capture is to measure and quantify inter-session marker placement variability, and gather preliminary data for a study. There are no risks involved in taking part in this experiment.

If you are interested in hearing more about the research after you have taken part, then you can always read a more detailed description in debriefing sheet that the experimenter will give you afterwards.

Queen Mary
University of London

Consent form

Please complete this form after you have read the Information Sheet.

Title of Study: Towards Flexibility in Motion Capture Systems.
Queen Mary Research Ethics Committee Ref: QMREC120

Thank you for considering taking part in this research. The person organizing the research must explain he project to you before you agree to take part.

If you have any questions arising from the information Sheet or explanation already given to you, please ask the researcher before you decide whether to join in.

- *I understand that if decide at any other time during the research that I no longer wish to participate in this project, I can notify the researchers involved and be withdrawn from it immediately.*
- *I consent to the processing of my personal information for the purposes of this research study. I understand that such information will be treated as strictly confidential and handled in accordance with provisions of data protection act 1998.*

Participant's Statements:

I _____ agree that the research project named above has been explained to me to my satisfaction and I agree to take part in the study. I have read both the notes written above and the Information Sheet about the project, and understand what the research study involves.

Signed: Date:

Investigator's Statement:

I, Roya Haratian, confirm that I have carefully explained the nature, demands and any foreseeable risks (where applicable) of the proposed research to volunteer.

Signed: RoyaHaratian Date: 15 Jun 2013

Appendix C: An Example of the Possible Applicability of the Proposed Approach within Wireless Communication

To investigate the applicability of the proposed filtering technique for body-centric wireless communications, we used the approach to filter ultra wide band (UWB) channel response data. Measurement data of UWB radio channels for body-centric wireless communication where various units/sensors are scattered on/around the user needs to be cleaned from unwanted variations.

In the UWB frequency range, from 3.1 to 10.6 GHz, the antenna of on-body sensing system behaves like a filter in both spatial and frequency domains and tends to introduce unpleasant signal distortion and degradation. In addition, the human body affects the performance of the UWB on-body antenna. It is shown in [153] that there are differences in measured channel impulse response of the received pulses for the various designed scenarios performed in the Body-Centric wireless lab.

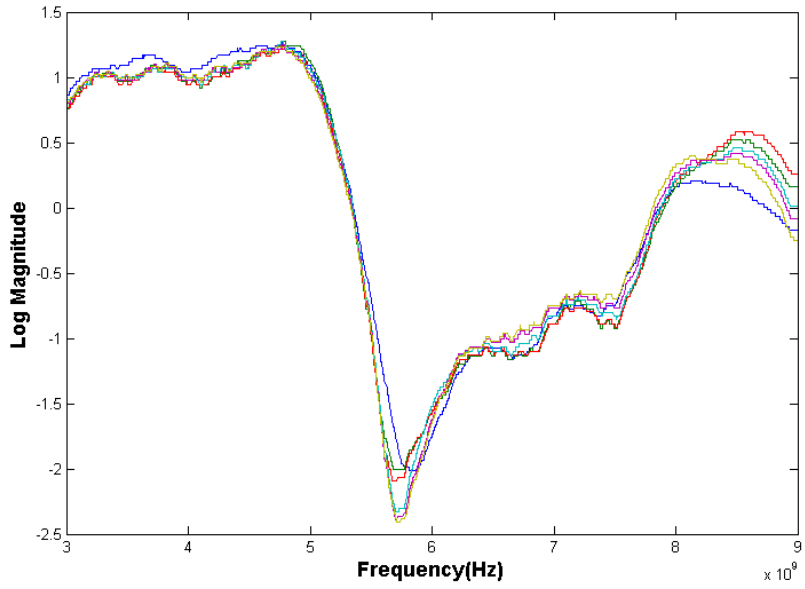

Figure 16, Logarithm magnitude of channel frequency responses for 6 different measurements before applying the proposed filtering technique.

In general, there should be several measurements of channel frequency response to estimate wireless channel parameters. To enhance the repeatability of measurement data and hence reduce the need for a larger number of trials and measurements, we can apply the filtering technique. This will provide a better methodology for extracting on-body channel data without the need for longer measurement times and only requires a few traces. This can be achieved by deriving functional principal components of the data. By keeping the first functional principal component and rejecting the rest and then transferring the data back to the first domain by projecting the data of the retained components, the filtering can be performed.

The channel frequency response with different measurements, as explained in [153], is presented in figure I. As we see there is variation in channel frequency response between measurements. It is shown in figure II that the variation in data of channel frequency response measurements can be compensated for by using the proposed approach although it needs further investigation to achieve reliable results.

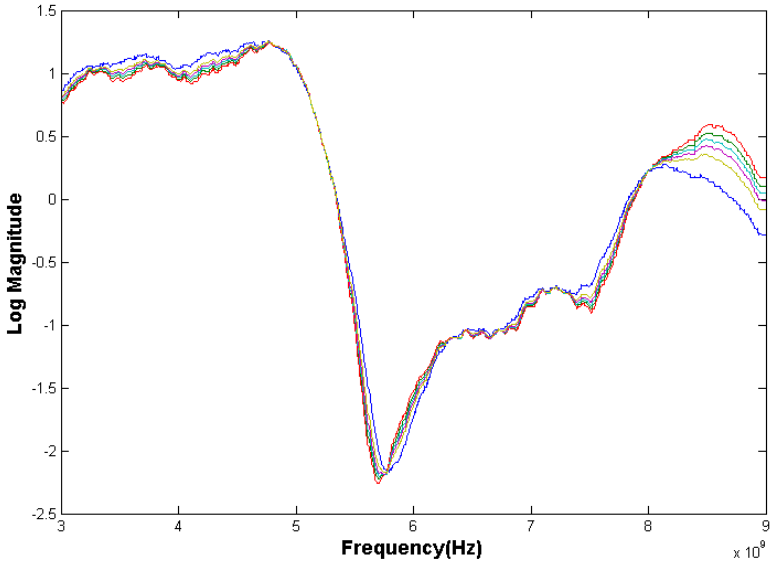

Figure II, Logarithm magnitude of channel frequency responses for 6 different measurements after applying the proposed filtering technique.